International Journal of Engineering Technologies (IJET)

Volume:8
No:1
March 2023

Printed ISSN: 2149-0104
e-ISSN: 2149-5262

Istanbul Gelisim University Press,
2023

International Journal of Engineering Technologies is an international peer–reviewed journal and published quarterly. The opinions, thoughts, postulations or proposals within the articles are but reflections of the authors and do not, in any way, represent those of the Istanbul Gelisim University.

CORRESPONDENCE and COMMUNICATION:

Istanbul Gelisim University Faculty of Engineering and Architecture
Cihangir Mah. Şehit P. Onb. Murat Şengöz Sk. No: 8
34315 Avcilar / Istanbul / TÜRKİYE
Phone: +90 212 4227000
Fax: +90 212 4227401
e-Mail: ijet@gelisim.edu.tr
Web site: http://ijet.gelisim.edu.tr
https://dergipark.org.tr/en/pub/ijet
Twitter: @IJETJOURNAL

Printing and binding:
Anka Matbaa
Certificate Number: 44889
Phone: +90 212 5659033 - 4800571
E-mail: ankamatbaa@gmail.com

International Journal of Engineering Technologies (IJET) is included in:

International Journal of Engineering Technologies (IJET) is harvested by the following service:

Organization	URL	Starting Date
The OpenAIRE2020 Project	https://www.openaire.eu	2015
GOOGLE SCHOLAR	https://scholar.google.com.tr/	2015
WORLDCAT	https://www.worldcat.org/	2015
IDEALONLINE	http://www.idealonline.com.tr/	2018

INTERNATIONAL JOURNAL OF ENGINEERING TECHNOLOGIES (IJET)
International Peer–Reviewed Journal
Volume 8, No 1, March 2023

Scientific Advisory Board

Asst. Prof. Dr. Seda Yamac AKBIYIK, Istanbul Gelisim University, Türkiye
Asst. Prof. Dr. Seda ERBAYRAK, Istanbul Gelisim University, Türkiye
Asst. Prof. Dr. Samuel MOVEH, Istanbul Gelisim University, Türkiye
Asst. Prof. Dr. Sajedeh NOROZPOUR SIGAROODI, Istanbul Gelisim University, Türkiye
Asst. Prof. Dr. Safar POURABBAS, Istanbul Gelisim University, Türkiye
Asst. Prof. Dr. Nihal ALTUNTAS, Istanbul Gelisim University, Türkiye
Asst. Prof. Dr. Neslihan OZDEMIR, Istanbul Gelisim University, Türkiye
Asst. Prof. Dr. Mustafa TUNAY, Istanbul Gelisim University, Türkiye
Asst. Prof. Dr. Mustafa NURI BALOV, Istanbul Gelisim University, Türkiye
Asst. Prof. Dr. Mukhallad Mohammed Mawlood AL-MASHHADANI, Istanbul Gelisim University, Türkiye
Asst. Prof. Dr. Mesut BARIS, Istanbul Gelisim University, Türkiye
Asst. Prof. Dr. Meltem UZUN, Istanbul Gelisim University, Türkiye
Asst. Prof. Dr. Mahmoud H. K. ALDABABSA, Istanbul Gelisim University, Türkiye
Asst. Prof. Dr. Khalid O.Moh. YAHYA, Istanbul Gelisim University, Türkiye
Asst. Prof. Dr. Hasan Emre OKTAY, Istanbul Gelisim University, Türkiye
Asst. Prof. Dr. Hadi ERCAN, Istanbul Gelisim University, Türkiye
Asst. Prof. Dr. Gulsum Yeliz SENTURK, Istanbul Gelisim University, Türkiye
Asst. Prof. Dr. Gokay Burak AKKUS, Istanbul Gelisim University, Türkiye
Asst. Prof. Dr. Ferhat KURUZ, Istanbul Gelisim University, Türkiye
Asst. Prof. Dr. Elham PASHAEI, Istanbul Gelisim University, Türkiye
Asst. Prof. Dr. Didem Yilmaz CAPKUR, Istanbul Gelisim University, Türkiye
Asst. Prof. Dr. Cansu NOBERI, Istanbul Gelisim University, Türkiye
Asst. Prof. Dr. Bora TAR, Istanbul Gelisim University, Türkiye
Asst. Prof. Dr. Binnur GURUL, Istanbul Gelisim University, Türkiye
Asst. Prof. Dr. Ayse KARAOGLU, Istanbul Gelisim University, Türkiye
Asst. Prof. Dr. Aylin Ece KAYABEKIR, Istanbul Gelisim University, Türkiye
Asst. Prof. Dr. Ali SAKIN, Istanbul Gelisim University, Türkiye
Asst. Prof. Dr. Ahmet Yucel URUSAN, Istanbul Gelisim University, Türkiye
Asst. Prof. Dr. Ahmed Amin Ahmed SOLYMAN, Istanbul Gelisim University, Türkiye
Asst. Prof. Dr. Abbas AKKASI, Istanbul Gelisim University, Türkiye
Asst. Prof. Dr. Mehmet Akif SENOL, Istanbul Gelisim University, Türkiye
Asst. Prof. Dr. Kyungnam KO, Jeju National University, Republic of Korea
Asst. Prof. Dr. Hulya OBDAN, Istanbul Yildiz Technical University, Türkiye
Asst. Prof. Dr. Hidenori MARUTA, Nagasaki University, Japan
Dr. Youcef SOUFI, University of Tébessa, Algeria
Dr. Tuncay KAMAS, Eskişehir Osmangazi University, Türkiye
Dr. Rafael CASTELLANOS-BUSTAMANTE, Instituto de Investigaciones Eléctricas, Mexico
Dr. Nobumasa MATSUI, Faculty of Engineering, Nagasaki Institute of Applied Science, Nagasaki, Japan
Dr. Jorge Guillermo CALDERÓN-GUIZAR, Instituto de Investigaciones Eléctricas, Mexico
Dr. Hiroyuki OSUGA, Mitsubishi Electric Corporation, Japan
Dr. Hector ZELAYA, ABB Corporate Research, Sweden
Dr. Guray GUVEN, Conductive Technologies Inc., United States
Dr. Cristea MIRON, Politehnica University in Bucharest, Romania

From the Editor

Dear Colleagues,

On behalf of the editorial board of International Journal of Engineering Technologies (IJET), I would like to share our happiness to publish the 29th issue of IJET. My special thanks are for members of Editorial Board, Publication Board, Editorial Team, Referees, Authors and other technical staff.

Please find the 29th issue of International Journal of Engineering Technologies at http://ijet.gelisim.edu.tr or https://dergipark.org.tr/en/pub/ijet. We invite you to review the Table of Contents by visiting our web site and review articles and items of interest. IJET will continue to publish high level scientific research papers in the field of Engineering Technologies as an international peer-reviewed scientific and academic journal of Istanbul Gelisim University.

Thanks for your continuing interest in our work,

Prof. Dr. Necmettin MARAŞLI
Istanbul Gelisim University
nmarasli@gelisim.edu.tr

---

http://ijet.gelisim.edu.tr
https://dergipark.org.tr/en/pub/ijet
Printed ISSN: 2149-0104
e-ISSN: 2149-5262


International Journal of
Engineering Technologies
IJET

Table of Contents

Volume 8, No 1, March 2023

International Journal of Engineering Technologies, IJET

e-Mail: ijet@gelisim.edu.tr
Web site: http://ijet.gelisim.edu.tr
https://dergipark.org.tr/en/pub/ijet
Twitter: @IJETJOURNAL

Production, and Analysis of a Two-Axis Food Liquid Pouring Machine

Muhammed Ömer Erdogan*‡, Ali Okatan**, Umut Uz*, Furkan Yılmaz*, Ali Çetinkaya*

*Technology Transfer Office Application and Research Centre, Istanbul Gelisim University, Avcilar, Istanbul, Türkiye.
**Department of Software Engineering, Faculty of Engineering, Istanbul Aydın University, Küçükçekmece, Istanbul, Türkiye.

(moerdogan@gelisim.edu.tr, aliokatan@aydin.edu.tr, uuz@gelisim.edu.tr, fuyilmaz@gelisim.edu.tr, alcetinkaya@gelisim.edu.tr)

‡ Corresponding Author; Muhammed Omer Erdogan, Technology Transfer Office Application and Research Centre, Istanbul Gelisim University, Avcilar, Istanbul, Türkiye.
Tel: +90 212 422 70 00/7188 moerdogan@gelisim.edu.tr

Received: 07.02.2022 Accepted: 24.08.2022

Abstract- People always want to feel special and different. This demand has not left us alone in the food sector and has improved itself as culinary arts and presentations. So much so that there are masters who can transform food liquids, such as pancake liquids, into art by making special shapes on them based on demand. As in every sector, the effects of technology are also seen here. Considering these needs and developments, this study focused on the production and tests of machines that would convert the drawings designed by people with the help of computers into food liquid. The machine, produced in the context of the study, has a two-axis mechanical structure and gives shape to the food liquid with the commands coming from a computer and the liquid pouring chamber. While this machine aims to provide convenience to people in terms of time and ability, it also contributes to the developing technology in the kitchen sector. As the machine's working principle, a drawing is created first with shapes that people can draw on a tablet or a computer in front of them if they want, or they can choose ready-made. Then, this drawing is converted to g code via the program and the movement coordinates of the pouring mouth of the machine are created. The system, controlled by a microprocessor, drives the motors and performs the operation. While the pouring process is supported with the help of a chamber air control system in which the food liquid is located, the cooking of the food liquid is ensured by the heat-adjustable tray under it.

Keywords Two-axis machine, Kitchen, Pancake

1. Introduction

It is an undeniable fact that the invention of machines and the mechanization process have made human life easier. For example, mobile phones and transportation vehicles that we use every day are machines that provide convenience for us in all areas of life. The mechanization process continues to affect the flow of life by growing and renewing.

Machines allow us to do many small or big jobs easier now and they provide many conveniences in all aspects of our lives. Jobs that were done by many people in the past can now be done with less cost and in a shorter time thanks to one machine. Today, autonomous devices and machines have moved toward systems that are called artificial intelligence.

Three- and two-axis autonomous machines, which are among the commonly used devices today, are the focus of this study. These machines are used in many fields such as industry, military, health, and agriculture. While these machines that shape materials such as plastic, metal, and wood continue to be effective in the market, the machine that we have chosen in this study is used to serve people in the kitchen and food field by shaping food liquids.

The capacity of the systems of these machines, which differ structurally in terms of the way they work, depends on the direction and number of their movements on the axes of motion. The differentiation of usage areas makes devices into systems that require research and development works at many points in terms of both software and hardware.

In this study, the designed and manufactured machine was created by inspiring the infrastructure of two-axis computer-controlled systems. In terms of its design, thanks to its portable feature, this machine is a device that facilitates life and will be able to be used in everyday life and even at home. A literature review and similar projects related to the topic of the study are presented below.

2. Literature Review

The machines manufactured today consist of many infrastructures and systems. These infrastructures and systems include mechanical, electronic, and software stages.

For example, biaxial food liquid pouring machines consist of mechanical parts, electronic control units, air flow systems, liquid flow, and heating plate units [1]. With Computer Numerical Controls (CNCs) and cartesian robots, processing, design, and manufacturing operations on raw materials can be performed [2-6]. Electronic control on CNCs can be provided on computers via embedded electronic systems [7-10]. During this control phase, communication can be carried out using wired, Wi-Fi, or IOT (Internet of Things) systems [11-12].

Elements produced by using the 3D printing method are actively used in robotic systems, mobile robots, and CNC production area [13-14]. The software control of robotic systems can be planned to include artificial intelligence algorithms depending on their usage areas [15-17]. In machine design, analysis and evaluation of software systems in terms of the control of devices, and the design of machines' axis movements are very important [18-24]. In a study conducted by Kurt et al. [23], which production methods or manufacturing techniques were used for the production of machine elements were examined based on the production drawings and taking into account the science of technology. In the literature review, it was seen that older food-liquid cooking machines (pancake machines) used a hopper filled with pancake batter that was manually dropped on a rotating grill, and the pancakes were manually turned and coated when cooking was complete [25].

Based on the usage areas, the steel to be used in the structure of the machines should be stainless. Studies have shown that the chromium and passivation rate in stainless steel determines the stainless quality of the steel, and the oxide layer formed on the material surface is too thin to be seen with the naked eye and is waterproof [26].

3. Design of Mathematical Modeling

3.1. Equipment and Elements Used in the System

The system developed in this study is basically composed of two sections: a control unit section and a mechanical section. In the mechanical section, commands from the control section gain function. In this section, motors, belts, plates, pulleys, linear bearings, and rails constitute the system. In the control part, the commands given from the computer are transferred to the mechanical part with the microprocessor, engine drivers, air pump, and power supplies. Our system saves time and labor by processing a shape drawn from a computer with a control unit and then transferring it to a mechanical part. The food liquid reservoir located in the mechanical system is drawn on the cooking plate by a two-axis movement mechanism and drained. While two stepper motors provide movements, the air pump ensures the pushing of the flow of food liquid into the pouring mouth.

3.2. Mechanical Elements in the System

The elements used in the system were selected in accordance with the food. For example, while stainless steel was used in the Plate parts, hoses and hoppers were supplied from the food sector. In the mechanical part, the transmission of two stepper motors is ensured by belt, pulley, and linear bearing systems. In order to provide this motion control, limiters were used. The food liquid is kept in a container and transmitted to the mouth of the pourer with the help of a hose, while the movable arms shape this pouring process. In Figure 1, the complete mechanical components of the system is shown. While the white food liquid container is located on the top, the moveable lever to which the container is connected can also be seen in the figure. As seen, the hose and belt systems are located behind the mechanism.

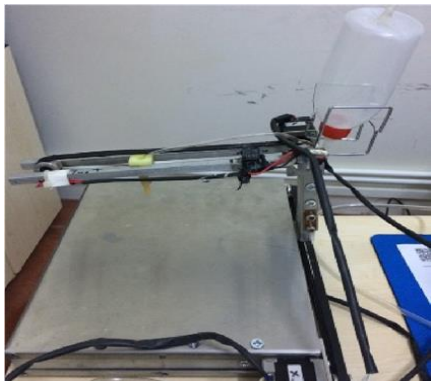

Fig. 1: Mechanical Part of the System

3.3. Stainless Plates

The 304 stainless steel plate used for the main lines and chassis of our machine was processed and assembled in accordance with our machine (Figure 2). The features such as being lightweight, giving results that we want in terms of durability, and being suitable for food use were among the main reasons for using this steel plate in our machine. In addition, its low cost stood out as a separate positive factor for us. The fact that the main frame of our machine is durable makes it possible not to be easily affected negatively as a result of any impact that the machine will face during the operation process.

Fig. 2: Stainless chassis of the machine

3.4. Movement and Transmission Elements

We used linear bearings so that our robot, which moves on two axes and also works with 3D printer logic, can perform the movements we want it to do on the axes without errors and smoothly. In addition, the linear bearing was the most logical choice because we used an induction shaft in the region where the bearing would move. The linear bearing where we use the SCE 10 UU model prevents axis leaks that may occur. In this way, the error rate that may emerge in the movements of our machine was minimized. Moreover, thanks to its lightweight structure, it did not create a disadvantage in the weight of the machine that we determined at the design stage. Figure 3 shows the selected bearing.

Fig. 3: Linear Bearing

Induction shaft: This shaft type with high strength works at full performance with the SCE 10 UU linear bearing that we use in our machine. In this way, our machine can move properly between the axes. The shaft used in the machine has a length of 270 mm and a diameter of 10 mm. The selected shaft is shown in Figure 4.

Fig. 4: Induction Shaft

In order to ensure the connection between the motors and the pulleys of our machine, a three-groove v-belt was used. Three-groove v-belts, which work in a full performance manner with specially processed pulleys, were used both because we did not use a process requiring high torque and because it was the best choice for movement between axes. In addition, the fact that v-belts have a long service life is another positive factor for our machine. In Figure 5, an example of a v-belt used in the system is shown.

Fig. 5: The v-Belt Used in the Machine

The pulley system used in the system was manufactured as a three-groove in accordance with this belt system; and this, in turn, minimizes the likelihood of the belt coming off due to the overload coming to the system.

3.5. Electronic Elements in the System

While two stepper motors were used in the system, the Toshiba Tb6560 stepper motor driver was used to control them. For fluidity, the air engine was used and the air pump control unit was used to control it. Limit switches were used for the notification of the limits of motor movements. These elements are controlled by an AT mega 328 microprocessor and power is provided to the system by a 12V DC power

supply.
Two stepper motors were used in the system: the Nema 14 and Nema 17 stepper motors. They provide x- and y-axis movement. Nema 17 moves the carrier arm on the x axis, while the Nema 14 motor moves the pouring mouth on the carrier arm on the y axis.

Fig. 6: Nema 17 Motor

It was decided that Nema 17, a type of stepper motor, was suitable for this project. In the system, one Nema 17 motor was used. In terms of its characteristics, the Nema17 operates at 4 V and 1.2 A. The purpose of use of it in hardware design with its holding torque of 3.2 kg-cm is to ensure the movement of the liquid pouring system and the X axis carrying the Y axis on it. This motor is shown in Figure 6.

Fig. 7: Nema 14 Motor

Nema14 is a kind of stepper motor and in the system, one Nema 14 motor was used. Nema 14 is powered by 2.7 V and 1000 mA. With its holding torque of 1.4 kg-cm, it provides the movement of the Y axis as integrated with the liquid pouring system in the hardware design. Figure 7 presents this motor.
To drive the Nema14 and Nema17 stepper motors used in the machine, two Toshiba Tb6560 Stepper motor drivers were used. This type of stepper motor driver, which can work with 24V and 3A, is suitable for 2, 4, and 6 phase stepper motors. A general view of the stepper motor driver is presented in Figure 8 and a connection diagram is shown in Figure 9.

Fig. 8: Tb6560 Stepper Motor Driver

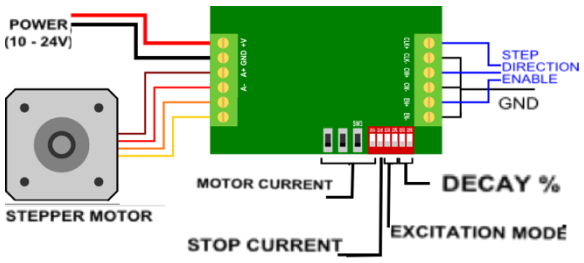

Fig. 9: Schematic Diagram for the connections of the motor driver

In order for the machine to transfer the food liquid onto the grill, an air pump powered by 220V and through which we can pour the food liquid was used. In this way, the movement of the food liquid on the axes of the designed system was ensured.
Another method is to perform this operation with a liquid pump. This pump, which was used to perform the spraying process that is the main task of Hexatar, provides the operation and stopping of the irrigation system by applying the start or stop commands that it received from the relay triggered by a pulse width modulation (PWM) signal. There are two hoses connected to this motor.

One of these hoses is located inside the fuel tank, while the other hose is fixed to the spraying apparatus. However, when we applied the literature [14] we examined, efficiency could not be achieved in terms of fluidity when we did not give the liquid to the container where it was in.

When tested with a DC 12 volt liquid pump, it was observed that no continuous fluidity could be achieved, and such a method was used to keep the air in the bottle constant. In Figure 10, a sample air pump motor is shown.

Fig. 10: Air Pump Motor

With the operation of the air pump, the food liquid was poured from the unit where it was located to the heater plate by the air pump control unit. This part is located in the control unit of the designed system and is controlled by the microcontroller board. This driver is shown in Figure 11.

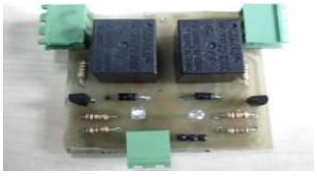

Fig. 11: Air Pump Motor Driver

A power supply is an electrical device that supplies electricity to an electrical load. The main function of a power supply is to convert the electric current from a source to the correct voltage, current, and frequency to supply the load.

Therefore, power supplies are also sometimes called electrical power converters. A 12 volt 5 A power supply was used to supply all the electronic components in the system. All the necessary energy is supplied from this power supply. An example of the power supply used in the system is presented in Figure 12.

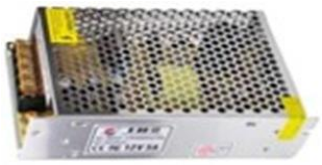

Fig. 12: Air Pump Motor Driver

To ensure that the internal components are in the correct position for the operation and to prevent operation when the access doors are opened, the Miniature Snap Action Switch can be used as components of devices such as copy machines, computer printers, convertible tops, or microwave ovens. A set of adjustable limit switches is installed on a garage door opener to turn off the motor when the door is in the fully raised or fully lowered position. A numerical control machine such as a lathe should have limit switches to define maximum limits for machine parts or to provide a known reference point for incremental movements. Therefore, in our system, we also used limiters to control movement limits in the system and obtain more useful results. An example of the limiter in the system is shown in Figure 13.

Fig. 13: The Limiters

Arduino Uno is a microprocessor development board based on ATmega 328 (Figure 14). The card has 14 digital input/output connections (of which 6 can be used as a P W M output), 6 analog inputs, a 16 Mhz crystal oscillator, a USB connection, a power connection, an ICSP connection, and a reset button. Connecting to the computer via the USB port is sufficient for the card to work. In addition, it can also be used with a battery or an adapter.

Fig. 14: Arduino Uno

In the machine designed in this study, we used AT mega 328. In order for the software created for the system to work simultaneously with the motor and drivers, the Arduino UNO-R3 was used. It was preferred both because of the variety of its code library and because it can be encoded very easily with the C codes. The card, which is also widely used in prototype projects today, has added practicality in terms of use in this project as well. In the study, this card was used as a processing and control card when driving the motors of the machine with the driver.

Another element of the system is the heater plate. It is the part where the food liquid that will flow through the liquid flow system with the air control unit will be cooked. Data related to food liquid is created on the computer interface in the system. A 220 V AC mains voltage was applied to supply the system. The heater plate (baking plate) was supplied as a ready-made product and added to the system. The heater plate used in the system is shown in Figure 15.

Fig. 15: Heater Plate

3.6. The Structure of the Software in the System

To control the motion system of the machine, the software developed within the Istanbul Gelisim University Technology Transfer Office (IGU TTO) was used in the software section. In the software system, the user data sent to the machine from the computer interface is directed by the TTO Pankek 4.1 interface software. The interface software used in the machine is comprised of six sections. The first is the “connection settings” section where the communications protocol is provided between the machine and the computer interface. The second is the “Manual Movement” section where manual position control of the machine is provided. In the third section, “Pancakes fluid flow control” is carried out by ensuring the manual control of the air flow system in the control unit. The fourth section is the drawing area where drawings will be created with the mouse. The fifth section is the “Incoming - outgoing data” section where outgoing–incoming data will be displayed during communication between the port and the machine and the possibility of manually sending codes can be provided. In the sixth section, on the other hand, there is an area where the created pancake data will be uploaded to the robot. The interface of the software used in the system is shown in Figure 16.

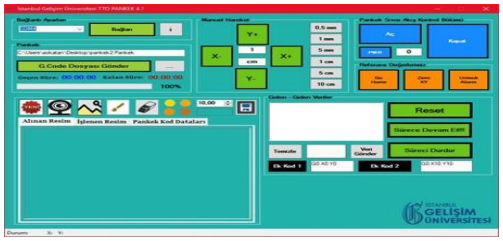

Fig. 16: Program Interface

As an example, when we type the inscription "İGÜ", an image is formed in the program as in Figure 17.

Fig. 17: "IGU" Interface image

While writing, the cooking priority can be determined with the color options on the tab at the top of the interface. While the parts drawn in a dark color are cooked more, the ones drawn in light color are poured later so that they are cooked less. The resulting G codes of this writing appear as in Figure 18.

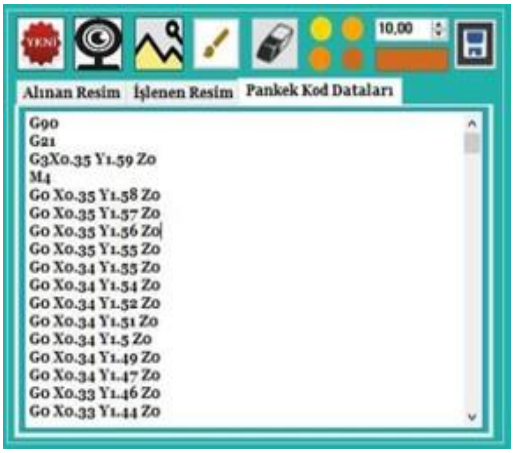

Fig. 18: G code view

It has been found that G-code instructions are mostly used in vertical machine tools and they are machine messages that tell motors where to move, how fast to move, and which path to follow [20].

3.7. The Principle of Operation of the System

After activating the power buttons on the system, the user makes sure that the microprocessor is working and its lights are on. The drawing program on the computer is run, the desired shape is drawn with the mouse, or the desired shape is transferred to the program. The heater plate is turn on and the pressure command is pressed with the control of the limit switches, then the pouring process of the food liquid is started. In case of any emergency, the printing process can be stopped via the program.

4. Conclusion and Recommendations

The control unit of the Food Liquid Machine can make axis movements in accordance with the air-flow system and liquid flow systems. In various tests conducted, it was observed that the software worked compatible with the control system and the air-flow system. In the project where the single-lever system was used for the first time on such machines, ease of use came to the fore, and it became easy to interfere with the product and the heater plate. However, it was noticed that the sensitivity of the liquid being poured was poor due to the mechanical system, and arrangements were made to prevent this. The system is shown in Figure 19.

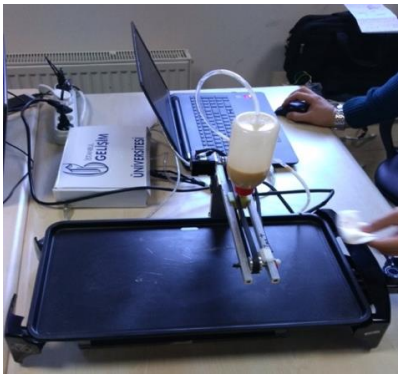

Fig. 19: Food liquid printing

In terms of arrangements, the height between the machine's arm carrying the liquid pouring system and the heat plate was decreased. With the shortening of the arm length, the delay margin between the motion of the movement mechanism and the shape made by the liquid on the plate also reached an ideal level. For example, when the pouring height was reduced to four centimeter and the temperature was set to 180 degrees Celsius, the cooking time was recorded as 3 minutes. Another arrangement is that the liquid container previously located above the pouring mouth was placed on top of the conveying arm, and the pouring mouth and the chamber mouth were separated from each other. Thus, the liquid chamber performed a healthier pouring by not weighing on the movement arm and not creating vibration on the pouring mouth. In addition, we made a new addition to the pouring mouth, and we done this with 3D printer. Today, precision, reproducibility, and the variety of materials have shown that some 3D printing processes can be considered industrial production technology.

One of the main advantages of 3D printing is the ability to produce very complex shapes or geometries. There are no prerequisites for the production of any part printed on a 3D machine. A digital 3D model or a CAD (computer-aided design) file is enough. Considering these, it was profitable to produce the material by this method.

In terms of recommendations that can be made: The software part currently transfers what is drawn over the computer via cable. In the future, remote ordering logic can be placed wirelessly on devices such as phones, tablets, and computers. By covering the device with plexy, a protection shield can be created and a healthier pouring process can be performed. Cases and unit containers can be made on the machine by using plastic injection molds, the cost of which will not cause problems in mass production. Finally, it can be also said that if a linear bearing, which could not be purchased because of its high price, had been able to be used in the sleigh system, the movement mechanism would give a smoother result.

References

[1] Erdoğan, M. Ö. (2019). İki eksenli gıda sıvısı döken makinenin tasarımı, analiz, talaşlı ve talaşsız imalat ile üretimi (Master's thesis, İstanbul Gelişim Üniversitesi Fen Bilimleri Enstitüsü).

[2] Kuncan, M., Kaplan, K., Ertunc, H. M., & Küçükateş, S. (2018). CNC lastik kalıbı işleme makine tasarımı, imalatı ve özgün NC takım yolu oluşturulması. Gazi Üniversitesi Mühendislik Mimarlık Fakültesi Dergisi, 33(3), 1183-1200.

[3] Iliyas Ahmad, M., Yusof, Y., Mustapa, M. S., Daud, M. E., Latif, K., Kadir, A. Z. A., ... & Hatem, N. (2022). A novel integration between service-oriented IoT-based monitoring with open architecture of CNC system monitoring. The International Journal of Advanced Manufacturing Technology, 1-12.

[4] Aslan, R. (1999). Step Motor Ile Tahrik Edilen Iki Eksenli Bir Kartezyen Robotun, 8051 Mikrodenetleyici Çerçevesinde Tasarlanması (Doctoral dissertation, Marmara Universitesi (Türkiye)).

[5] Yazıcı, S. (2004). İki eksenli dairesel enterpolasyon yapabilen CNC kontrol devresi tasarım, Fen Bilimleri Enstitüsü, Kocaeli Üniversitesi.

[6] Suh, S. H., Kang, S. K., Chung, D. H., & Stroud, I. (2008). Theory and design of CNC systems. Springer Science & Business Media.

[7] Yalçın, Ü. (1996). Bilgisayar kontrollü iki eksenli bir oksijenle kesme tezgahı tasarımı ve imalatı, Yüksek Lisans Tezi, Fen Bilimleri Enstitüsü, Selçuk Üniversitesi.

[8] Yılmaz, M. (2005). Punto makinasının iki boyutlu grafik ekseni kullanılarak bilgisayarlı kontrolü. Fen Bilimleri Enstitüsü, Gazi Üniversitesi.

[9] Khan, M. N., Maheshwari, A., & Verma, H. (2022). Study and Design of Arduino Based CNC Laser Cutting Machine. In IOP Conference Series: Materials Science and Engineering (Vol. 1224, No. 1, p. 012008). IOP Publishing.

[10] Arunachalam, A., & Andreasson, H. (2022). RaspberryPi-Arduino (RPA) powered smart mirrored and reconfigurable IoT facility for plant science research. Internet Technology Letters, 5(1), e272.

[11] Aebersold, S. A., Akinsolu, M. O., Monir, S., & Jones, M. L. (2021). Ubiquitous Control of a CNC Machine: Proof of Concept for Industrial IoT Applications. Information, 12(12), 529.

[12] Saray, T. (2017). Radyo dalgaları kullanarak yeraltı maden ocağında çalışan madencilerin izlenmesi (Master's thesis, Fen Bilimleri Enstitüsü).

[13] Malaeb, Z., AlSakka, F., & Hamzeh, F. (2019). 3D concrete printing: machine design, mix proportioning, and mix comparison between different machine setups. In 3D Concrete printing technology (pp. 115-136). Butterworth-Heinemann.

[14] Yılmaz, F. (2019). Elektrik jet motorlu havadan karaya seyir füzesinin tasarımı, analizi ve 3 boyutlu yazıcı yardımı ile üretimi (Master's thesis, İstanbul Gelişim Üniversitesi Fen Bilimleri Enstitüsü).

[15] Uz, U. (2019). Hexacopter yapısında bir insansız hava aracı ile elektronik ilaçlama/sulama sisteminin oluşturulması (Master's thesis, İstanbul Gelişim Üniversitesi Fen Bilimleri Enstitüsü).

[16] Allahverdi, N., Çetinkaya, A., Saray, T., & Afaghani, A. Y. (2017). Fuzzy Position Control Approach for Autonomous Robot Controller.

[17] Jond, H. B., Nabiyev, V. V., & Akbarimajd, A. (2014). Planning of mobile robots under limitted velocity and acceleration. In 2014 22nd Signal Processing and Communications Applications Conference (SIU) (pp. 1579-1582). IEEE.

[18] Madekar, K. J., Nanaware, K. R., Phadtare, P. R., & Mane, V. S. (2016). Automatic mini CNC machine for PCB drawing and drilling. International Research Journal of Engineering and Technology (IRJET), 3(02), 1107-1108.

[19] Yılmaz, M. (2007). Step motor ile iki eksenli robot kol tasarımı. Yüzüncü Yıl Üniversitesi.

[20] Apro, K. (2008). Secrets of 5-axis machining. Industrial Press Inc. ISBN 987-0-8311-3375-7

[21] Kaygisiz, H., & Çetinkaya, K. (2010). Cnc Freze Eğitim Seti Tasarımı ve Uygulaması. Uluslararası Teknolojik Bilimler Dergisi, 2(3), 53-71.

[22] Liptak, B (2005) GX. Instrument Engineers' Handbook: Process Control and Optimization

[23] Kurt, H., Onurcu, Ş., Şen, İ. Z., (2012) Uygulamalı Makine Tasarımı ve Esasları, Deha Yayıncılık.

[24] Flather, J. J. (1895). Rope-Driving: A treatise on the transmission of power by means of fibrous ropes.

[25] Kiwanis Seeking Names for Pancake Machine. Ocala Star-Banner. November 26, 1977. Retrieved August 6, 2015.

[26] Paslanmaz Çelik, https://borsenboru.com/paslanmaz-celik-nedir (Access time; 02, 01, 2022).

Estimation of Combustion Properties of Briquettes Produced from Palm Fruit Shell

Francis Inegbedion*, Andrew Amagbor Erameh**‡

* Department of Production Engineering, University of Benin, Benin City, Nigeria

**Department of Mechanical Engineering, Igbinedion University Okada, Nigeria

(*francis.inegbedion@uniben.edu, **erameh.andrew@iuokada.edu.ng)

ORCID ID: *0000-0002-2142-8079, **0000-0002-6463-143X

‡Corresponding Author; Francis Inegbedion, Department of Production Engineering, University of Benin, Benin City, Nigeria, Tel: +234 803 412 4035, francis.inegbedion@uniben.edu

Received: 23.02.2022 Accepted: 15.06.2022

Abstract- Agricultural residue briquettes can be used as a fuel for heating, cooking and other domestic and industrial applications. This article explored the potential of using palm fruit shells to make briquettes as an alternative fuel for both domestic and industrial use. This will significantly reduce the problem of deforestation and excessive dependence on fossil fuels and reduce the impact of greenhouse gas emissions generated by trees as a fuel for wood. Cassava starch was used in an amount of 100:15 by weight and the burning properties of the produced palm fruit briquettes were determined. The combustion characteristics of the palm fruit briquettes produced are 7.56% average moisture, 17.45% average volatiles, 6.68% average ash, 68.28% average bound carbon and 9717.74 kcal /kg of average calorific value. These results, compared with the literature, showed that briquettes made from palm husks have good combustion properties, which makes them suitable for domestic applications and small industries.

Keywords: Briquettes, palm fruit shell, calorific value, domestics use, agro residues

1. Introduction

Biomass briquetting is the compaction of loose agricultural residues with or without binder into compact solid composites of various sizes by the application of pressure [1]. Briquettes are the products formed by the physical-mechanical conversion of dry, loose material, of small particle size, with or without the addition of an additive, into a solid state of regular shape [1]. Briquettes are mainly used where heat applications are required (steam generation, metal smelting, space heating, brick kilns, tea treatment, etc.) and for energy generation through the gasification of biomass briquettes and for domestic use [1].

Reference [2] referred to the huge agricultural residue waste management problem facing developing countries. They said these agricultural and sawmill residues are usually burned on roadsides or in landfills, causing pollution problems. However, they identified the need to convert these residues into usable fuels. These residues are very difficult to handle and store and, if burned directly, result in very low thermal efficiency and high levels of air pollution. However, they concluded that these problems could be avoided by briquetting the residual biomass into a usable fuel that produces energy. This will make biomass briquettes an alternative to fossil fuels, improve waste management and reduce air pollution.

Reference [3] in his work observed that the caloric values of briquettes of mixed sawdust from three tropical hardwoods, bound with starch, cow dung and wood ash as binding agents, were high. He mixed the sawdust of each species with the binder in a ratio of 70:30 for cow dung and wood ash and 70:15 for starch. He used a 1: 1 ratio to mix the sawdust for each combination of briquettes he produced. His results showed that the best combination of briquettes was sawdust mixed with starch.

Reference [4] conducted an experimental test on the effect(s) of starch and gum arabic as binders on the combustion

properties of sawdust briquettes in different ratios. The briquettes were produced by mixing with the binders. The blends were compressed to 110 kN using a manually operated hydraulic briquetting machine and the products were dried in the sun. They estimated the calorific values, the volatiles and the flame temperature of the briquettes produced. In their results, briquettes formed using starch as a binder had better combustion properties than briquettes formed using gum arabic as a binder.

Reference [1] compared the calorific values of briquettes produced by the binary and tertiary combination of biomass briquettes made from sawdust from Afzelia africana, Daniella oliveri and rice hulls with binder contents of 20%, 30% and 40% starch. They carried out an immediate analysis of the briquette samples and observed significant differences ($p>0.05$) between the densities, the percentage of ashes, the percentage of volatiles and the percentage of bound carbon. They observed a gradual increase in the calorific value of biomass briquettes produced with increasing intensity. They found that briquettes made from the tertiary combination of Afzeliaafricana + Daniella oliveri + rice husk biomass had the highest and lowest calorific values of 4827.20 kcal/kg and 4586.72 kcal/kg at 40% and 20% starch, respectively. They also found that the tertiary combination had the highest and lowest ash content of 9.29% and 4.30% at 20% and 40% starch content, respectively. They therefore recommended using a starch content of 40% for the production of biomass briquettes.

Reference [5] had produced biobriquettes using Napier grass, Spear grass and Biochar at moderate pressure and temperature. They performed extensive analyzes and compared their results with wood samples. Their goal was to replace firewood with briquettes in rural Nigerian households.

Briquetting biomass is a way to generate energy from agricultural waste. Biomass briquettes were developed using different types of agricultural waste. The production of biomass briquettes from agricultural and municipal waste streams could lead to viable fuel production. In this research, we estimated the combustion properties of briquettes made from palm fruits shells.

2. Materials and Methods

Palm fruits shell were homogeneously mixed with cassava starch in a weight ratio of 100:15 as described by Sotannde et al. [6], Martin et al. [7]. This mixture was fed into a briquetting machine designed and manufactured by Inegbedion and Francis-Akilaki [8] to produce the briquettes required. This machine, a single extrusion screw press, mainly consisted of a drive motor, speed reducer, feed auger, die and housing containing a hopper. The drive motor directly transfers the power to the auger through the speed reducer. While the machine is working, the raw materials are fed into the compression chamber through the hopper, the raw materials are compressed into the barrel by the screw and extruded through the nozzle. The screw continuously pushes the materials into the die. In an extrusion die screw press, pressure builds up along the screw rather than in a single area as in piston machines. Figure 1 shows briquettes made from palm bark bound with cassava starch.

Fig. 1. Briquettes produced using from Palm Fruits Shell

2.1 Determination of Moisture Content of the Palm Fruit Shell Briquettes Produced

To estimate the percentage moisture content (PMC), 1.5g samples of the palm fruit peel briquettes produced were weighed using a crucible of known mass and placed in an oven set at 105 °C±5°C. The crucible and its contents were removed from the furnace after one (1) hour and allowed to cool to room temperature, after which the crucible and its contents were reweighed. This procedure was repeated until a constant weight was recorded. Equation (1) was used to estimate the percentage moisture content of the sample briquettes produced.

$$PMC = \frac{W_1 - W_2}{W_2} \times 100\% \quad (1)$$

W_1 is the initial weight, while W_2 is the final weight of briquette sample respectively.

2.2 Determination of Volatile Matter of the Palm Fruit Shell Briquettes Produced

The percentage volatile matter (PVM) of the palm fruit shell briquettes produced was estimated by placing 1.5 g of the briquette sample in a crucible and keeping it in a furnace at a temperature of 550°C. ± 5°C for 8 minutes, then weighed after allowing it to cool to room temperature. The percentage volatile matter of the briquette samples produced was estimated using equation (2).

$$PVM = \frac{W_2 - W_3}{W_3} \times 100\% \quad (2)$$

W_2 is the weight of the oven-dried sample (g) while W_3 the weight of the sample after 8 min in the furnace at 550 °C (g)

2.3 Determination of Ash Content of the Palm Fruit Shell Briquettes Produced

1.5 g samples of the produced palm fruit briquettes were stored in a controlled oven and completely burned. An electronic scale was used to record the weight of the residue. Equation (3) was used to estimate the percentage by weight of the residue, which is the ash present in the sample.

$$PAC = \frac{W_4}{W_2} \times 100\% \quad (3)$$

2.4 Determination of Fixed Carbon of the Palm Fruit Shell Briquettes Produced

The percentage fixed carbon (PFC) of the palm fruit shell briquettes produced were determined using equation (4) [9].

$$PFC = 100\% - (PMC + PVM + PAC) \quad (4)$$

2.5 Determination of Calorific Value of the Palm Fruit Shell Briquettes Produced

The calorific values of the briquettes produced were determined using a bomb calorimeter. We completely burned 1.5 g of the briquette sample in oxygen oxides. The heat released during combustion was absorbed by the water and the calorimeter. The heat lost due to the combustion of the briquettes was the heat gained by the water and the calorimeter. We used equation (5) to estimate the calorific value (CV) of the briquettes produced from the measured data [10].

$$CV = \frac{BFx\ \Delta t - 2.3\ length\ of\ wire}{W} \quad (5)$$

Where: BF = Burn Factor; Δt = Change of temperature ($t_2 - t_1$)°C; t2 = final temperature; t_1 = initial temperature; W = mass of the sample used and BF = constant = 13,257.32.

3. Results and Discussion

The estimated combustion properties of the palm fruit shell briquettes produced were: percentage moisture content, percentage volatile matter, percentage ash content, percentage fixed carbon, and calorific value.

Table 1. Percentage Moisture Content (PMC) of Palm Fruit Shell Briquettes

Sample	PMC (%)
1	7.65
2	7.52
3	7.60

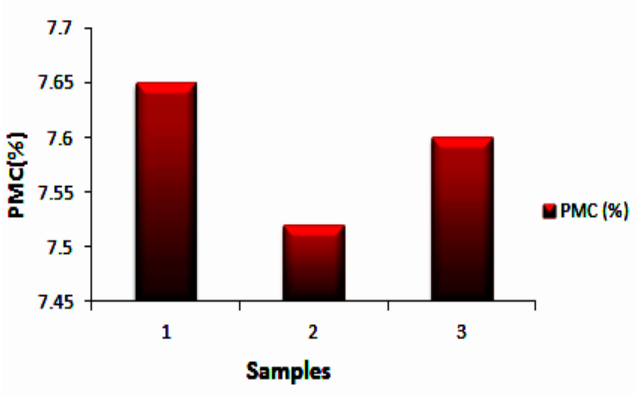

Fig. 2. Percentage Moisture Content (PMC) for Palm Fruit Shell Briquettes

In Table 1 and Figure 2, we present the results of the average percent moisture content (APC) of the produced palm fruit shell briquette being 7.56%. These results compared to the work of Pallavi et al. [11] agreed with their recommendation of 5-10% moisture content for quality briquettes. Reference [9] indicates that briquettes are easy to ignite when the moisture content is low and have a high calorific value.

Table 2. Percentage Volatile Matter (PVM) for Palm Fruit Shell Briquettes

Sample	PVM (%)
1	17.45
2	17.48
3	17.42

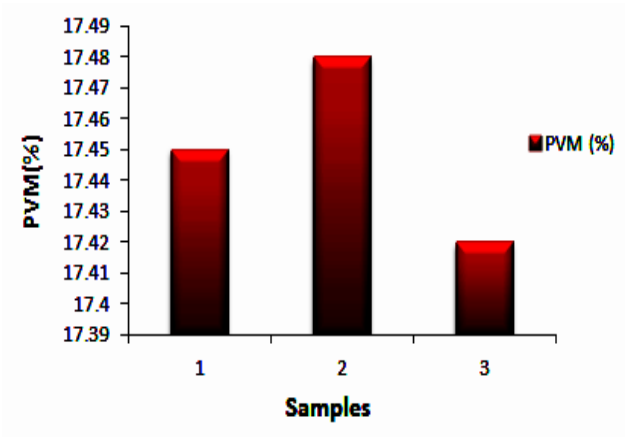

Fig. 3. Percentage Volatile Matter (PVM) for Palm Fruit Shell Briquettes

Table 2 and Figure 3 showed the results of the average percentage volatile matter (PVM) for the palm shell briquette produced being 17.45%. High volatile matter indicates easy ignition, rapid burning, and proportional elongation of flame length, but low calorific values [12]. The briquette produced

from palm fruit shell has a percentage volatile matter between 10% and 25% for good quality briquettes, as reported by [12].

Table 3. Percentage Ash Content (PAC) for Palm Fruit Shell Briquettes

Sample	PAC (%)
1	6.58
2	6.98
3	6.47

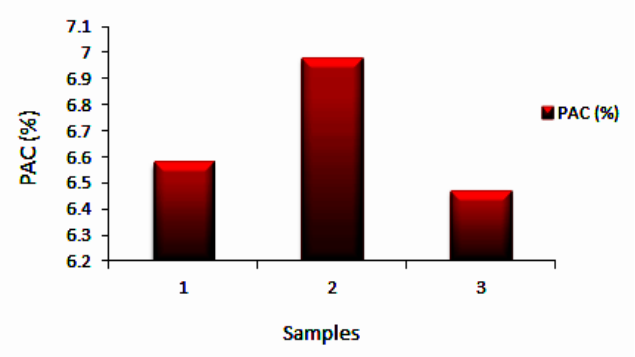

Fig. 4. Percentage Ash Content (PAC) for Palm Fruit Shell Briquettes

In Table 3 and Figure 4, we have presented the results of the average percentage ash content of the palm fruit shell briquettes produced as 6.68%. Reference [10] reported that low ash content indicates higher calorific values for briquettes, but high ash content leads to high dust emissions affecting combustion volume and briquette efficiency. Reference [13] noted that high ash content resulted in a lower calorific value and vice versa, as it minimizes the heat transfer to the internal parts of the fuel and the diffusion of oxygen on the brick surface during coal burning, which affects the burning rate.

Table 4. Percentage Fixed Carbon (PFC) for Palm Fruit Shell Briquettes

Sample	PFC (%)
1	68.32
2	68.02
3	68.51

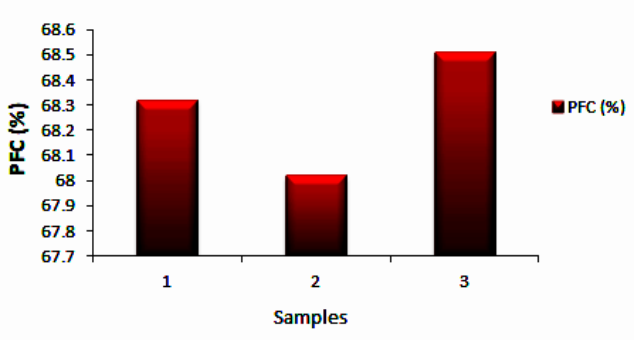

Fig. 5. Percentage Fixed Carbon (PFC) for Palm Fruit Shell Briquettes

Table 4 and Figure 5 showed that the average percentage of fixed carbon for the palm fruit shell briquettes produced was 68.28%. These results compared to the result of Pallavi et al. [11] reporting the suitability of solid carbon briquettes at 80.5% for domestic applications shows a good agreement. Reference [14] reported that the higher the fixed carbon content of a fuel, the higher the calorific value, the lower the volatile matter, the lower the ash and moisture content and the better the fuel quality.

Table 5. Calorific Values (CV) for Palm Fruit Shell Briquettes

Sample	CV (kcal/kg)
1	9,710.53
2	9,721.12
3	9,721.56

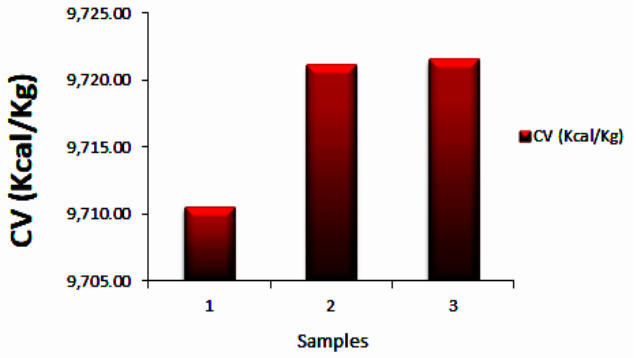

Fig. 6. Calorific Values (CV) for Palm Fruit Shell Briquettes

Calorific value is the amount of thermal energy present in a material. In Table 5 and Figure 6 we presented the average calorific value for the palm fruit briquette produced as 9717.74kcal/kg. Reference [1] in their work obtained caloric values ranging from 4586.72kcal/kg to 4827.20kcal/kg and reference [3] in their work obtained caloric values ranging from 33116kcal/kg to 23991kcal/kg when compared to the results obtained from this work showed that the briquettes samples produced have good combustion properties that are good enough for domestic use and small-scale industrial applications.

4. Conclusions

Fossil fuels, gases and wood fuels are the main source of energy for such household activities. Excessive use of these fuels can lead to problems such as global warming, air pollution and deforestation. It is high time to transform agricultural, sawmill and municipal waste into useful briquettes which will be good substitutes for these fuels. This work focused on estimating the calorific values of palm husk briquettes to determine their suitability for domestic and small-industrial application. The results obtained indicate that the briquettes obtained from the shell of palm fruits have high combustion properties sufficient for domestic use and for small-scale industrial applications.

References

[1]. Y.I. Ogwu, T.E. Tembe, and A.S. Shomkegh, "Comparative Analysis of Calorific Value of Briquettes Produced from Sawdust Particles of Daniella oliveriand Afzelia africana Combination at Binary and Tertiary Levels with Rice Husk", Journal of Research in Forestry, Wildlife and Environmental, vol. 6, no 2, pp.13 – 21, 2014.

[2]. G. Agidi, N.A. Efomah, and A.S. Alake, "Assessment of the Performance of a Disc Actuated Briquette Production Machine Developed at the National Cereals Research Institute, Badeggi", Global Journal of Engineering Science and Research Management, Gbabo., vol. 2, no. 7, 2015

[3]. A.E. Emerhi, "Physical and combustion properties of briquettes produced from sawdust of three hardwood species and different organic binders", Advances in Applied Science Research, vol.2, pp.236-246, 2011.

[4]. O.J. Olawale, A. B. Hassan, M. Abubakar, and I.J. Barakat, "Effect of Starch and Gum Arabic Binders in the Combustion Characteristics of Briquette Prepared from Sawdust", International Journal of Scientific & Engineering Research, vol. 5, no. 3, 2014

[5]. U.T. Onuegbu, M.I. Ogbu, and C. Ejikeme, "Comparative analyses of densities and calorific values of wood and briquettes samples prepared at moderate pressure and ambient temperature" Int. J. Plant Anim. Environ. Serv., vol. 2, pp. 40–45, 2011.

[6]. A.O. Sotannde, O.A. Oluyege, and B.G Abah, "Physical and Combustion Properties of Briquettes from Sawdust of Azadirachta indica", Journal of Forestry Research, vol. 21, no. 1, pp.63 – 67, 2010

[7]. F.J. Martin, A.M.R. Pineda, A.J. Manaay, A.R.S. Handa, and A.B. Ocreto, "Design and Development of Charcoal Briquetting Machine", USM R & D, vol. 16, no. 2, pp.85 – 90, 2008.

[8]. F. Inegbedion, and T.I. Francis-Akilaki, "Design and Fabrication of a Briquetting Machine", Journal of Energy Technology and Environment, vol. 4, no. 1, pp. 11 – 20, 2022.

[9]. J. Akowuah, F. Kemausuor, and S.J. Mitchual, "Physiochemical characteristics and market potential of sawdust charcoal briquettes", International Journal of Energy and Environmental Engineering, vol. 3, no. 20, pp.1−6, 2012.

[10]. F.O. Obi, O.C. Akubuo and I.W. Okonkwo, "Development of an Appropriate Briquetting Machine for Use in Rural Communities", International Journal of Engineering and Advanced Technology, vol. 2, no. 4, pp.578-582, 2013.

[11]. V.H. Pallavi, S. Srikantaswamy, M.B. Kiran, R.D. Vyshnavi, and A.C. Ashwin, "Briquetting Agricultural Waste as an Energy Source", Journal of Environmental Science, Computer Science and Engineering & Technology, vol. 2, no. 1, pp.160-172, 2013.

[12]. A.O. Akintaroa, A.I. Musab, J.A. Ajobo, and T.F. Oyewusi, "The Potentials of Using Carbonized Corncob to Produced Briquettes as an Alternative to Fuel wood". FUTA Journal of Research in Sciences, vol. 13, no. 1, pp.137-145, 2017

[13]. J.O. Chaney, "Combustion Characteristics of Biomass Briquettes", Fuel Processing Technology, vol. 30, no. 2, pp.219-230, 2010.

[14]. A.D. DahamShyamalee, U.S. Amarasinghe, and N.S. Senanayaka, "Evaluation of different binding materials in forming biomass briquettes with sawdust", International Journal of Scientific and Research Publications, vol. 5, no. 3, 2015.

Finite Element Analysis for the Static Response of Functionally Graded Porous Sandwich Beams

Sura Kareem Abbas Al-Itbi*‡, Ahmad Reshad Noori*

*Department of Civil Engineering, Istanbul Gelisim University. Istanbul, Türkiye

(surak985@gmail.com; arnoori@gelisim.edu.tr)

‡ Corresponding Author; Istanbul Gelisim University. Istanbul, Türkiye
Tel: +90 212 422 70 00 206, surak985@gmail.com

Received: 13.08.2022 Accepted: 24.08.2022

Abstract- In this paper, the finite element method is used to analyze the static response of the functionally graded porous (FGP) sandwich beams subjected to uniformly distributed loads along the beam span. The core of the beam is made up of functionally graded porous material while the top and bottom layers are made up of isotropic homogenous materials. Uniform distribution and symmetric distribution of pores are used as two different types of porous material. Shear deformation is considered in the analysis by utilizing BEAM189 in ANSYS which is a finite element package program. This element is based on the first-order shear deformation theory. The influence of porosity coefficient, boundary conditions, and type of the porous material on the static response of the considered structures is presented in detail. The results demonstrate that the porosity coefficient has an important impact on the static response of the FGP sandwich beams.

Keywords Static analysis, Finite element method, FGM, Porous materials, Sandwich beam

1. Introduction

Engineering designers are aimed to provide superior structure performance regards various aspects. The structure needs to withstand applied loads in addition to other requirements that need to be met. Users and designer requirements are continuously developed to the level that conventional materials cannot give acceptable performance. Damping, strength, stiffness, thermal isolation, lightweight, environmental needs, vibration characteristics, and many more properties that may not be met with separate materials. For this reason, functionally graded materials (FGMs) should be preferred. Although fabrication technology of FGMs is in its beginning, they provide various benefits such as high stiffness, lightweight, and thermal isolation.

Sandwich beams and plates that were found in the 1980s showed acceptable performance, durability, and multi-objective structures. These structures can be used in civil, mechanical, aerospace, manufacturing, automobiles, and many more fields. VARTM technology is applied to manufacture sandwich structural elements like sandwich beams or plates [1]. The sandwich beam is considered from cellular materials that its properties can be modified according to its usage [2].

The sandwich beams have a variety of characterizations. Strong, durable, thin load member, stiffness, and strength over weight ratios for sandwich beam are very high. The solid metal faces give an acceptable stiffness. Where the core may be used as graded porous in different patterns. The core materials can be bone, coral, ceramic, polymer, wood, and many more. The core porosity can be formed based on the required final performance. The increase of the porosity may reduce the overstrength, but it will provide superior characteristics in other aspects [3]. A review paper can provide more knowledge about functionally graded sandwich beams like in [4-6]. Higher-order shear deformation theory [7], Euler-Bernoulli beam theory [8], quasi-3D theory [9], and first-order shear deformation theory [10] can be applied in the case of structural elements analysis for various types of structures. In functionally graded beams, an analysis was implemented by [11] with the aid of the Ritz method on the basis of Timoshenko revealed that material selection and modulus of Elasticity have a major role in beam behavior related to stress distribution and displacement. The research was performed by [12] on some basic sandwich beam concepts for their fitness of application to uni-dimensional functionally graded sandwich beams. A perfect convention is found between finite element analysis and higher-order theory. A finite element model was developed by [13] to analyze stress distribution for functionally graded sandwich beams across the cross-section thickness. The model was validated using numerical methods results.

The quasi-3D theory was used by [14] to present the static behavior of functionally graded sandwich beams, which includes both thickness stretching and shear deformation effects. In [15], it is carried out that functionally graded sandwich beams with less length to height (L/h) ratio than five can be simulated, and solved using symmetric smoothed particle hydrodynamics method combined with applying of quasi-3D theory. Damping properties of sandwich cantilever beams were investigated by [16] where they mentioned that viscoelastic core thickness has a great effect in reducing the damping factor. Wang et al [17] utilized shock tube experiments to represent the dynamic behavior of sandwich panels. Model analysis for functionally graded beams was built by [18] depending on shear deformation from first order regarding static bending behavior under different boundary conditions. The model verification process of [18] was successfully determined for accuracy and efficiency by comparison of their results with those of the available literature. They considered the slenderness ratio, the thickness of the core, and metal faces, and power low index in their research. Through the application of the repeated shear deformation theory, the static analysis of functionally graded beams was performed by [19].

The displacement aspect established on higher-order shear deformation theory is applied by [20] to study the static behavior of functionally graded metal-ceramic functionally graded material beams under surrounded temperature. By the method of complementary functions, the bending of functionally graded beams is defined by [21]. Depending on the theory of Bernoulli, and Timoshenko the equations governing the bending response of sandwich beams were obtained by [22]. Furthermore, the method of complementary functions is applied in order to solve the obtained equations numerically. Also, they studied the effects of (L/h) ratios, different boundary conditions, layer ratios, and material difference coefficients on the bending response of the beams. In [23] it is carried out that functionally graded core sandwich beam which is loaded by the transverse load can be analyzed using elasticity solution. Core properties variation was not affected by normal stress which varies linearly with cross-section thickness. Results of [24] show that the sandwich beam behavior is dependent on the power-law index, porosity, and FG porous metal core thicknesses. Under different types of distributed loads, linear and nonlinear flexural analyzes of sandwich beams in which the core was functionally graded have been performed by [25].

The literature survey shows that the bending response of functionally graded porous sandwich beams has not been investigated by using the BEAM189 element via ANSYS [26] yet. This paper aims to examine the static response of FGP sandwich beams with the aid of the finite element method. The sandwich beams are assumed to have isotropic homogenous face sheets and an FGP core. Results are obtained and compared for various values of porosity coefficients and clamped - clamped, clamped - pinned, clamped - free, and pinned - pinned boundary conditions. The influence of the porosity coefficients on maximum vertical displacement and stress values is presented. The effect of shear deformation is taken into account in the analysis procedure. The uniform porosity and symmetric porosity are used as two different types of FGP materials.

To present this research paper in a better way, it is organized as follows: Section 2 shows the functions of FGP materials and gives information about the finite element type used in the analysis. Section 3 presents the numerical results and discussion. and Section 4 gives the most important conclusion of this paper.

2. Materials and Method

The functionally graded porous (FGP) sandwich beam

shown in figure 1 with length L, thickness h, and width b is considered. In this paper, it is assumed that the sandwich beam is consist of three layers with different thicknesses. The top and bottom layers of the beam are isotropic homogenous and the core layer is FGP. Two different types of porosity distributions are used.

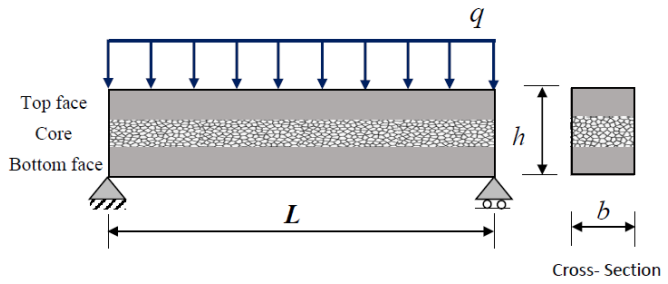

(a) FGP sandwich beam with uniform porosity distribution

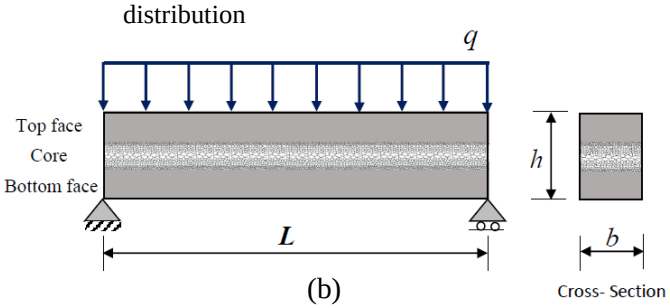

(b)

(b) FGP sandwich beam with symmetric porosity distribution

Fig. 1: Simply supported FGP sandwich beam with different porosity distributions

These types are symmetric and uniform porosity distributions. The Poisson's ratio is taken as constant. The symmetric FG porosity can be described by Eq. 1 and the uniform FG porosity can be expressed by Eq. 2 [27].

$$E\,(z) = E_1\left[1-e_0 cos\left(\frac{\pi z}{h_c}\right)\right] \quad (1)$$

$$E\,(z) = E_1[1-e_0\varphi] \quad (2)$$

where h_c is the core thickness and the value of φ can be calculated as follows:

$$\varphi = \frac{1}{e_o} - \frac{1}{e_o}\left(\frac{2}{\pi}\sqrt{1-e_o} - \frac{2}{\pi} + 1\right)^2 \quad (3)$$

In these equations e_o is the porosity coefficient, h is the thickness of the cross-section, E_1 is the maximum value for the modulus of elasticity. The distribution of the elasticity material along the cross-section of the beam is given as follows:

$$\begin{aligned} E &= E_1 && -\frac{h}{2} \le z \le -\frac{7h}{18} \\ E &= E(z) && -\frac{7h}{18} \le z \le +\frac{7h}{18} \\ E &= E_1 && +\frac{7h}{18} \le z \le +\frac{h}{2} \end{aligned} \quad (4)$$

In the finite element solution of the problem in the hand with ANSYS, the BEAM189 element is used. This element is a quadratic element that has three nodes. There are six degrees of freedom at each node of this element. The shear deformation is considered in this element based on the first-order shear deformation theory. For more detailed information about the assumptions and restrictions of this element see [28].

To define the functionally graded materials for the FGP sandwich beam the modulus of elasticity is calculated and entered into the ANSYS model. The section of the beam is divided into 36 layers (Figure 2) along the thickness direction, similar to [29]. To obtain detailed values of stress along the length of the beam, it is divided into 100 finite elements in the longitudinal direction. The boundary conditions are given in Table 1. The load is implemented in the z-direction.

Table 1: Boundary conditions

Type of the support	Boundary conditions	
	i	j
Fixed – Fixed (F-F)	Rotz = Roty = Rotx= Uz = Uy = Ux = 0	Rotz = Roty = Rotx= Uz = Uy = Ux = 0
Fixed – Pinned (F-P)	Rotz = Roty = Rotx= Uz = Uy = Ux = 0	Uz = Ux = Uy = 0
Pinned – Pinned (P-P)	Uz = Ux = Uy = 0	Uz = Ux = Uy = 0
Fixed – Free (F-FR)	Rotz = Roty = Rotx= Uz = Uy = Ux = 0	-----

Fig. 2: The finite element model of an FGP sandwich beam

3. Numerical results and discussion

The analyzed beam dimensions are (3 × 0.5 × 0.5) m as length, width, and height respectively. The beam is a functionally graded sandwich beam by thickness direction with a varied elasticity value. The implemented load is 10 N/m as a uniformly distributed load. It is worth to be mentioned that there is no specific reason for choosing these loads. It is considered only to investigate the effect of porosity on the static response of the FGP beams.The outer faces are made up of steel material, and the core is FGP material. Two main groups used are symmetric material constitutive relationships (SMCR) FG beam and uniform porosity distribution FG beam. For each one of these two FGP material groups, forty-four different models were generated and analyzed using the finite element procedure.

To outline the effect of porosity on the static response of the considered structure, results are obtained for several values of porosity coefficients and boundary conditions. The material properties are assumed to be E_1= 210 GPa and ν = 0.3. The maximum displacement values are obtained and presented in Tables (2 -3).

Table 2: Maximum transverse displacement values for FGP sandwich beam with symmetric distribution (m)

e_o	F-F	F-FR	P-F	P-P
0.10	2.81E-09	1.02E-07	5.14E-09	1.10E-08
0.20	2.90E-09	1.04E-07	5.28E-09	1.13E-08
0.25	2.96E-09	1.04E-07	5.35E-09	1.14E-08
0.30	3.01E-09	1.05E-07	5.44E-09	1.15E-08
0.40	3.14E-09	1.07E-07	5.61E-09	1.18E-08
0.50	3.30E-09	1.10E-07	5.83E-09	1.21E-08
0.60	3.50E-09	1.12E-07	6.09E-09	1.24E-08
0.70	3.78E-09	1.15E-07	6.45E-09	1.28E-08
0.75	3.97E-09	1.16E-07	6.69E-09	1.31E-08
0.80	4.23E-09	1.18E-07	7.01E-09	1.35E-08
0.90	5.23E-09	1.24E-07	8.19E-09	1.46E-08

Table 3: Maximum transverse displacement values for FGP sandwich beam with uniform distribution (m)

e_o	F-F	F-FR	P-F	P-P
0.10	2.83E-09	1.03E-07	5.20E-09	1.12E-08
0.20	2.95E-09	1.07E-07	5.40E-09	1.16E-08
0.25	3.02E-09	1.09E-07	5.51E-09	1.18E-08
0.30	3.08E-09	1.11E-07	5.62E-09	1.20E-08
0.40	3.24E-09	1.15E-07	5.88E-09	1.25E-08
0.50	3.42E-09	1.20E-07	6.17E-09	1.31E-08
0.60	3.64E-09	1.25E-07	6.52E-09	1.37E-08
0.70	3.92E-09	1.32E-07	6.96E-09	1.45E-08
0.75	4.10E-09	1.35E-07	7.23E-09	1.49E-08
0.80	4.31E-09	1.40E-07	7.55E-09	1.55E-08
0.90	4.94E-09	1.51E-07	8.46E-09	1.69E-08

It can be seen in Table (2-3) that the material porosity coefficient has a significant influence on the maximum displacement of FGP sandwich beams. The minimum displacement occurs in fixed-fixed support with a porosity coefficient of 0.1 while the maximum displacement occurs in the cantilever beam with a porosity coefficient of 0.9.

To better interpret the given results in Tables (2-3) the graphical form of the results is illustrated in Figures (3- 10).

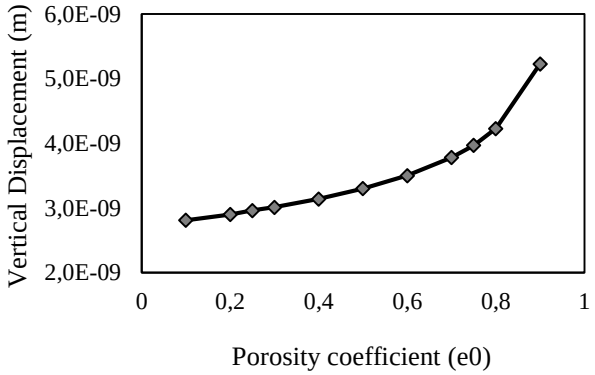

Fig. 3: Porosity – deflection curve for fixed – fixed FGP sandwich beam with symmetric distribution

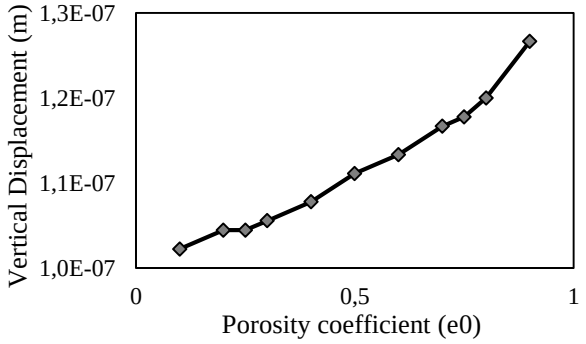

Fig. 4: Porosity – deflection curve for fixed – free FGP sandwich beam with symmetric distribution

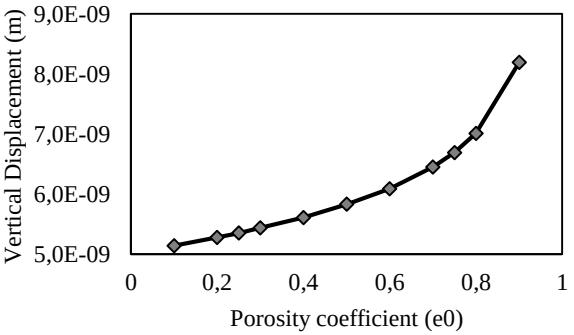

Fig. 5: Porosity – deflection curve for fixed – pinned FGP sandwich beam with symmetric distribution

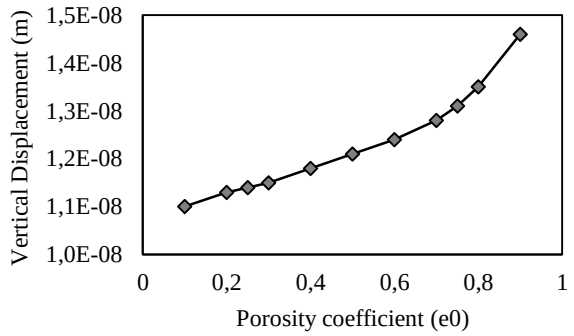

Fig. 6: Porosity – deflection curve for pinned – pinned FGP sandwich beam with symmetric distribution

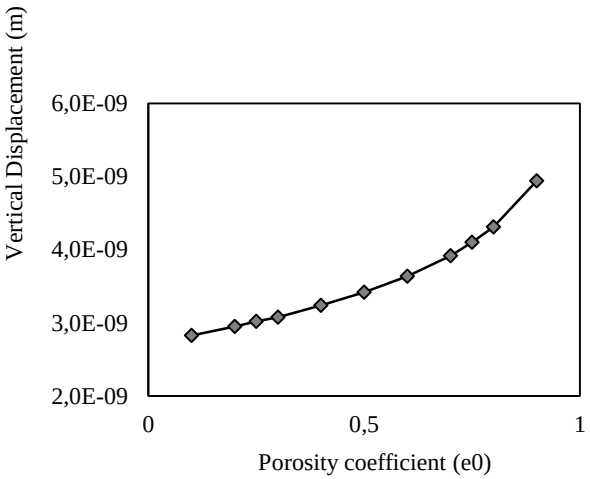

Fig. 7: Porosity – deflection curve for fixed – fixed FGP sandwich beam with uniform distribution

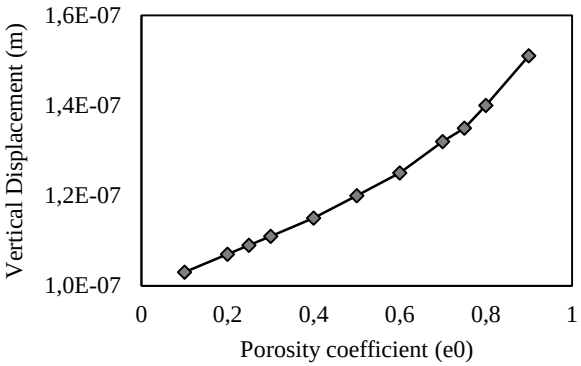

Fig. 8: Porosity – deflection curve for fixed – free FGP sandwich beam with uniform distribution

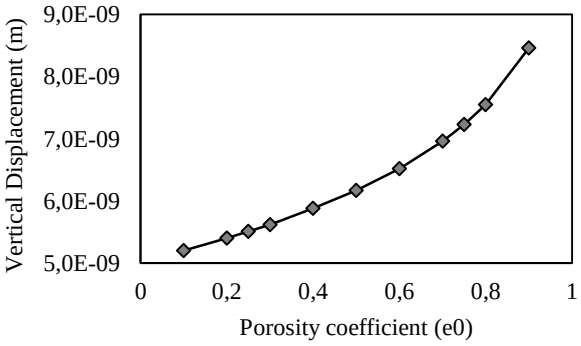

Fig. 9: Porosity – deflection curve for fixed – pinned FGP sandwich beam with uniform distribution

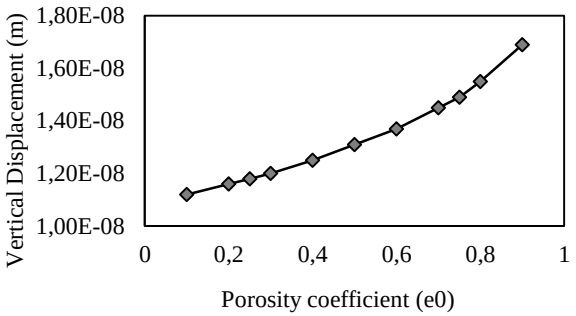

Fig. 10: Porosity – deflection curve for pinned – pinned FGP sandwich beam with uniform distribution

As can be clearly observed in Figures (3-10) the results reveal a positive correlation between porosity and deflection. In other words when the porosity coefficient increase higher deflection will be recorded. From the results gained we can arrange the beam from lower to higher deflection based on the beam supports comparison: fixed – fixed, fixed – pinned, pinned – pinned, and lastly fixed – free.

The diagrams for the vertical displacement and rotations along the axis of the beam are obtained for all cases discussed above. But only the vertical displacement (Uz) is illustrated in this section for fixed–fixed FGP sandwich beam with symmetry distribution (Figure 11). The material porosity coefficient is considered to be 0.5. The dashed line shows the undeformed shape.

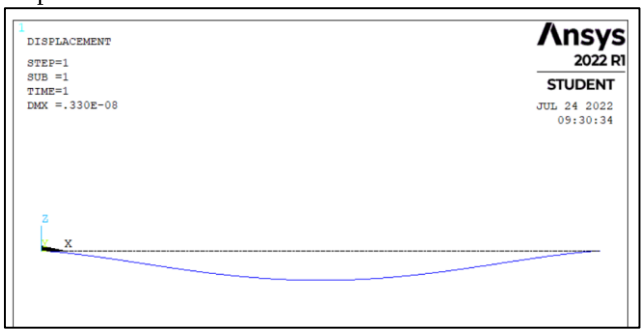

Fig. 11: Deformed shape of fixed – fixed FGP sandwich beam with symmetric distribution (e0=0.5)

The von Mises stress values are obtained for several cases and presented in Figures (12-16).

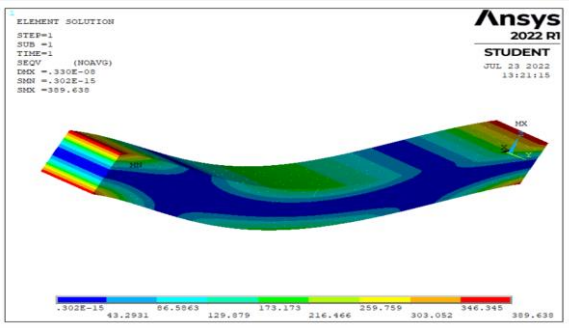

Fig. 12: The von Mises stress distribution for fixed – fixed FGP sandwich beam with symmetric distribution (e0=0.5)

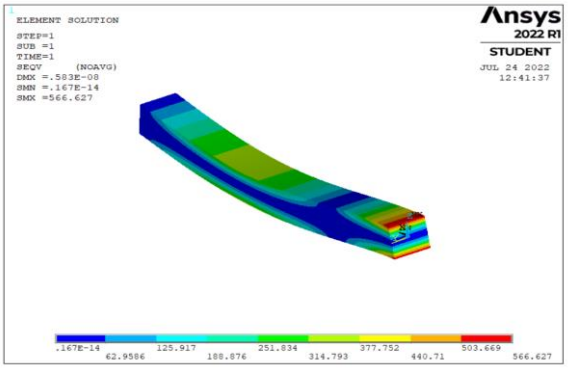

Fig. 13: The von Mises stress distribution for fixed – pinned FGP sandwich beam with symmetric distribution (e0=0.5)

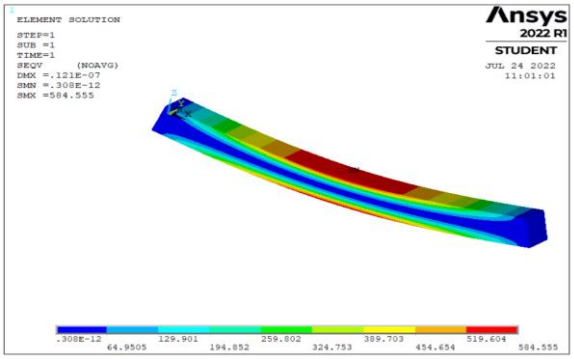

Fig. 14: The von Mises stress distribution for pinned-pinned FGP sandwich beam with symmetric distribution (e0=0.5)

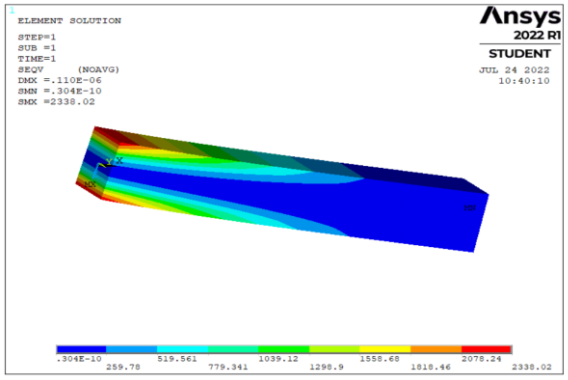

Fig. 15: The von Mises stress distribution for fixed – free FGP sandwich beam with symmetric distribution (e0=0.5)

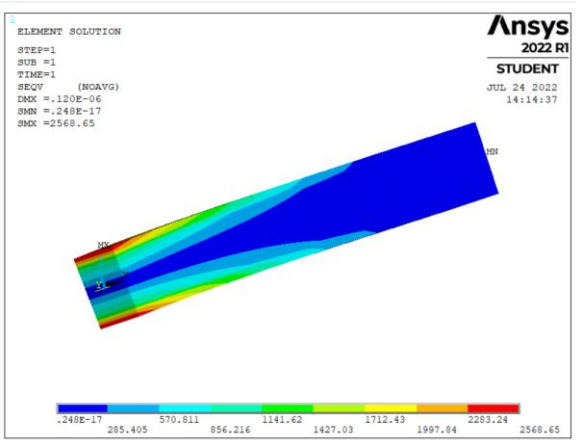

Fig. 16: The von Mises stress distribution for fixed – free FGP sandwich beam with uniform distribution (e0=0.5)

In Figures (12-15) it can be clearly seen that type of the support has a significant influence on the von Mises stress values of FGP sandwich beams. The maximum von Mises stress values for fixed–fixed, fixed–pinned, pinned–pinned, and fixed–free FGP sandwich beams with symmetric distribution (e0 = 0.5) are 389.63 Pa, 566.63 Pa, 584.56 Pa, and 2338.02 Pa. The same stress value for the cantilever FGP sandwich beam with uniform distribution (e0 = 0.5) is obtained as 2568.65 Pa (Figure 16). This indicates that the fixed–free beam has the highest von Mises stress while the fixed–fixed beam has the lowest. When symmetric and uniform porosity distributions are compared it can be carried out that for e0 = 0.5 porosity coefficients the stress values are greater in the uniform porosity distribution of FGP sandwich beams.

4. Conclusions

In this study, the impacts of porosity coefficient on the static response of FGP sandwich beams are investigated by the method of finite element. The results are obtained for several boundary conditions and material indices. Two types of porosity distribution, symmetric and uniform, are considered in the research. The analysis is done based on the Timoshenko Beam Theory.

Porosity is to decrease the weight of sandwich beams, but it also decreases the strength. The results showed that the values of the maximum displacement are directly proportional to porosity coefficients. Increasing the value of the porosity coefficient increases the values of displacements. The comparison between the symmetric and uniform distribution of the FGP materials indicates that the transverse displacement is greater when the uniform distribution is used for the values of e_0 less than 0.9. But for 0.9 it is vice versa. As one of the main results of this paper, it can be concluded that variations in von-Mises stresses depend on the boundary conditions and on the types of porous distribution and porosity coefficient at the core of the sandwich beams.

5. References

[1] M.A. Dweib, B.Hu, A.O'Donnell, H.W.Shenton and R.P.Woo, "All natural composite sandwich beams for structural applications". *Composite structures*, *63*(2), pp. 147-157, 2004.

[2] L. J. Gibson and M.F. Ashby. *Cellular solids: structure and properties*. United Kingdom: Cambridge Univrsity Press, 1999.

[3] T. George, V. S. Deshpande and H. N.G. Wadley, "Mechanical response of carbon fiber composite sandwich panels with pyramidal truss cores." *Composites Part A: Applied Science and Manufacturing* 47, pp. 31-40, 2013.

[4] A. S. Sayyad and Y. M. Ghugal,"Modeling and analysis of functionally graded sandwich beams: A review." *Mechanics of Advanced Materials and Structures* 26.2, pp. 1776-1795, 2019.

[5] E. K. Njim, M. Al-Waily and S. H. Bakhy,"A review of the recent research on the experimental tests of functionally graded sandwich panels." *Journal of Mechanical Engineering Research and Developments* 44.3, pp. 420-441, 2021.

[6] H. Wu, J. Yang and S. Kitipornchai, "Mechanical analysis of functionally graded porous structures: A review." *International Journal of Structural Stability and Dynamics* 20.13 2020.

[7] T.Nguyen, T. T. Nguyen, T. P. Vo and H. Thai, "Vibration and buckling analysis of functionally graded sandwich beams by a new higher-order shear deformation theory." *Compos. Part B Eng.* 76, pp. 273–285, 2015.

[8] B.V. Sankar, "An elasticity solution for functionally graded beams." *Compos. Sci.Technol.* 61, pp. 689–696, 2001.

[9] T. P. Vo, H. Thai, T. Nguyen, F. Inam and J. Lee, "Static behaviour of functionally graded sandwich beams using a quasi-3D theory,." *Compos. Part B Eng.* 68, pp. 59–74, 2015.

[10] H. Thai and D. Choi, "A simple first-order shear deformation theory for the bending and free vibration analysis of functionally graded plates." *Compos. Struct.* 66.101, pp. 332–340, 2013.

[11] M. Şimşek, "Static analysis of a functionally graded beam under a uniformly distributed load by Ritz method." *International Journal of Engineering and Applied Sciences (IJEAS)* 1.3, pp. 1-11, 2009.

[12] N. A. Apetre, B. V. Sankar and D. R. Ambur, "Analytical Modeling of Sandwich Beams with Functionally Graded Core." *Journal of Sandwich Structures and Materials* 10.1, pp. 53-74, 2008.

[13] S. Das and S. K. Sarangi, "Static analysis of functionally graded composite beams." *IOP Conference Series: Materials Science and Engineering*. Bangalore, 2016.

[14] T. P. Vo, H. Thai, T. Nguyen, F. Inam, J. Lee. "Static behaviour of functionally graded sandwich beams using a quasi-3D theory,." *Compos. Part B Eng.* 68, pp. 59–74, 2015.

[15] A. Karamanlı, "Bending behaviour of two directional functionally graded sandwich beams by using a quasi-3d shear deformation theory." *Composite Structures* 174, pp. 70-86, 2017.

[16] J. H. Yim, S. Y. Cho,Y. J. Seo, B. Z. Jang, "A study on material damping of $0°$ laminated composite sandwich cantilever beams with a viscoelastic layer." *Composite Structures* 60.4, pp. 367–374, 2003.

[17] E. Wang, N. Gardner and A. Shukla, "The blast resistance of sandwich composites with stepwise graded cores." *International Journal of Solids and Structures* 46, pp. 3492–3502, 2009.

[18] P. V. Van, "Static bending analysis of functionally graded sandwich beams using a novel mixed beam element based on first-order shear deformation theory." *Forces in Mechanics* 4 2021.

[19] T. P. Vo, H. Thai, T. Nguyen, F. Inam and J. Lee, "Static behaviour of functionally graded sandwich beams using a quasi-3D theory,." *Compos. Part B Eng.* 68, pp. 59–74, 2015.

[20] R. Kadoli, K. Akhtar and N. Ganesan, "Static analysis of functionally graded beams using higher order shear deformation theory." *Applied mathematical modelling* 32.12, pp. 2509-2525, 2008.

[21] A.R. Noori, T. A. Aslan and B. Temel, "Static analysis of FG beams via complementary functions method." *European Mechanical Science* 4.1, pp. 1-6, 2020.

[22] A.R. Noori, H. Rasooli, T. A. Aslan and B. Temel, "Fonksiyonel Derecelenmiş Sandviç Kirişlerin Tamamlayıcı Fonksiyonlar Yöntemi ile Statik Analizi." *Çukurova Üniversitesi Mühendislik-Mimarlık Fakültesi* 35.4, pp. 1091-1102, 2020.

[23] B. Srikarun, W. Songsuwan and N. Wattanasakulpong, "Analysis of sandwich beams with functionally graded core." *19th AIAA Applied Aerodynamics Conference*. Anaheim,Canada,U.S.A, 2001

[24] E. K. Njim, M. Al-Waily and S. H. Bakhy, "Experimental and Numerical Flexural Properties of Sandwich Structure with Functionally Graded Porous Materials." *Engineering and Technology Journal* 40.1, pp. 137-147, 2022.

[25] B. Srikarun, W. Songsuwan and N. Wattanasakulpong, "Linear and nonlinear static bending of sandwich beams with functionally graded porous core under different distributed loads." *Composite Structures* 276, 114538, 2021

[26] ANSYS, Inc Release 15.0, Canonsburg, PA, 2013.

[27] N. Wattanasakulpong and S Eiadtrong, “Transient responses of sandwich plates with a functionally graded porous core: Jacobi-Ritz method.” *International Journal of Structural Stability and Dynamics*,2022, https://doi.org/10.1142/S0219455423500396.

[28] Mechanical APDL Element Reference, 2013, Inc., 275 Technology Drive, Canonsburg, PA 15317

[29] A.R. Noori, T. A. Aslan and B. Temel, "Dynamic analysis of functionally graded porous beams using complementary functions method in the Laplace domain." *Composite Structures* 256, 113094, 2021.

A Mathematical Model to Evaluate the Impact of Yoga Poses on Body

Sajedeh Norozpour*‡

*Department of Civil Engineering, Istanbul Gelişim University. Istanbul, Türkiye

(snorozpour@gelisim.edu.tr)

‡ Corresponding Author; Istanbul Gelisim University. Istanbul, Türkiye
Tel: +90 212 422 70 00 206, snorozpour@gelisim.edu.tr

Received: 27.07.2022 Accepted: 19.08.2022

Abstract- Daily Yoga activities are part of a ten-posture series with linked relaxation and aerobic exercise, resulting in a balancing of flexibility and extensions. Because this series is often repeated and advocated by several yoga professionals, structural modeling to justify its purported health advantages is needed. Older is recommended to do more workouts to maintain activity, given the increasing pressures in societal, economical, and health issues as a result of the elderly society. They are, regrettably, unable to do so due to a variety of physical and psychological obstacles. The whole body form changes significantly as people get older, and sag. One of the most important variables in regaining their drive and comfort throughout social activities might be the layout of their apparel. The impact of athletics on older is investigated in this study. Depending on rigid body movements and free-body diagrams, a numerical model is built for each position in the yoga exercises. The idea of static equilibrium is used to calculate the forces and moments that different joints experience. The model given in this study was developed under a variety of assumptions. But what is discovered in practice is that the knees carry the maximum joint action while the ankle and wrist are discovered to play a major part in transferring the ground response forces throughout yoga. Thus, it would imply that the model is a good tool for forecasting the forces and durations that happen not just during the yoga positions but also during other situations.

Keywords: Digitalization, Linear Regression, Mathematical Approach, IT, ICT.

1. Introduction

Most elements, when mixed properly and in the correct proportions, produce an alloy with unique qualities. The best ensembles feature a well-balanced mix of components. Similarly, comprises a precise sequence of yoga positions executed while breathing in perfect balance. This series is made up of ten energetic positions that are executed in a single, mindful, and beautiful movement as (Figure 1) [1, 2]. The movements cleverly contrast forward-bending movements with backward-bending positions. The sequencing of all these positions is said to assure that 'energy' hits all areas of the body, whilst the sunrays cover all regions of the world. The older population is among the most widespread global phenomenon, posing significant social, financial, and healthcare issues. Seniors are motivated to become more active and fit to address the problems posed by the aging workforce. Yoga is one of the most prominent and age-friendly low-intensity physical exercises for elderly ladies since it has no age restrictions.

Fig. 1: Yoga Poses

Yoga is well-known for its diverse positions and distinct levels of difficulty for learners of various physical abilities. Yoga can help with not only body activities like muscular endurance, bodily balance, and metabolism system, but also psychological processes like stress, late-life depression, and nervousness. Regular exercise is well proven as being important for older persons and it can be used as a strategy for improving late-life quality and achieving effective aging. Although seniors have more free time after retirement, the quantity and levels of physical activity participation tend to [3] decline as they et older.

1. Literature Review

The reasons for passive activity in older adults can be divided into two categories: one is the elderly's failure to trust in their ability to exercise; another is their decreasing health state. Seniors perceive themselves as a population at danger of damage throughout exercise, and they tend to exaggerate the risks associated with physical activities. Those are commonly regarded as impediments to elderly persons participating in physical activity. Some exercising psychological studies have discovered a range of psychological concepts and theories that describe older individuals' workout activities, including what encourages them to begin regular exercise and how to keep it up. A study examined the realm of health-related actions impacted by social and cognitive elements using the Information-Behavioral Skills (IMB) theories [4]. Knowledge, intention, and cognitive abilities are the primary elements of beginning activities, according to his approach. The most persuasive hypothesis, social cognitive theory (SCT), is frequently used to describe and anticipate the workout behaviors of the elderly. Self-efficacy, motives, aspirations, surroundings or social influences, and result expectations are the basic mental factors that make up that theory [5].

In other aspects, it is understandable that people may be driven to begin and sustain exercise activities if they believe they are able of doing so. This reinforces the goal to enhance their considered efficacy for adhering to the activity. According to the study self-determination model (SDT), workout inspiration stems from physiological or mental demands that lead to an action aimed at achieving a goal. The level of engagement was determined by how the location of causality was viewed. Exercise Motivational Assessment identified several motives for starting to exercise based on the frequency of SDT in the strength and conditioning behavior area [6].

Stress reduction, pleasure, difficulty, social recognition, associations, competitiveness, health demands, poor health, avoiding, favorable health, weight maintenance, attractiveness, stamina, and dexterity are some of these motives. By these ideas, the most important thing to do to encourage individuals to do yoga is to figure out what types of motives they respond to some of the most and how to internalize external reasons. Boosting their motivation can help them start and maintain this practice [7].

Yoga, as a type of fitted facility, can enable workouts to meet their physical and psychological requirements. It's also been recognized as significant athletic apparel that plays a vital part in boosting exercising capacity, preventing exercise-induced diseases, and increasing mental stability. Furthermore, just a few studies have looked into physical development for seniors beyond the age of 55. Many people in this age group have different health beliefs, which has affected their physical and psychological requirements.

Yoga assessment study has traditionally emphasized the assessment of human body movements. A most extensively adopted technology for tracking the users' motions placed upon the human body throughout Yoga activities has been the performance capture system. There have been few studies on measuring people when they are engaged in activities. The acceleration is regulated by the supported rate and also modifying the exercise intensity, according to one finding from the dynamic measurements (yoga, walking versus running, rope skipping).

It's therefore important to describe the causes for seniors' participation in yoga workouts to keep improving their encouragement in yoga workouts through having a mental high level of satisfaction. As per prior research, senior citizens weighed the projected advantages against the cost and risk involved with participating in physical activities. The elderly on the other hand, are greatly motivated by health-related aspirations that try to keep them healthy. As a response,

research into elderly perceptions of the consequences of yoga fitness is required [8].

The next approach has been to look at how seniors participate in yoga activities and what types of yoga aspects affect their attitudes and requirements. As a result, this question has been included in the survey. Different yoga workout histories have been presumed to have various impacts on senior choices and expectations, and the evaluated variables while exercising have been also involved in the questionnaire and intended as multiple-choice questions, that can also be utilized to develop criteria specializing for seniors.

2. Design of Mathematical Modeling

Because measuring forces and moments can be difficult, mathematics techniques are commonly applied to approximate these pressures within rigid body motion. The hard body dynamics technique assumes several things about the body, like non-deformability, a stable center of gravity, and substance uniformity. We should identify facts such as bending stresses, geometry, and supportive practices to do appropriate analysis. The concept of superposition is used to calculate forces and instances that assert that "the present on any level owing to the entire stress is the arithmetic average of the instants due to different sections of the pressure." The theory of superposition is highly useful in determining the duration acting at any point on a body exposed to multiple pressures. There are ten poses in Yoga. As a result, the duration exerted on the muscles is determined by the body's arrangement in each position. As a result, the load to be addressed while computing the moments is varied. Because the body is separated into several parts that are each applied to a distinct loading, the bending moment at each location must equal the sum of the individual bending moments. When a tissue simply supports the body at its ends, it performs the function of load transmission and no time is formed. However, if there is an overhanging over the joints that support the body, the weight of the body will cause a small quantity of action [9, 10].

Knowing free body models are required for evaluating the elements that determine normal and prosthetic joint strength. A free-body chart is used to illustrate all of the forces applied graphically operating on a joint. The wrists, elbows, shoulders, hips, knees, and ankle joints were all taken into consideration. The body can be separated into 4 major divisions for the assessment of such 6 joints: head, arms, trunk, and legs (Table 1). The idea of equilibrium is crucial for comprehending and estimating the forces and times that occur throughout specific Yoga poses. The joint reactive forces and times for various situations can be calculated by using the equation of plane equilibrium state.

Table 1: The proportional weight and size of the human body segments

Segment	Relative weight	Relative length
Head	0.07	0.121
Arm	0.0311*2	0.241
Trunk	0.314	0.127
Leg	0.1114*2	0.423

To evaluate the weights at every segment, we have to determine the body's overall weight and length variation. It was accomplished with the help of Table.1's dispersion graph. While estimating the joint values, the following conditions are formed: The body has already been described as an array of stiff links joined by the 6 primary pivot joints that include the wrists, elbows, shoulders, hip, knee, and ankle. The hips and lower back have already been combined into one ideal joint. The human body has now been simplified as a one-dimensional system that moves in the sagittal plane. The sagittal view was chosen since the Yoga actions take place largely in this plane. The outcomes of sagittal plane kinetic assessment have produced extremely useful characteristics for evaluating normal and abnormal gait muscle processes.

3. Results and discussion

We offer a sample computation of the values at every one of the 6 joints arising from position 8 to explain the study of yoga positions (Figure 1). Figure 2 depicts the equivalent free-body graph using the data from Table 1.

Consider the following equation for the ankle joint's energy balance;

$$\sum M_A = 0 \tag{1}$$

$$\begin{aligned}(0.324W)(0.1242L) + (0.3214W)(0.3574L) \\ + (0.07W)(0.3258L) \\ + (0.052W)(0.4251L) - R\_w\,(0.568L) \\ = 0\end{aligned}$$

Here R_w (ground reaction force on wrist) $= 0.5221W$ and R_A(Ground reaction force on Ankle) $=1 - R_w = 0.4121W$.

$$A_K = Knee\ activity = R_A = (0.1235L) = (0.4212\,W)(0.3214\,L) = 0.0645\,WL \tag{2}$$

$$A_H = Hip\ activity = R_A = (0.2255L) - (0.4011\,W)(0.2201\,L) + 0.0045\,WL = 0.1541WL \tag{3}$$

$$A_E = Elbow\ activity = R_W = (0.1375L/2) = (0.4011\,W) \tag{4}$$

$$A_S = Shoulder\ activity = R_W = (0.1043L) - (0.602\,W)(0.6174\,L) + 0.214 = 0.094WL \tag{5}$$

$$A_A = Ankle\ activity = 0\,WL \tag{6}$$

$$A_w = Wrist\ activity = 0\,WL \tag{7}$$

Where W and L are the weight and length of body, respectively.

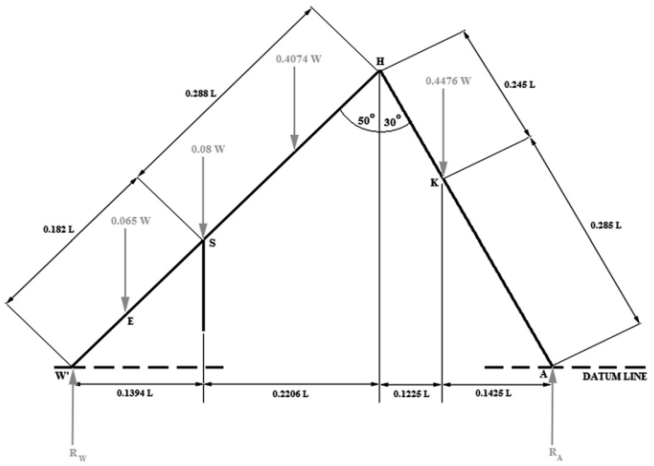

Fig. 2: Eight Postures of W0 = Wrists, E = Elbows, S = Shoulders, H = Hips, K = Knees, A = Ankles, W = Weight of Body, L = Length of Body

Because the individual is upright in posture 1, there is no action occurring on either of the joints. Caused by the weight of the body, the foot experiences a reaction effect. This position strengthens the posture musculature and improves lower back wellness. In posture 2, the person tries to lean backward as far as feasible, lengthening the back as far as potential and bending the arms well above the forehead.

The person leans forward into postures 3 and 10 and puts their hands below their feet. The position of the arm is diminished in this position, and the hip, knee, and ankle take up a large portion of the weight and motion produced by this position. The hamstrings and gluteal musculature benefit from enhanced flexibility in this position.

In position 4, the individual crosses one leg in front of another. The hip (which is shown by the highest hip motion in Table 1) and leg are attempting to expand forward in this position. The knee and ankle of the forward-moving leg endure a significant situation. This position encourages movement. The analysis of stance 4 applies to posture 9, with the exception that in the former, the driving leg now makes room for the opposite leg and moves backward.

We examine the durations on another leg that is now leading and see that the knee action increases significantly when it is exposed to the response force that was previously overtaken via the ankle in position 4.

The shoulder and ankle help the entire body in position 5, maintaining the trunk horizontal to the floor. As a consequence, the hip receives a lot of attention. The elbow is extended and the body is perpendicular to the floor in position 6.

4. Conclusion

Daily Yoga activities are part of a ten-posture series with linked relaxation and aerobic exercise, every position combatting the one before it, resulting in a balancing of flexibility and extensions. Because this series is often repeated and advocated by several yoga professionals, structural modeling to justify its purported health advantages is needed. The requirements of elderly yoga participants are investigated using the special effects data of older participants. Age-friendly design specifications for multiple elements and structures will be beneficial to the growth of yoga. Extrinsic motivation is more successful than internal motivation in the early phase, thus age-friendly will not only fulfill physical demands but also emotional needs, motivating participants to perform yoga and to start and maintain a fitness routine. Those who have exercised regularly for a prolonged period are more self-sufficient when performing yoga postures.

References

[1] Zhao, P., Ji, Z., Wen, R., Chen, Q., & Jiang, G. (2020). Biomechanical Characteristics of Lower Limbs of Yoga Posture Based on AnyBody Simulation. Journal of Medical Biomechanics, E698-E704.

[2] Bhavanani, A. B., & Ramanathan, M. (2018). Psychophysiology of yoga postures: Ancient and modern perspectives of Asanas. In Research-based perspectives on the psychophysiology of yoga (pp. 1-16). IGI Global.

[3] Kim, R. (2019). The Effects of Yoga as an Adjunct to Traditional Core Stability Exercise on Non-Specific Chronic Low Back Pain (Doctoral dissertation, Azusa Pacific University).

[4] Anuradha, P. (2020). Posture modification through Sunjeevan Yoga. GSC Advanced Research and Reviews, 5(3), 053-058..

[5] Gupta, A., & Gupta, R. K. (2021). A literature review on behavioral attributes of yoga postures and cognition. Yoga Mimamsa, 53(2), 141.

[6] Whissell, E., Wang, L., Li, P., Li, J. X., & Wei, Z. (2021). Biomechanical Characteristics on the Lower Extremity of Three Typical Yoga Manoeuvres. Applied Bionics and Biomechanics, 2021.

[7] Błażkiewicz, M. (2020). Nonlinear measures in posturography compared to linear measures based on yoga poses performance. Acta Bioeng. Biomech, 22, 15-21.

[8] Gautam, S., Kumar, U., & Dada, R. (2020). Yoga and its impact on chronic inflammatory autoimmune arthritis. Frontiers in Bioscience-Elite, 13(1), 77-116..

[9] Myers, P. S., Harrison, E. C., Rawson, K. S., Horin, A. P., Sutter, E. N., McNeely, M. E., & Earhart, G. M. (2020). Yoga improves balance and low-back pain, but not anxiety, in people with Parkinson's disease. International journal of yoga therapy, 30(1), 41-48.

[10] Panakkat, H. F., & Merrick, D. (2020). An Anatomical Illustrated Analysis of Yoga Postures Targeting the Back and Spine through Cadaveric Study of Back Musculature. International Journal of Cadaveric Studies and Anatomical Variations, 1(1), 33-38.

Parameter Optimization of Bidirectional Three-Phase DC-AC Power Inverter by an Improved Particle Swarm Optimization based Fractional Order PI Controller for the Grid Forming Operation

Mehmed Çelebi*‡, Abdullah Başçi**

* Department of Electrical and Electronics Engineering, Harran University, Şanlıurfa, Türkiye

** Department of Electrical and Electronics Engineering, Atatürk University, Erzurum, Türkiye

‡ Corresponding Author; Mehmed Çelebi, Department of Electrical and Electronics Engineering, Harran University, Şanlıurfa, Türkiye, celebim@harrane.edu.tr

Received: 11.09.2021 Accepted: 06.09.2022

Abstract- Nowadays, it is becoming more remarkable for bidirectional power conversion from battery energy sources. These structures can be used for three-phase loads and they also have a common application in Micro-grid systems. This paper is mainly focused on parameter optimization of the system by using improved particle swarm optimization (PSO) in grid forming operation of dual active bridge series resonant converter (DABSRC) topology, in term of total harmonic distortion (THD). Fractional order proportional integral (FOPI) controller is used to simulate DABSRC regarding to THD factor in this system. The results are also compared to genetic algorithm (GA) and conventional PSO. While all algorithms achieved the same optimum control parameters, a significant reduction of computation time has been reported by improved PSO in terms of THD.

Keywords: THD, Optimization, PSO, Fractional order control

1. Introduction

GA-based optimization and other optimization methods have been used extensively in inverter and DC / DC converter design. Emara et al., have compared the modified PSO algorithm with other known optimization techniques such as conventional PSO, line search and GA to find out the superior model that minimizes error of the currents for an induction machine between simulation and test system [1]. The simulation results show that the modified PSO is better than other optimization techniques in obtaining machine parameters that reduce errors occurring in the system. Kaviani et al., have presented some methods to overcome and minimize low voltage harmonics at the output of multilevel inverter by using PSO, continuous genetic algorithm (CGA) and sequential quadratic programming (SQP) [2]. The results show that PSO has better performance in terms of eliminating or minimizing harmonics in the multilevel inverter output compared to CGA and SQP. Modified species-based PSO algorithm has been used with adaptive adjustment of niche radius to apply a related problem that involves lots of switching angels [3]. To show the validity and effectiveness of the proposed technique, it was first proven in theory then successfully applied in real time to an eleven level cascaded H-bridge inverter. Shindo et al., have presented a single phase inverter design by using the PSO algorithm to perform effective switching [4]. Firstly, they have designed inverter in a simulation environment. Then, they confirmed the results of simulation via using an implementation circuit. The results show that the simulation result was consistent with the results of implementation circuit. Ganguly has proposed a PSO-based algorithm for compensation of reactive power in networks [5]. When it is optimistically apportioned, served in a desired good

case, it can excellently minimize the power loss. Mohammadi and Akhavan, have used GA and PSO methods together for selective harmonic elimination problem to obtain the base voltage constant, for DC energy in the cascaded multilevel inverters [6]. The aim of the proposed methods is to determine the matching fire switching values of the inverter. The results show that PSO is better than GA in finding the proper and desired values that are needed for the inverter to operate in healthy condition. In another study, a different and unusual optimization technique is implemented by using PSO to find switch forms of CMOS inverter [7]. The proposed new method was compared with the real coded genetic algorithm (RCGA) and classical PSO. Results show that the PSO with constriction factor and inertia weight approach (PSO-CFIWA) has significant characteristics such as finding desired inverter parameters and has satisfactory switching angles to reduce harmonics. Baskin and Caglar, have introduced a PSO-based PID controller for permanent magnet synchronous motor (PMSM). To show the effectiveness and superiority of the proposed controller, the PID controller whose parameters were obtained by using the Ziegler Nichols method is also applied to the same system and the results obtained for both controllers were compared [8]. The results show that the PSO-based PID controller is the best choice for stabilizing the speed loop of PMSM.

In this paper, an improved particle swarm optimization based FOPI controller is used to optimize the THD of bidirectional three-phase DC-AC power inverter for grid forming operation of dual active bridge series resonant converter. In addition, in order to examine the performance of the proposed PSO, genetic algorithm and conventional PSO methods are also used to find the optimum parameters of the controller and the results obtained were compared.

2. Theoretical Approach of Dabsrc

As shown in Fig. 1, the topology includes three-phase expanding circuit that means unfolder to feed AC load by DC-side that contains two dual-active bridge series-resonant converters (SRC) circuits [9].

Both SRCs are controlled one by one to produce variable DC-link for the unfolding in DC/AC mode in the grid forming operation. These DC-link voltages are converted to AC by the unfolder. The operation will be reversed in AC/DC mode. PID controllers, reference generation, look up table and Unfolder are controlled by FPGA. Look up table is used to control switching sequences of the unfolder [10]. The advantages of this structure are removing PWM inverter and filter, decrement of the capacitance of DC-link, the optimization of THD by relating advances in control strategy of the SRCs [9]. Parallelization of the two DC-links with the AC circuits, it remodels or rectifies from the three-phase AC to conventional 60 degree segments of sinusoidal wave forms which exist at the variable DC-link nodes [11], [12]. More to clarify that, the capacitors of DC-link which placed among the unfolder and SRC do not stock network energy and are basically required by filtering of the output current of SRC.

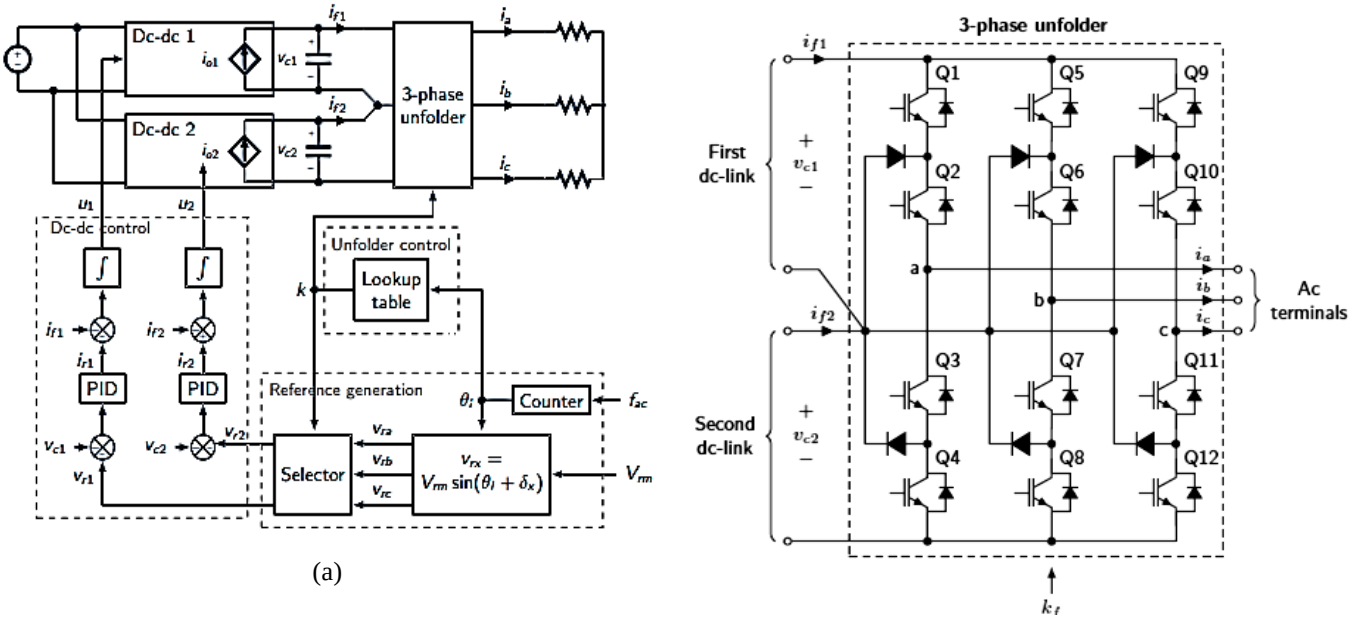

(a) (b)

Fig. 1. a) Block Diagram, b) Unfolder circuit of the system

3. Fractional Order PI Controller

The fractional-order integral-differential operator is represented by and defined as follow [13],

$$ {}_aD_t^r = \begin{cases} \dfrac{d^r}{dt^r} & r\rangle 0 \\ 1 & r=0 \\ \displaystyle\int_a^t (dt)^{-r} & r\langle 0 \end{cases} \tag{1} $$

where and are the upper and lower limits of operator a and t is the fractional order. Several mathematical definitions for this type of differentiation could be listed in the references but three of them is enough here, that are Caputo, Grünwald–Letnikov (GL) and the Riemann–Liouville (RL), are accepted. The mentioned definitions have its own properties and are given below. The definition of GL [14] is,

$$ {}_aD_t^r f(t) = \lim_{h\to 0} h^{-r} \sum_{j=0}^{\left[\frac{t-a}{h}\right]} (-1)^j \binom{r}{j} f(t-jh) \tag{2} $$

Where $\left[\dfrac{t-a}{h}\right]$ is the integer part. On the other hand, for $n-1\langle r\langle n$ the RL definition can be defined as,

$$ {}_aD_t^r f(t) = \frac{1}{\Gamma(n-r)} \frac{d^n}{dt^n} \int_a^t \frac{f(\tau)}{(t-\tau)^{r-n+1}} d\tau \tag{3} $$

where $\Gamma(.)$ is the gamma function. Finally, for $n-1\langle r\langle n$ the Caputo method can be written as [15,16].

$$ {}_aD_t^r f(t) = \frac{1}{\Gamma(n-r)} \int_a^t \frac{f^n(\tau)}{(t-\tau)^{r-n+1}} d\tau \tag{4} $$

In this paper, Caputo definition is used due to extensively been used in engineering application. FOPID controller is generally donated by $PI^{\lambda}D^{\mu}$ and the equation below shows the transfer function,

$$ G_c(s) = K_p + K_i s^{-\lambda} + K_d s^{\mu} \tag{5} $$

Here λ and μ are real positive numbers. P, I and D defines proportional gain, integration and differentiation of constant K respectively. Determination of these parameters makes a significant improvement on PID. Therefore, several optimization methods are proposed to find the optimum value for the FOPID controller parameters. In this paper, we used PSO for the determination of the controller parameters.

3.1 Tuning of The FOPI Controller by PSO

3.1.1 Improved PSO

The improvement flowchart which basically focuses on handling of the population (particles) has presented in Fig. 2. The weighted selection method is used to decrease the swarm size population. Reducing the swarm size by half will undoubtedly reduce CPU time in terms of optimization issue.

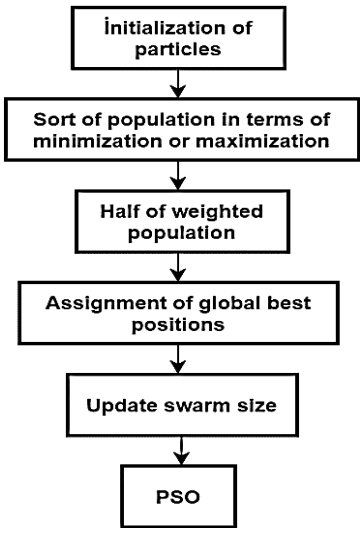

Fig. 2. Flowchart of improved PSO

Simulation results of revised PSO and conventional PSO are compared in Table 1. The simulations are tested for thousand times for the same initial conditions. The improve PSO was first simulated on traditional test functions as shown in Table 1. A brief information about these functions; first function is De Jong 1 function which is simple to apply, shows a stable and convex form. While two methods achieved the optimum value of the De Jong 1 function, a significant decreasement of CPU time has been retrieved (58 %). Second function De Jong 2 which is a typical function used in optimization testing, and also known as a "banana function". Score point is located at a deep figurative valley; difficult to get the minima considering this shape, that's why it is used for tests. Similarly, about 40 % gain is marked as in De Jong1. De Jong 3 has a feature of incoherent, uniform modal, separativity and extensitivity. Optimum value of the De Jong 3 function is related with the variable number. A reduction of 20 % was achieved for three variables but 48 % for ten, that's great for advanced PSO. The fourth is De Jong 4 function which has a Gaussian noise. 45 % ratio is indicative for three variables and 20 % for more variables. The other name of De Jong 5 is called Shekel's function, furthermore a_{ij} and ci are some constants which can be found in literature. This function differs with separability with local maxima associated with the a_{ij} matrix. Superior results and excellent performance (62 %) for three variables, unfortunately 10 % for ten. Our last function is Rastrigin function which is presented by customizing De Jong 1 with a cosine factor.

Table 1. Calorific Values (CV) for Palm Fruit Shell Briquettes

Test Functions	Number of Variables	Mathematical Expression	PSO		Improved PSO		Reduction in CPU time (%)
			Iterations	CPU time (s)	Iterations	CPU time (s)	
DeJong1	3	$f(x)=\sum_{i=1}^{n} x_i^2$	80.1	35.99	59.308	15.23	**58**
	10		168.8	75.64	128.4	31.52	**58**
DeJong2	3	$f(x)=\sum_{i=1}^{n-1} 100(x_{i+1}-x_i^2)^2+(1-x_i)^2$	62.248	9.138	45.6	5.71	**38**
	10		123.4	28.6	113.2	16.652	**42**
DeJong3	3	$f(x)=\sum_{i=1}^{n} \text{int}(x_i)$	116.4	35.44	79.42	28.28	**20**
	10		107.25	106	98.25	55.25	**48**
DeJong4	3	$f(x)=\sum_{i=1}^{n} i x_i^4+Gauss(0,1)$	19011	8276	488.6	4512	**45**
	10		21237.6	10411.6	548.4	8452	**19**
DeJong5	3	$f(x)=\sum_{i=1}^{m} \frac{1}{\sum_{j=1}^{4}(x_j-a_{ij})^2+c_i}$	63.4	89.12	43.688	33.78	**62**
	10		111.92	511.25	200.9	461.75	**10**
Rastrigin	3	$f(x)=10n+\sum_{i=1}^{n}(x_i^2-10\cos(2\pi x_i))$	112.12	133.5	114.125	79.7	**40**
	10		178.3	605.83	170	294.4	**51**

3.1.2 Improved PSO

Simply application, lower variables and high convergence are basic assets of this algorithm. As an alternative of the structures require long CPU times, PSO appears. Thus, this algorithm is preferred in this complex system and also compared with GA. Improved PSO shows better CPU time results with better optimization as it is referred above. The boundaries of the algorithm are presented in the Table 2.

PSO optimization results based FOPI control, advanced PSO and GA are displayed in Table 3 for 2 kVA RL load. Why it is displayed for one load, because the others reach also about the same time scales reasonably. Focusing on the Table 4 one can see each algorithm carried out the optimum value, but it took enormously distant CPU cycles. The table shows GA need more CPU time drastically. Another convincing improvement is the reduction in CPU times as predicted: 42 % lower CPU time. PSO should be selected for complex systems in terms of simulation time as it is seen in this Table. On the other hand, simulation was run for different load types for testing as it is shown in the Table 4.

Table 2. Parameter Boundaries for PSO and GA

Parameters	Lower	Upper
K_p	0.01	0.03
K_I	50	180
K_D	0.1	0.2
λ	0.4	0.9
μ	0.3	0.8

Table 3. Comparison of Simulation Times of the Algorithms for the load of RL (2 kVA).

Algorithm	K_p	K_i	λ	K_D	μ	THD	CPU time
PSO	0.0255	52	0.477	0.22	0.663	1.65 %	62 h
Improved PSO							36 h
GA							144 h

It could be seen that FOPI dominates PI ones in some loads. More inductive loads cause more corruption in THD values as expected.

Table 4. Comparison of PI and FOPI in terms of THD Values

Load	PI	FOPI	
Resistive (100 Ω)	0.44	1.34	THD (%)
RL (2.5 kVA)	3.49	2.9	
RL (2 kVA)	2.45	1.65	
RL (1 kVA)	0.95	0.98	
IM (1.5 kW)	0.92	5.6	

Also inductive loads have some glitches in Voltage characteristic as seen in the Fig. 3. Since the system is optimized for worst conditions with different loads, the resistive load has higher THD value than 1 kVA load. The system was tested up to 2.5 kVA load because of saturation limits. On the other hand, the Induction Machine (IM) load result of PI controlled algorithm achieved impressively higher performance over FOPI one. But however FOPI can get the same result with different control parameters that require dynamic parameter tuning for FOPI.

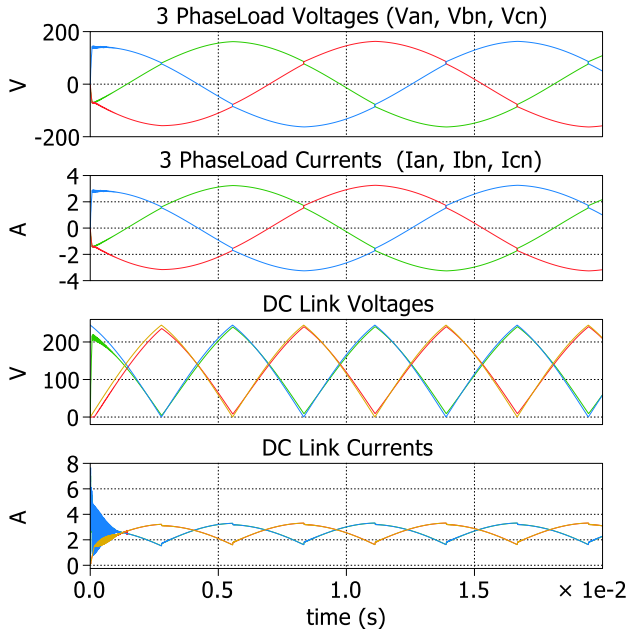

Fig. 3. Illustration of Simulation results for 2 kVA load optimized by Improved PSO.

4. Conclusions

In this paper, the THD Optimization of a FOPI controlled Bidirectional Three-Phase DC-AC Power Conversion in Grid Forming Operation is presented by an improved PSO. The main goal of this design is to minimize switching complexity of conventional inverter and to obtain pure sinusoidal wave form without harmonic elimination methods. In the first stage, the comparison between PI and FOPI expose the superiority of fractional controller over PI except IM load. However, FOPI can get the same result with different control parameters, dynamic tuning of parameters is mandatory. In the second stage, significant reduction in CPU time proves that the new approach makes the algorithm more optimistic. Dominating the CPU time for GA presents that PSO is an alternative solution for optimization of sophisticated architectures which need hard CPU time. The future work will be the FPGA implementation of FOPI controller and verification of optimum in hardware. Another future work will be multi variable optimization in terms of efficiency and different loads. Also online optimization methods can be implemented because of nonlinearities. A dynamic FOPID / PID control should exactly give the best results for this system. The full paper will include better optimized simulation results, dynamic load response of the system for the proposed optimization algorithm, objective function and comprehensive introduction.

References

[1] H. M. Emara, W. Elshamy, A. Bahgat, “Parameter identification of induction motor using modified Particle Swarm Optimization algorithm”, IEEE International Symposium on Industrial Electronics, pp. 841 - 847, 2008.

[2] A. K. Kaviani, S. H. Fathi, N. Farokhnia, A. J. Ardakani, “PSO, an effective tool for harmonics elimination and optimization in multi-level inverters”, 4th IEEE Conference on Industrial Electronics and Applications, pp. 2902 - 2907, 2009.

[3] M. T. Hagh, H. Taghizadeh, K. Razi, “Harmonic Minimization in Multilevel Inverters Using Modified Species-Based Particle Swarm Optimization”, IEEE Transactions on Power Electronics, Vol. 24, pp. 2259 – 2267, 2009.

[4] T. Shindo, K. Jin'no, “Switching angles optimization of single phase PWM DC-AC inverter by particle swarm optimizations”, Joint of 6th International Conference on Soft Computing and Intelligent Systems (SCIS) & 13th International Symposium on Advanced Intelligent Systems (ISIS), pp. 65 – 70, 2012.

[5] S. Ganguly, “Multi-Objective Planning for Reactive Power Compensation of Radial Distribution Networks with Unified Power Quality Conditioner Allocation Using Particle Swarm Optimization”, IEEE Transactions on Power Systems, Vol. 29(4), pp. 1801 – 1810, 2014.

[6] H. R. Mohammadi, A. Akhavan, “A new adaptive selective harmonic elimination method for cascaded multilevel inverters using evolutionary methods”, IEEE 23rd International Symposium on Industrial Electronics (ISIE), pp. 1484 – 1489, 2014.

[7] B. P. De, R. Kar, D. Mandal, S. P. Ghoshal, "Design of symmetric switching CMOS inverter using PSOCFIWA", International Conference on Communications and Signal Processing (ICCSP), pp. 1818 – 1824, 2014.

[8] M. Baskin, B. Caglar, "A modified design of PID controller for permanent magnet synchronous motor drives using particle swarm optimization", 16th International conference on Power Electronics and Motion Control Conference and Exposition (PEMC), pp. 388 – 393, 2014.

[9] C. Weilun, R. Zane, D. Seltzer, L. Corradini, "Isolated bidirectional DC/AC and AC/DC three-phase power conversion using series resonant converter modules and a three-phase unfolder", Workshop on Control and Modelling for Power Electronics (COMPEL), pp. 1 - 6, 2014.

[10] D. Seltzer, L. Corradini, D. Bloomquist, R. Zane, and D. Maksimović, "Small Signal Phasor Modelling of Dual Active Bridge Series Resonant DC/DC Converters with Multi-Angle Phase Shift Modulation", Energy Conversion Congress and Exposition (ECCE), pp. 2757 – 2764, 2011.

[11] B. Jacobson and E. Holmansky, U.S. Patent 7,839,023, "Methods and apparatus for three-phase inverter with reduced energy storage," Nov 22, 2010.

[12] K. Oguchi, E. Ikawa, Y. Tsukiori, "A three-phase sine wave inverter system using multiple phase-shifted single-phase resonant inverters," Industry Applications, IEEE Transactions on, Vol. 29(6), pp. 1076-1083, Dec 1993.

[13] K. Orman, A. Basci, and A. Derdiyok, "Speed and Direction Angle Control of Four Wheel Drive Skid-Steered Mobile Robot by Using Fractional Order PI Controller, Elektronika Ir Elektrotechnika, vol.22, no.5, pp.14-19, 2016.

[14] I. Podlubny, "Fractional differential equations," New York: Academic Press, 1999.

[15] D. Valerio and J. S. Costa "Time domain implementation of fractional order controllers," IET Proceedings-Control Theory and Applications, vol.152, no.5, pp.539-552, October 2005, doi.10.1049/ip-cta:20045063

[16] K. Orman, K. Can, A. Basci and A. Derdiyok, "An Adaptive-Fuzzy Fractional-Order Sliding Mode Controller Design for an Unmanned Vehicle", Elektronika Ir Elektrotechnika, vol.24, no.2, pp.12-17, 2018. doi.org/10.5755/j01.eie.24.2.20 630.

Shaping Effects on Long Span Bridge Deck Aerodynamics

Ali Etemadi*‡

* Department of Civil Engineering, Faculty of Engineering and Architecture, Istanbul Esenyurt University, Istanbul, Türkiye.

(alietemadi@esenyurt.edu.tr)

‡ Corresponding Author; Department of Civil Engineering, Faculty of Engineering and Architecture, Istanbul Esenyurt University, Istanbul, Türkiye,

Tel: +90 444 9 123, Fax: +90 (212) 699 09 90, alietemadi@esenyurt.edu.tr

Received: 24.09.2022 Accepted: 29.09.2022

Abstract- An aerodynamic circumstance of wind pressure surrounding the long-span bridge allocates many theoretical and experimental research to this topic. Determination of the materials and optimal cross-sectional shape of bridge decks that affected a dynamic behavior of long span bridge deck is still included in current research issues and works to be continued in this path. These include the Lack of sufficient awareness of wind forces, stemming from complex nature, and the unpredictability of the wind nature. In this study, in addition to recognizing the aerodynamic behavior of the flutter, the acting pressure forces on the bridge deck are investigated. The geometrical shape of decks, wind velocity, and flutter conditions are adopted as design variables that affected the dynamic forces exerted on bridge decks. A common type of geometric sections of the long-span bridge deck and effective aerodynamic phenomena are examined. The hollow box steel suspended deck and double cells box girder linked via upper flanges and cells linked via the top and bottom flanges are adopted for Computational Fluid Dynamic (CFD) approach. Thus, aerodynamic instability and turbulent torsional flutter flows, as well as a trail of shedding vortices around the bridge decks, are investigated. By changing some geometrical parameters of commonly used bridge sections, the optimal cross-section in terms of turbulence created above and below the deck section is examined and an optimal cross-sectional shape variable is proposed. The shape variable and section dimensions adopted for CFD-Simulations are similar to the dimensions and materials used in previous laboratory specimens of wind tunnels to be able to interpret the results and possibly verify them with the result of the current study.

Keywords: Wind load, hollow box steel suspended deck, box girder deck, aerodynamic instability, trail of shedding vortices.

1. Introduction

Construction of bridges with long spans on valleys, lakes is increasingly underway and in turn, new techniques must be adopted to calculate and estimate the forces acting on bridge components, building materials, and the type of bridge deck cross-section, both in the design and construction phase. One of the major forces acting on bridges is wind pressure. Lack of sufficient knowledge and careful study of the forces applied by the wind loads can cause severe vibrations on the bridge deck and may occurrence of a resonance condition that can lead to complete failure of the bridge. The collapse of the Tacoma Bridge in the United States (1940) and Brington Bridge in China (1879) are the examples of a bridge collapse due to unexpected wind loads.

In general, the effect of wind depends on factors such as geographical location, height of the area above sea water level, topography of the bridge site, and geometric characteristics of the bridge. The wind speed increases at higher elevations above ground level, and thus we face more air pressure at higher elevations. Since the fluctuations caused by turbulent wind currents on bridges are of great importance, the study of the geometric shape of the bridge deck is one of the most important issues in bridge engineering and requires more comprehensive studies. The compressive pressure is exerted on the windward surface, while there is the suction on the leeward sides or parallel surfaces of the wind flow, and the wind does not flow steadily, the air particles collide with the turbulence as they move. Vortex shedding tails is created which put more local pressure around bridge components. This

is reason that an additional local pressure is created around the decks and should be taken into consideration in structural design process.

In general, wind load is dynamic in nature, meaning that its magnitude varies with time and space. As a result, the analysis and modeling of such a load and its relative effects on structures can be complex, and requires a great deal of knowledge in mathematics, CFD, and structural analysis. For instance, the structure starts to fluctuate with the wind flow and then following the deck vibration itself affects the wind flow interactively, sometimes its increases and sometimes its decreases turbulence currents. Such an inactive effect can be examined by CFD-Simulation and experimental procedures like wind tunnel tests.

The regulations for the design of bridges against wind forces, such as European EN-1991-1-4 (Eurocode 1), [1] have special design criteria for structural designers against incoming wind forces on surfaces of structures, dynamic and static responses of long-span bridges. Despite the complex nature of wind forces, the regulation proposes relatively simple methods for the modeling of wind flutter phenomena and their corresponding effects on bridge structures, as well as determine the aeroelastic and dynamic responses of structures. However, sufficient knowledge of the context and logic applied in the simplified proposed method is required for using these criteria. It should be ensured that the results of the hypotheses and limitations of the suggested methods should reflect the real conditions at the bridge construction site. On the other hand, the relationships provided for the responses toward wind direction and the reciprocal wind responses (outside the wind direction) are not considered in simplified method. According to the regulation criteria, single bridges with a main span length of more than 50 meters need to be dynamically checked and the wind load coefficients provided by simplified method is not accurate enough for use in practice. The simplified criteria are true for bridges with a simple geometric shape with the dominant first mode. More precise dynamic analysis is required for several complex deck shapes such as long span suspension bridge decks exposed to strong turbulent wind flow.

The aerodynamic stability of bridges is determined largely based on wind tunnel tests. Since CFD-Simulations methods have developed, it has been used as a complement to test ways. Although very time consuming and costly, wind tunnels have become popular with researchers and bridge design engineers. The use of CFD simulation is not a reliable alternative to wind tunnel testing and verification by experimental results is required. Nevertheless, it can be used as a powerful tool for documenting and examining various scenarios prior to laboratory simulations. This is also easily done by changing the modeling input parameters.

The main purpose of this study is to examine the aerodynamic stability of long span bridge decks subjected to strong wind flutter condition. The effects of the geometry of the bridge deck on the pressure distribution on the deck surface is also examined. In addition to introducing and examining the shape of common decks, an attempt has been made to estimate pressure caused by tail of vortex shedding. The CFD approach, assumptions and domain size considered in the analyzes are introduced. The effect of the geometric shape of the deck on the dynamic behavior under the influence of the wind current is evaluated and compared. Thus, recommendations on the optimal deck cross-sectional shape are introduced. As mentioned before, numerical simulations of wind flow will be valid and reliable if they can be reproduced by experimental tests. In this study, the author tried to construct structural models similar to laboratory samples tested in previous research in order to compare, adapt and validate the results obtained.

2. Literature Review on Previous Works

The following is a brief description of the papers used with the topic of the flutter phenomenon and the impact of deck shaping under wind flows and wind tunnels experiments.

The aerodynamic static coefficients of the 2-edge sloped box beam were assessed by Lee *et al.*, [2]. The static wind load coefficient sensivity angle of attack was evaluated for 2-edge sloped box girder. A series of wind tunnel tests were conducted by changing the the box slope angle from 0° to 17°, whereas the attack angle was arranged in between -10° to 10°. The consequences illustrated that the lateral wind force decreased significantly with increasing box slope angle, except when the physical angle was 8°–11°. For the practical range of angle of attack, the box slope must be greater than 15° to minimize the aerodynamic static lateral force on the beam. Ying *et al.*, [3] comprehensively investigated the limit cycle flutter characteristics of a bridge deck through use a fluid-structure interaction model. Its precision was confirmed by the flutter reactions of a thin plate with theoretical solutions. The aeroelastic responses of a bridge deck was numerically simulated. As the angle of attack increases, the section shape turns into much blunter, so it becomes more prone to limit cycle flutter. The advanced numerical simulation supplyes a robust instrument for limit cycle flutter analyses of bridges with large span. The sufficient precision of the numerical models is verified by comparison with the experimental results.

The flutter performance of a twin-box bridge girder at large angles of attack were investigated. Several central slot widths were taken into consideration. The stationary and dynamic flow field characteristics were changed. The results of both CFD-simulations and wind tunnel testing are compared (Tang *et al.*) [4]. The analysis results imply that the presence of the central slot benefits the bridge flutter stability at null angle of attack. However, the flow field around the girder is varied at large angles of attack. The incoming flow may run through the central slot and act on the vortex connecting to the girder. The upstream box draws energy from the wind flow easier than downstream, thus leading the bridge to torsional flutter instability at lower wind velocities. Montoya *et al.*, [5], proposed a methodology for performing the aerostructural design of bridges with large span in early design phases by taken into account a number of parameter variation to analyze the relations in between the geometric shape of deck and the buffeting repercussions. This information is used to tailor the deck shape aiming at keeping the buffeting response under a given threshold. This outcome is applied to adapt the shape of

the deck, which aims to keep the buffeting response below a certain threshold.

Kusano *et al.*, [6] carried out the CFD simulations of a single-box deck section to investigate the significance of railings and vortex attenuation tools on the bridge reaction subjected to wind pressure. Several cross section of bridge deck were investigated like a bare section and deck sections with attenuation tools and altering the width of deck. Coefficients of aerodynamic force get through CFD simulations were then applied to calculate flutter derivatives on the basis of quasi-steady formula. Flutter speed was computed for several cross sections. The deck section with the greatest width to depth ratio has the highest efficiency towards instability of flutte phenomenon. Although it appears the vortex attunation tools be in tendency to develop the aerodynamic behavior of the bridge through changing the flow field around the bridge deck. Liu *et al.*, [7] presented the properties of self-excited forces are in both in the time-domain and frequency-domain. The flutter calculation is performed subjected to both smooth flow and turbulent flow to evaluate the impact of wind turbulence on the instability condition of the flutter. By comparing of the results of several turbulence severites with that of the smooth flow, it was concluded that the turbulence has a stabilizing impact on flutter condition of bridge. The turbulence can alter the vibration patterns and decline the spatial vibration correlation in some degree. Consequently, the critical flutter speed could be augmented by 5% to 10%.

Yang *et al.*, [8] examined two critical flutter and vortex-induced vibration performance performance of closed-box girder bridges with lower inclined web angles and various wind fairing angles by experimental research and theoretical studies by performing a theoretical analysis and wind tunnel testing results. The results indicate that for a given inclined web angle, a closed box girder with a sharper wind fairing angle of 50° has better flutter and vortex-induced vibration performance than 60°, while a 14° inclined web angle reduces the best vortex-induced vibration performance. Furthermore, a wind fairing angle of 50° reduces a preferable flutter output by causing a single vortex shape and a balanced distribution of the strength of vorticity in both lower and upper sides of the wake zone.

Hansen, [9-11] analyzed the critical wind velocities of the flutter phenomenon on the bridge during the construction of the Great Belt East. This research was commissioned by Steinman Co. with the aim of reviewing the work done by COWI Consulting Engineers. The research report was based on wind tunnel experiments and they concluded that the most critical stage of construction is when the fifth section of the bridge is installed. The deck of the bridge at that stage was 249 meters long. The results of this research indicated the critical wind speed of the flutter is at about 43.3 m/s^2. They also observed that the phenomenon of vibration occurs at the collision of two characteristic modes of torsional and vertical transition. Frandsen, [12] conducted extensive studies on fluid dynamics analysis and proposed several structural fluid formulations to find the critical float velocities of the built bridges. Although the fluid range was relatively large, the results were surprisingly good. In that study, even the smallest mesh elements had a characteristic length of approximately one meter. He observed the beginning of the vortex shedding behind the bridge deck. The fluid range of 1900 nodes was modeled in an irregular mesh structure. The critical wind velocity of the float was calculated between 65 m/s and 70 m/s, which was slightly lower than the values measured from the Danish Maritime Institute's wind tunnel test in 1992 and 1993. The results of fluid dynamics analysis through the finite element model of structures to estimate the critical float wind speeds were presented with sufficient accuracy, but not enough to the extent that there is no need to conform and adapt to the laboratory results of wind tunnels.

Awruch and Braun [13] used two different methods to find flutter critical wind speeds. The forced vibration test was performed on a numerical model and the oscillations were simulated by altering the input wind angle. The experiment was performed to find aerodynamic derivatives and the critical wind velocity of the floater was 73 m/s. They also performed structural-fluid interaction analyzes. The analysis resulted in a critical flutter wind speed of 69 m/s. Both of these results were in good agreement with the quantities obtained from the wind tunnel test. The Strohall number was $S_t = 0.18$, which was close to the quantities of wind tunnel test measurements.

Cigada *et al.*, [14] introduced a new approach to simulate the bridge deck response to turbulent winds. The results show that the wind tunnel test has an important and fundamental role in determining the values of variables used in bridge deck simulation software against turbulent and tornado loads. The aerodynamic acceptance function is one of the hardest variables to estimate because it depends on the control of the incoming tornado spectrum as well as the ratio of the average wind-to-deck angle that varies in time and space. Larsen *et al.*, [15] examined a variety of box beam deck models and determined the optimal geometric shape to prevent the formation of wind vortex response. All models of this research have been made and tested in the laboratory and in the wind tunnel. The results indicated that a deck could be obtained without virtual vibration and also the angle between the lower horizontal plane of the deck and the sloping side plate is a fundamental variable to achieve this goal (Larsen *et al.*) [15].

Larsen *et al.*, [16] examined the dynamic effects of wind on two types of suspension and cable bridges. This study addresses the different types of wind dynamic effects that usually occur on suspension and cable bridges with emphasis on the importance of understanding the dynamics of the bridge structure. Anina *et al.*, [17] performed an experimental and analytical research of load coefficients and free vibrations of bridge decks. The results of the analysis are firstly compared with the quantites get from the wind tunnel and validated. In this model, two-dimensional model analysis is assumed and, in the analysis, the deck cross-section used in the wind tunnel was used. Han *et al.*, [18] investigated the impacts of aerodynamic variables on the dynamic response of road and deck vehicles and bridges under vertical wind loads on vehicle direction. At first, they simplified the vehicle and the forces applied from the wind to the vehicle using mathematical formulas, and then the result of these forces was applied to the bridge deck, and finally, the effects of wind on the bridge deck were obtained using mathematical calculations. The results

show the different and often increasing effects of these vehicles on the output of deck forces. Some recent literature review on the impact of deck cross section under wind loads are described in the following:

Pindado *et al.*, [19] investigated the impact of the cross-sectional deck shape on the aerodynamics of the uniform deflection-rotational torques of the cantilever bridges during construction. The oscillating torque applied on the deck of a reinforced concrete box was made experimentally, using a balanced cantilever installation method, during the bridge installation operation. The impact of the shape of the box beam deck was tested by wind tunnel using four models based on the different cross section for box bridges with different angles of the box girder. The parameter was taken to be a = 0.02 m (Fig. 4). The results of their experiments showed that the reduction of deflection oscillation torque coefficients decreases with the linearization of the bridge deck shape and when the length of the deck is close to twice the width of the deck, the Yawing moment coefficient attains its maximum quantity. Larose *et al.*, [20] performed laboratory measurements on the forces of wind blowing for different models of bridge decks at the Danish Maritime Research Center in Denmark. The results of the wind tunnel test were reported to investigate the volumetric distribution of wind loads as a function of deck width and sudden turbulent flow for different sections of the bridge deck. For the geometric variable of the cross-section, the ratio of width to height of the cross-section was considered, and laboratory models were tested with ratios of 5, 7.5, 10, and 12.67 (Fig. 6). They examined and reported a more detailed relationship between aerodynamic flow direction and forces along the bridge span.

Larsen and Wall [15] conducted research on the effect of deck shape to prevent vortex shedding from responding to the aerodynamics laboratory at the Ottawa National Research Center in Canada. The side edge angle of trapezoidal box decks was a geometric variable in the models tested for their research work (Fig. 7). The authors showed that free decks can be obtained from virtual vibration and that the angle between the bottom surface of the deck and the inclined side is a significant parameter to achieve this aim. The results of their experiments showed that the trapezoidal cross-section of the bridge deck can be adopted to prevent the formation of vortex shedding for specific structural damping. The experiments were performed for relatively small Reynolds numbers, but subsequent tests also confirmed the results for high Reynolds numbers. It was observed that the angle between the bottom plate and the side panel is about 15 degrees, which is almost the optimal value for the trapezoidal cross-section of the bridge deck. The vortex shedding was just below the side panel.

3. Aerodynamics and Wind-Induced Forces on Long Span Bridge Decks

In this section, a brief introduction to the load phenomena emerging on long-span bridge decks is expressed. This study focuses on the flutter phenomenon, but an understanding of other phenomena is necessary for fully grasping the nature of the wind-induced motions. The impacts that occured when long-span suspension bridges are under wind-induced forces can be rather excessive and in critical situations causing the full collapse of the bridge. The effect of the wind loads is dependent on the aerodynamic characteristics of the bridge deck. A bridge deck entangled in a flow interacts with the flow, and is, as a result, exposed to compressive or suction surface pressures. The applying turbulent flow will produce the dynamic forces on the bridge deck which causes the time-dependent lift force, drag force, and moment loads on bridge decks. The forces are classified into static forces, related to the mean wind speed, and forces associated with the pressure fluctuations (buffeting), due to the turbulence.

Wind-induced loads on long-span bridge decks are classified into three separate groups: (a) Extraneously induced excitation covers dynamic loads due to turbulence with very large movements in the applying wind. The motions due to fluctuating winds are called buffeting. (b) Instability due to turbulence developed by the bridge deck itself goes by the name of signature turbulence. This covers the well-known Von Kármán's Street which is likely to be in resonance with the bridge structure. (c) Aerodynamic instability (negative damping), where motion-induced wind loads arise on the bridge structure. This covers phenomena such as galloping and flutter. (Morgenthal) [21-22]. The origin of the loads can be classified into the motionless and moving bridge deck. An explanation of the wind-induced loads expressed in the following sections.

3.1 Aerodynamic Instability (Galloping and flutter phenomenon)

Flutter and galloping both occur for the wind which does not act in resonance with the structure, both are described as aerodynamic instability phenomena. In addition, the phenomena are independent of the turbulence of the incoming wind but can arise in a uniform flow. Galloping is the phenomenon occurring when the structural vibrations are almost perpendicular to the incoming wind and are characterized by negative aerodynamic damping as the driving force. Flutter is a combination of a coupled vertical motion and a rotational motion. It is important for the coupled flutter vibration, that there is a phase difference between the torsional and the vertical movement. If there is no phase difference between the two movements, the resulting work is zero. Flutter is said to occur when the energy input, from the wind velocity, is equal to the energy dissipated. This velocity is known as the critical flutter wind velocity. The aerodynamic damping loads become negative when exceeding the critical flutter wind velocity, and thereby further increasing the vibration amplitudes. For flutter to occur, the torsional frequency must exceed the vertical frequency for the bridge movements, but only marginally. This ensures the continued energy transfer to the system which is crucial for the phenomenon to arise. Other than, the energy transfer will dissipate due to structural damping. (Hansen and Dyrbye) [23].

Depending on the cross-section of the bridge deck, increasing wind velocity leads to aerodynamic instability. If the aerodynamic effects are continuous and gradually stronger due to aerodynamic forces in some places, they will experience self-induced increasing oscillating movements, which is called flutter. The flutter is basically a stability problem that causes the bridge to experience large and increasing vibrations (intensifying) to the point of failure.

In Fig. 1, a schematic flow around a stationary bridge deck profile is presented. On the windward side of the profile, a point of stagnation is expected for a bridge at rest. On the first two edges, the flow is expected to separate, forming two standing vortices. Due to the relatively large afterbody, it is expected that the flow reattaches to the bridge deck. This is expected as the width of the bridge is larger than the vortex formed on the edge. The global forces on the bridge deck are very sensitive to the reattachment, as this dictates the size of the vortex where the relative pressure is large. After the reattachment a turbulent boundary layer builds up until the end of the profile is reached. Due to the sharp edges on the leeward side of the profile, vortices are expected to be shed periodically forming a well-known vortex street in the wake. Strong adverse pressure gradients are expected to arise when the wind passes over the sharp edges on the top and bottom of the bridge. This will cause the flow to separate from the boundary, forming two standing vortices. The vortex on the top side of the bridge is formed on a sharper edge, resembling a backward-facing step.

Periodic movements of a structure may happen when the vortices formed around the body is shed at a frequency close to the eigenfrequency of the structure. Both vertical and torsional modes should be considered. Vortex induced motions can be avoided by providing that the frequencies of the vortices created are widely separated from the structure's natural frequencies. This is performed by altering the geometry of the bridge design or changing the natural frequencies. The shedding frequency is usually defined by the use of Strouhal's number. The necessary values for the determination of Strouhal's number for the bridge deck can be found by the use of two contour plots from the simulation, one illustrating the horizontal velocity and one illustrating the vortices. The Strohall number is a function of the Reynolds number:

$$\mathrm{R}_e = \frac{VD\rho}{\mu} \quad (1)$$

In this expression, V is wind velocity, D is the diameter of the cross-section, or in this instance the height of the deck, ρ is the specific gravity of air, μ is the coefficient of kinematic viscosity of air.

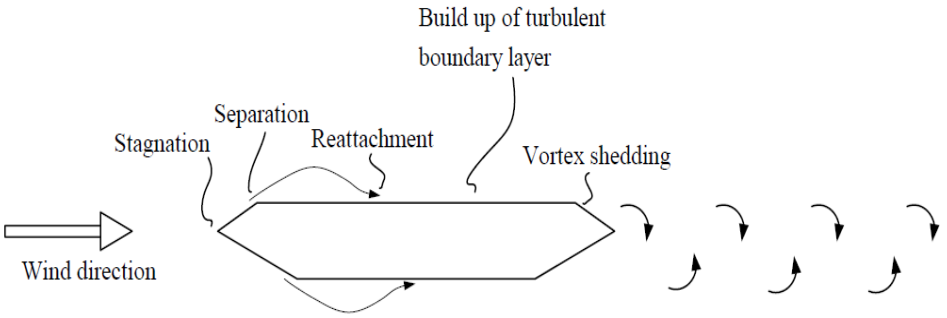

Fig. 1. Schematic view of the wind flow around the bridge deck

4. Basic Assumptions in Fluid Dynamics Analysis

To compute the critical flutter wind speed of the bridge deck float, the cross-sectional area of the box bridges and the flat deck with different edge angles have been adopted for CFD Simulation. In modeling, the cross-section is modeled as a rigid body. For this reason, the deformation of the bridge deck itself is not considered in the CFD-simulations. Since the deformations of the deck itself are very small compared to the vibrations of the bridge, it is assumed that they have very little effect on the movements created by wind loads.

The formation of periodic variable vortices The von Karman's vortex road, following the bridge deck, is very dependent on the meshing around the surface of the windward deck. Since eddies are formed by several meshing elements, the size of the eddies naturally determines the meshing size. In the shape of the road, a fully formed eddy current can be seen. Numerical models lead to more accurate results by increasing the mesh density and reducing the size of the loading steps. But the point is that the optimum mesh size and loading steps also lead to sufficiently acceptable results, but less time is spent solving the equations. Numerical models are less sensitive to the effects of boundary layers.

4.1 Design variables for selected flat trapezoidal and box girder decks

Design engineers use streamlined, box, and twin girders or the trapezoidal flat section types according to architectural issues and structural needs in the relevant project. The cross-section of bridges used in this study is divided into three main categories: simple trapezoidal, box girder beams, and double box girder types. The suspended deck of Fatih Sultan Mehmet Bridge over the Bosphorus strait is an example of flat trapezoidal used in this study as shown in Fig. 2. The main span between its towers is 1090 m. The underside of the deck is 64 m above sea level. The steel suspended deck is a hollow box composed of orthotropic, stiffened panels, having an aerodynamic cross-section. The deck has a 33.80 m x 3.00 m box section and two cantilever side walks of 2.8 m at each side. The total width of the deck is 39.40 m. Length of deck unit are variable and their weights are between 115-230 tons. Multiple advantages lie with this box form compared with the classical stiffened truss. Much less steel is required in the boxes which

means less material in the cables, towers, anchorages, and foundations. The “steam lined” shape improves aerodynamic performance and reduces the wind loading on the bridge. The large flat uncluttered surfaces are much easier to maintain than the truss girder. The deformation caused by the movements caused by the wind flow is the maximum value in the middle part of the bridge span, so it is assumed that the sections that are under flutter in the analysis of dynamic analysis are adopted from the middle part of the long-span bridge.

The selected section dimensions adopted for CFD-Simulations are similar to the dimensions and materials used in previous laboratory samples of wind tunnels to be able to interpret the results and possibly verify them with the result of the current study. Important parameters affecting the shape and behavior of both trapezoidal flat girders and box girders are examined. By changing the dimensional sectional ratios, the effect of shapes on wind flow around deck is investigated. In order to find the most suitable cross-sectional shape, the pressure distribution caused by the wind flow has been clarified.

The impact of the box beam deck was tested by Pindado *et al.*, [19] in a wind tunnel using four models based on the different cross-sections for box bridges with different angles of box girders are adopted for CFD-Simulations. The parameter was taken to be a = 0.02 m (Fig. 4). Trapezoidal flat cross-section models used by Larose *et al.*, [20] are adopted for this study. For the geometric variable of the cross-section, the ratio of width to height of the cross-section is considered, and simulation models are prepared with ratios of 5, 7.5, 10, and 12.67 (Fig. 6), similar to those used in experimental test specimens. The section dimension and deck shape (side edge angle) effects of trapezoidal box deck models conduced by Larsen and Wall, [15] are adopted for this research. The dimension details and geometric variables in the models tested for their research work shown in Fig.

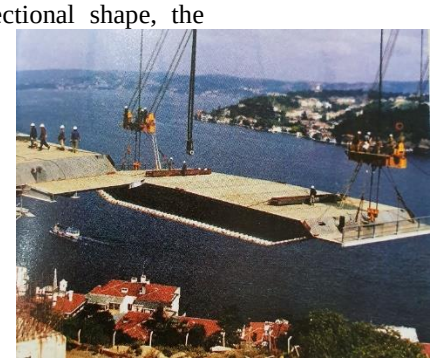

(a)

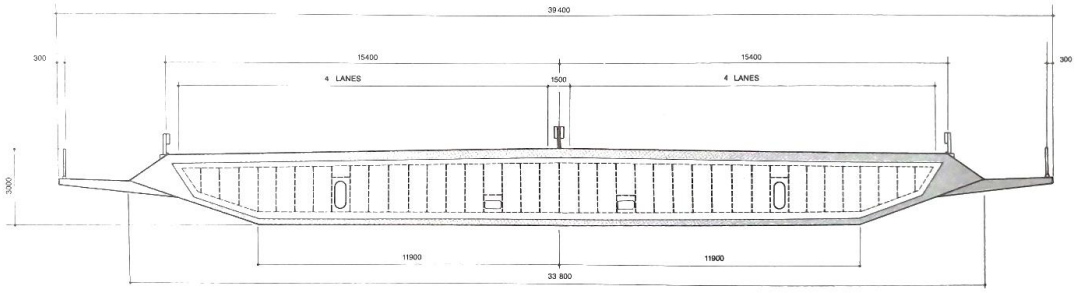

(b)

Fig. 2. (a) Deck view and (b) section from the deck of Fatih Sultan Mehmet Bridge

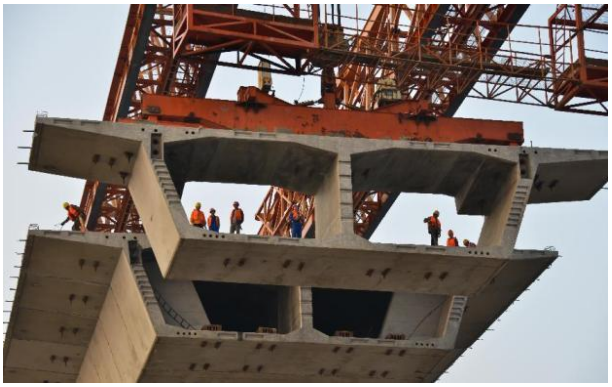

(a)

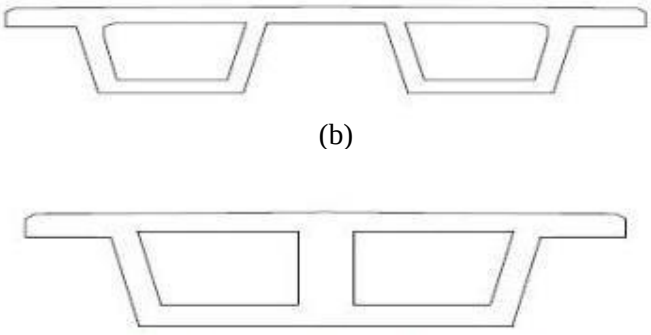

(b) (c)

Fig. 3. Box girder with cells linked by upper flanges and cells linked to both lower and upper flanges

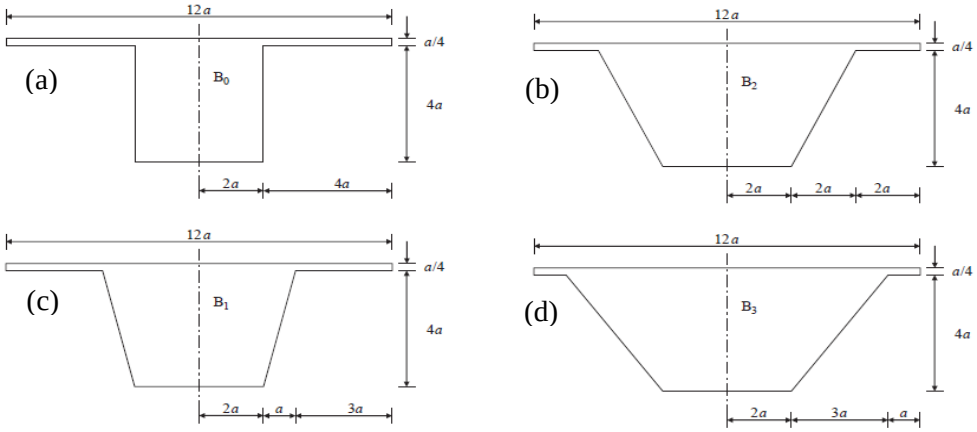

Fig. 4. Bridge deck model designed for CFD-Simulations wind analysis, with different cross section for bridges with different angles of box girder (a = 0.02m)

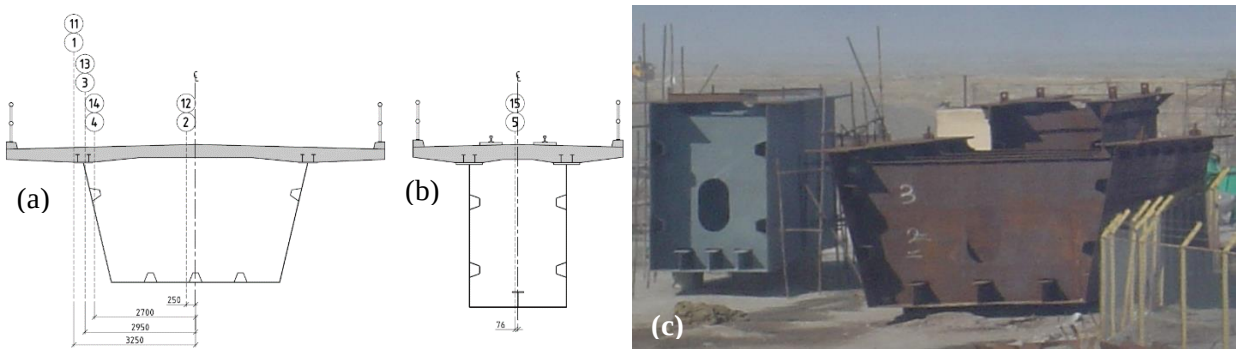

Fig. 5. Trapezoidal cross section bridge deck model with different length to width ratio (5,7.5, 10 and 12.67)

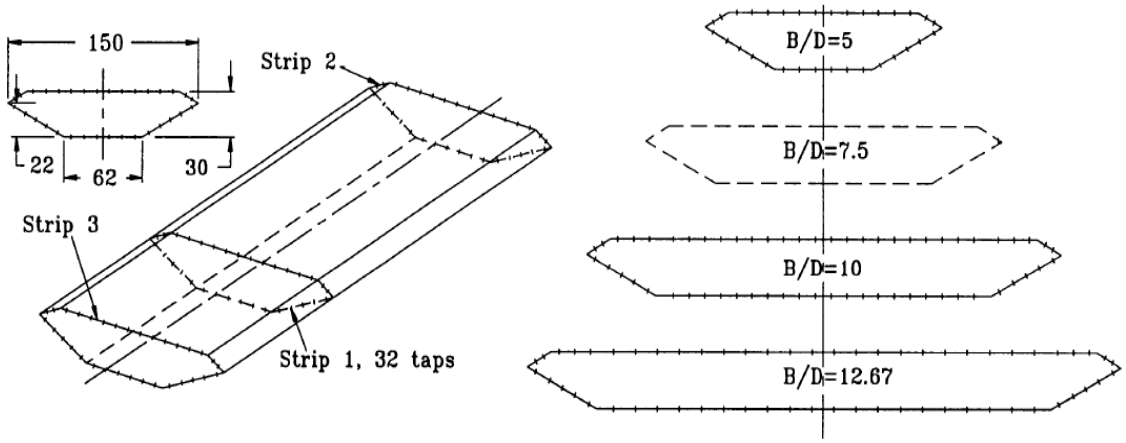

Fig. 6. Trapezoidal cross section model of bridge deck with different length to width ratio (5,7.5, 10 and 12.67)

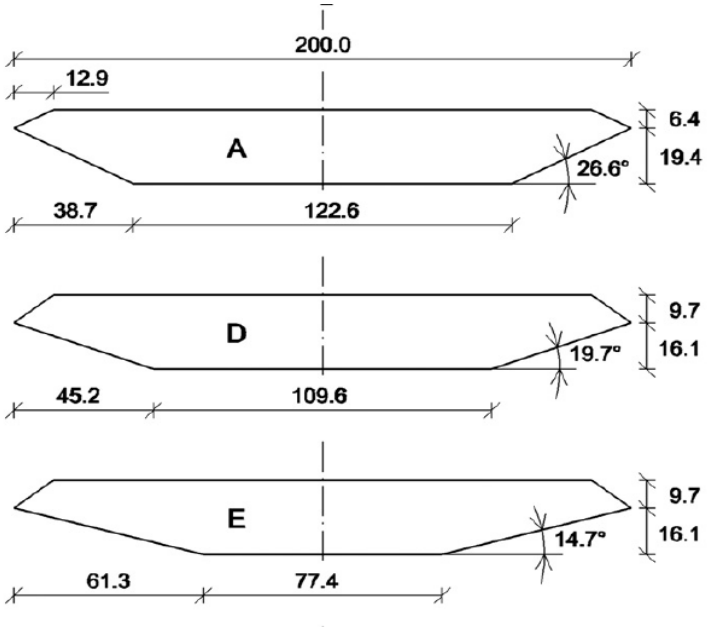

Fig. 7. Trapezoidal cross section model of bridge deck with different side angles $(26.6°,\ 19.7^{\circ},\ 14.7^{\circ})$

5. Fluid Dynamic Analysis

This analysis is a suitable tool for analyzing fluid flow in two-dimensional and three-dimensional modes. In a fluid analysis, the following seven general steps must be followed: (1) to identify the physical condition of the problem, (2) to determine the fluid regime, (3) to prepare a mesh model of finite elements, (4) to apply the border conditions. At this stage, it is necessary to adjust the parameters related to the dynamic analysis of the fluid, (5) perform analysis and problem-solving. In this step, the results are reviewed and the effect of each of the analysis variables is evaluated, and thus the optimal cross-sectional area of the bridge can be judged.

In fluid dynamic solution problems (CFD-Simulations), first, it is necessary to draw the fluid domain (wind flow) to be analyzed and then the solid domain (which in this research is the cross-section of the bridge deck) from the fluid domain.

The shape of the wind fluid domain and the cross-section of the deck for the model of bridges with box girders are shown in Fig. 8. The fluid domain is assumed that the distance between the upper and lower boundary plates and also the incoming flow is at the distance of the nominal diameter of the surface (D) of the cross-section from the center of gravity of the deck and the boundary surface of the flow outlet is at the distance (4D). The air temperature is considered to be 30 degrees Celsius. The characteristics of fluid (air) for atmospheric pressure at 30° C are given in Table 1. The element size around the bridge deck plays an important role in the forming of vortices behind the bridge. Very high values of velocity gradients near the surface require a very fine mesh. The vortices form in the sharp-edged body of the deck.

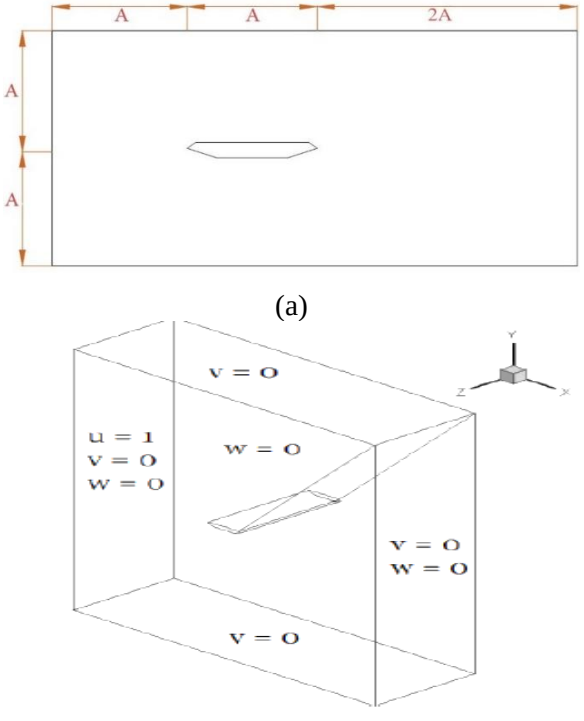

Fig. 8. (a) The size of the flow domain used for wind dynamic analysis, (b) Boundary conditions of current domain

Table 1. The characteristics of air for atmospheric pressure at 30° C

	VALUE
Mass density	1.166
Conductivity	0.0264
Specific Heat	1.005
Viscosity	1.604E-005
Expansion Coeff.	0.003315

The airflow is assumed to be uniform. The air pressure at the outlet edge is assumed to be zero. The behavior of the air on the deck wall is very important and the parameters related to the deck will need to be introduced to the program accurately. In both turbulent or turbulent fluid analyzes, it is necessary to calculate the pressure and flow distributions in two- or three-dimensional geometry. In these cases, the density and viscosity of the fluid need to be determined. Boundary conditions applied to different levels of the flow range are shown in Fig.8. Since the parameters are dimensionless, the upper bound has a unit velocity in the x-direction and is not a component in the y and z directions. And periodic boundary conditions are used in the z-direction. The output edge is assumed to be zero pressure. Non-slip conditions are considered on the deck surface.

In applying the boundary conditions of the edge in which the incoming flow into the domain. The incoming velocity is applied in one direction and equal to 100 km/h as per to the Iranian bridges loading code (139 regulation). The average speed wind at a height of 10 meters above the ground or river equal to 100 kilometers per hour is suggested. In the analyzes, the effect of wind velocity has also been investigated, for which wind velocities of 60, 100, and 120 km/h have been considered for dynamic analysis, respectively.

The transient flow from the float can be considered as slow or turbulent flow. In the slow flow of the fluid, the field velocity of the fluid changes slightly. This type of flow occurs in the field of fluid flow with high viscosity and low velocity. For example, fluids such as oil have such a flow field. In fluids, turbulent flow occurs if the velocity is high enough and the viscosity is low. Results of fluid dynamics analysis, comparison, and interpretation are expressed in the following section.

6. Results of Fluid Dynamics Analysis, Comparison and Interpretation

In this section, the shape of the flutter mode, the critical flutter wind velocity contour, the pressure distribution contours around the bridge deck of the trapezoidal flat bridges and the box girder are presented and examined. For different Reynolds numbers, the back-to-wind flow also follows different patterns, so that in very small amounts of Reynolds number $R_e \cong 1$, the flow remains parallel to the cylindrical body after passing through the deck body. As the Reynolds number increases up to $R_e \cong 20$ the flow around the body becomes symmetrical, but the flow separates from the deck body and large vortices shedding are formed at the lower surface of the deck body. At last, for $30 \leq R_e \leq 5000$ ranges, vortex street occurs downstream of the body (Benard-von Karman Vortex Street. Laboratory and theoretical research of this phenomenon for different cross-sections are still ongoing. In the following, the flow lines of the behind the bridge deck and the pressure distribution around the cross-section of the deck are examined.

6.1 Pressure contours around flat decks with different web edge angles (α=14.7, 19.7, 26.6 deg)

The variation of the web edge angle of the flat trapezoidal deck under the turbulence flow around the bridge decks is investigated in this section. Fig. 9 shows the velocity flow at the wind velocity of 100 km/h for different web edge angles (α=14.7, 19.7, 26.6 deg). The wind flow passes above and below the deck surface uniformly and the separation of the flow is not observed at the point of contact with the wall. By reduction of the side web edge angle, wind flow passes the deck steadily. Fig. 10 shows the pressure contours around flat decks with different outer edge angles. The pressure distribution around the cross-section reduces at a smaller web angle. It is observed that a smaller angle of approximately 15 degrees between the bottom plate and the side edge is the optimal value for the trapezoidal deck cross-section. It has a positive effect on the uniform passage of airflow around the deck and prevents oscillating flows to form vortex shedding behind the deck body and in turn, reduce the incoming forces and the probability of resonance condition.

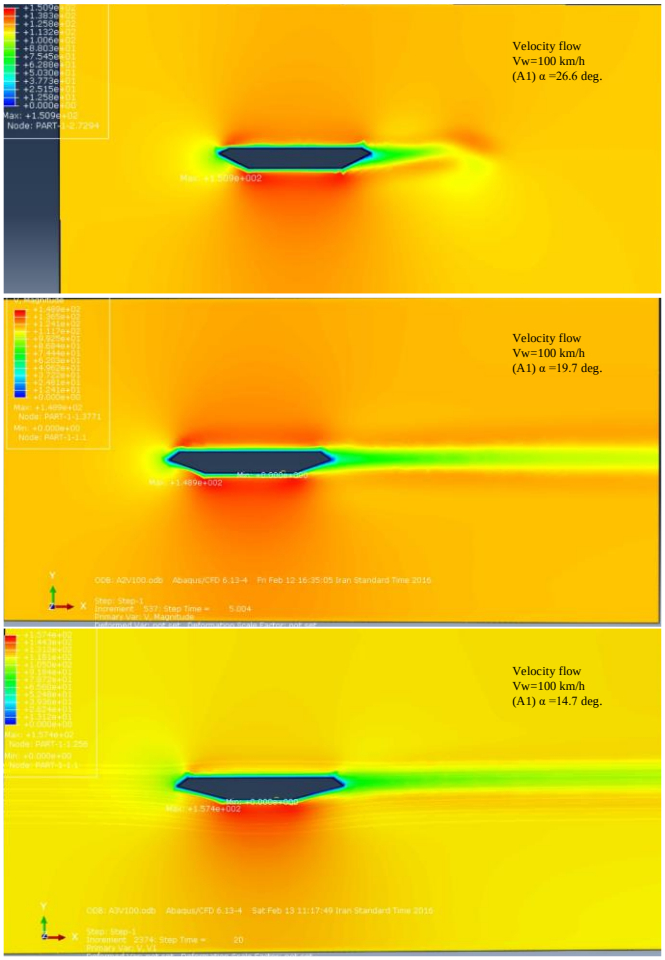

Fig. 9. Flow velocity on flat decks with different lateral edge angles (α=14.7, 19.7, 26.6 deg)

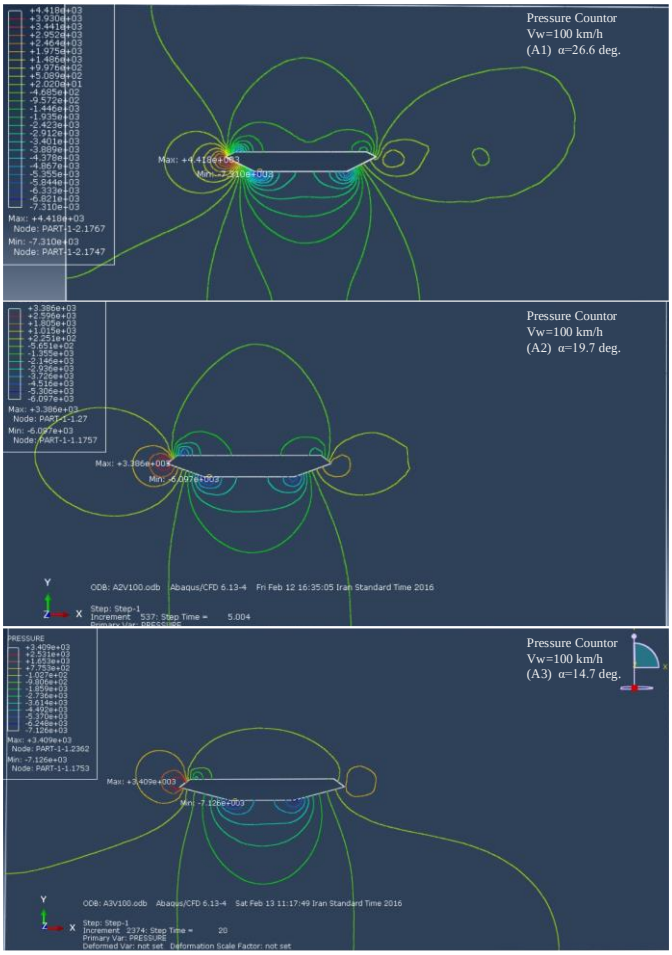

Fig. 10. Pressure contours around flat decks with different outer edge angles (α=14.7, 19.7, 26.6 deg)

6.2 Variation of Flow velocity and Pressure contours in flat decks with different width to height ratio of cross section (B/D ratio=12.67, 10, 7.5, 5)

The flow rate around the different flat decks with the ratio of width-to-height (B/D ratio = 5, 7.5, 10, 12.67) is examined in Fig. 11. By increasing this ratio, the velocity flow passes steadily up and down the deck without disturbing. A vortex road can be seen at low ratios, which causes shocks and severe vibration of the bridge deck. In general, by increasing the ratio of width to height of trapezoidal flat sections, the transient current crossing is improved and less vortex shedding is generated. It leads to a degradation of shocks and vibration on the bridge deck and fewer dynamic forces are applied to the surface of the deck.

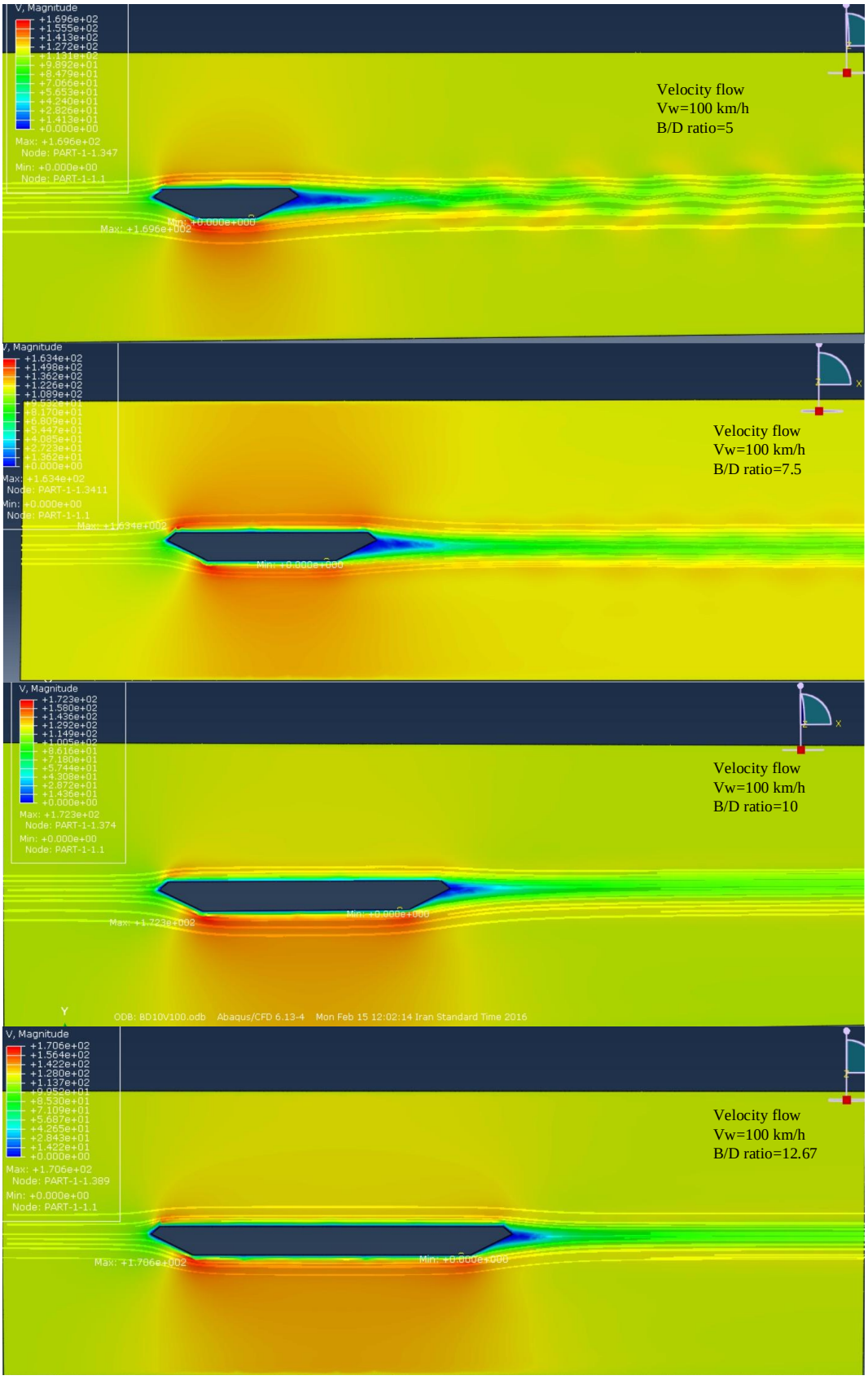

Fig. 11. Flow velocity in flat decks with different width to height ratio of cross section (B/D ratio=12.67, 10, 7.5, 5)

6.3 Variation of Flow velocity and Pressure contours around the box decks with different web angles (α=53, 63, 76, 90 deg)

The angle of the web plate to the vertical line is one of the important features of box decks. Despite the good performance

of box bridges against the gravity and seismic loads, their performance against strong wind forces also needs further investigation. In particular, the geometric characteristics of the deck section are among the important parameters that affected the aerodynamic behavior of bridge structures. In Fig. 12, box girders with various web angles (α = 53, 63, 76 90 degrees to the bottom flange are adopted to CFD-simulations. Generation of moving vortex shedding on the back of section at the upper side of the deck. The occurrence of such turbulences flow causes impact motions (Galloping) and severe vibration on the deck surface, which will lead to dynamic forces. The most critical case is the box section with a vertical web case. Vortex shedding operates in a counterclockwise direction to rotate the section body. Fig. 13 shows the pressure countors of the single-cell box section with different web angles. The pressure distribution around the section indicates that the pressure applied to the section with the vertical web is 25% higher than in the case where the web plate position at an angle of 53 degrees toward the bottom flange.

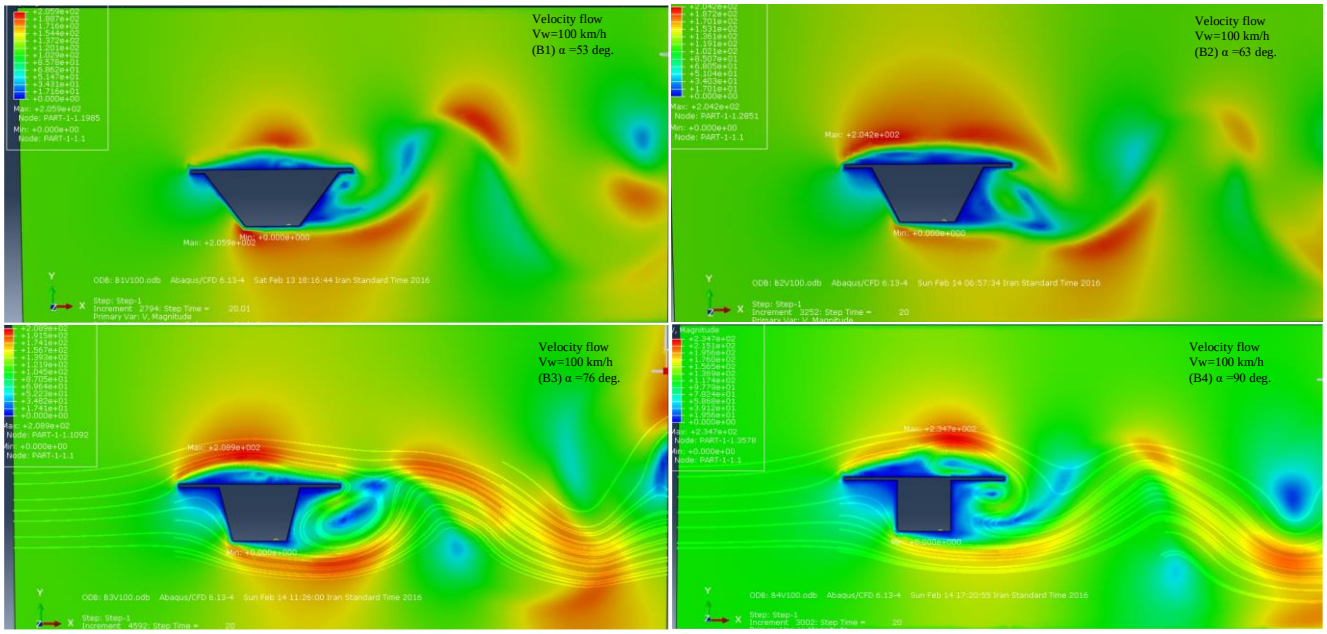

Fig. 12. View the flow velocity around the box decks with different web angles (α=53, 63, 76, 90 deg)

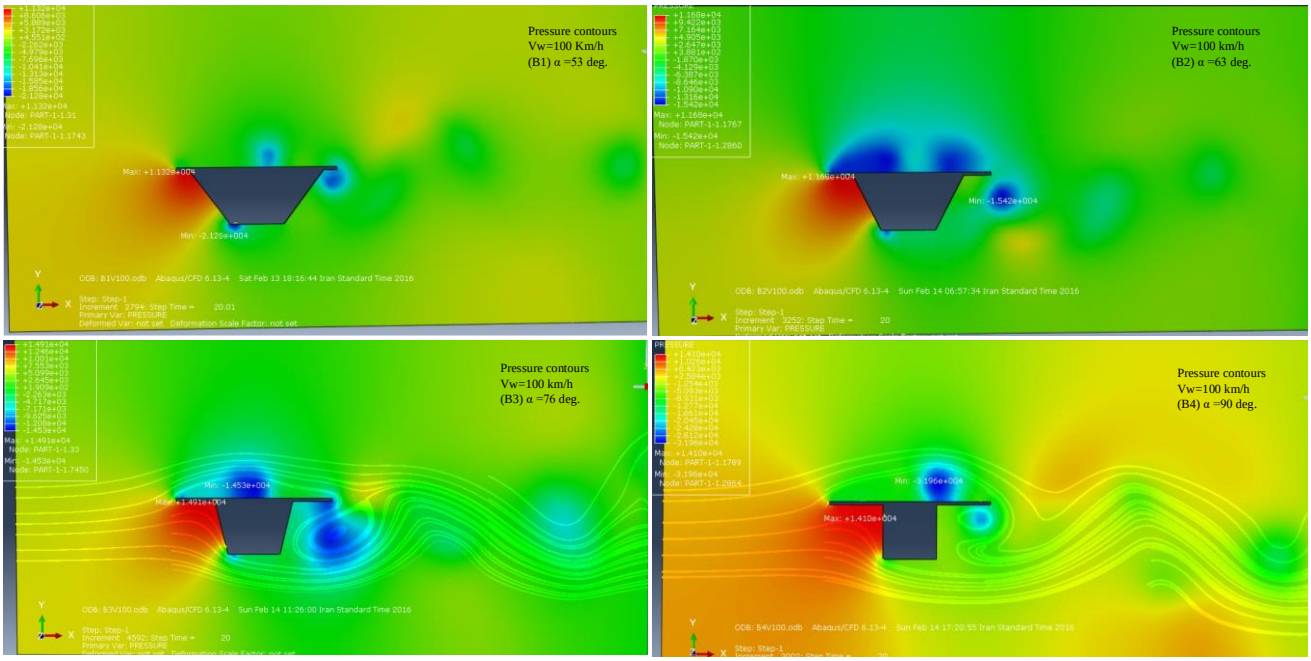

Fig. 13. Distribution of pressure and flow lines around box decks with different life angles (α=53, 63, 76, 90 deg)

6.4 Distribution of pressure and flow lines around box decks with different web angles due to increasing wind velocites

In this section, an attempt has been made to investigate the effect of increasing the critical flutter wind velocity on the box section with various web angles. To this aim, the flutter wind velocity is increased from 60 to 100 km/h. Fig. 14 shows the contours of wind flow lines around single-cell box decks. It can be seen that the wind turbulence condition has become more critical with increasing the box web angle. At an angle of 76 and above, a vortex shedding is formed on the leeward side of the deck. Increasing the flutter wind velocity causes the formation of longer vortices street leeward side of the deck section. The maximum flow velocity values at the top and bottom of the section cause severe vibration motions and in turn greater forces. The pressure distribution around the deck wall is also plotted for the same models (See Fig. 15). It is shown that with increasing flutter wind velocity, the pressure on the wall facing the wind increases by about 4.5 times so that this increase is more critical in the vertical wall and has increased up to 5 times. It is seen that increasing suction pressure on the leeward side of the deck generates the moment forces to rotate the section counterclockwise direction. The pressure distribution conditions around the decks indicate that the uplift forces applied at the windward edge of the deck. Vortices shedding on the leeward side of the deck are caused by negative pressures and acts against the uplift-edged pressure. The distributed negative pressure field affects the bridge deck almost uniformly. The pressure field increases due to the counterclockwise rotation moments. By vortex shedding of moving the vortex to the right side of the deck, an increase in positive moments is seen.

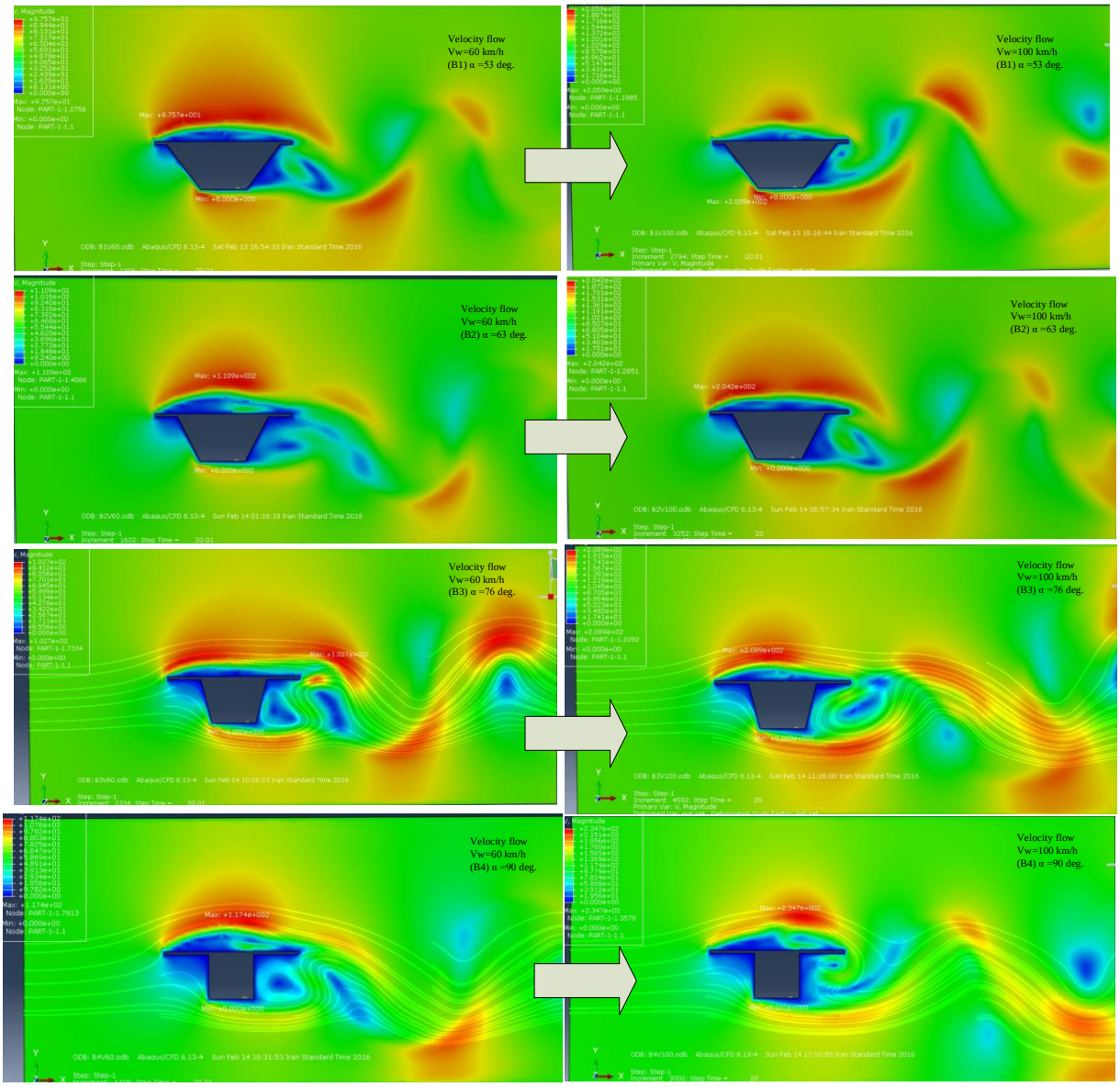

Fig. 14. Flow lines around box decks with different web angles with increasing the wind speed

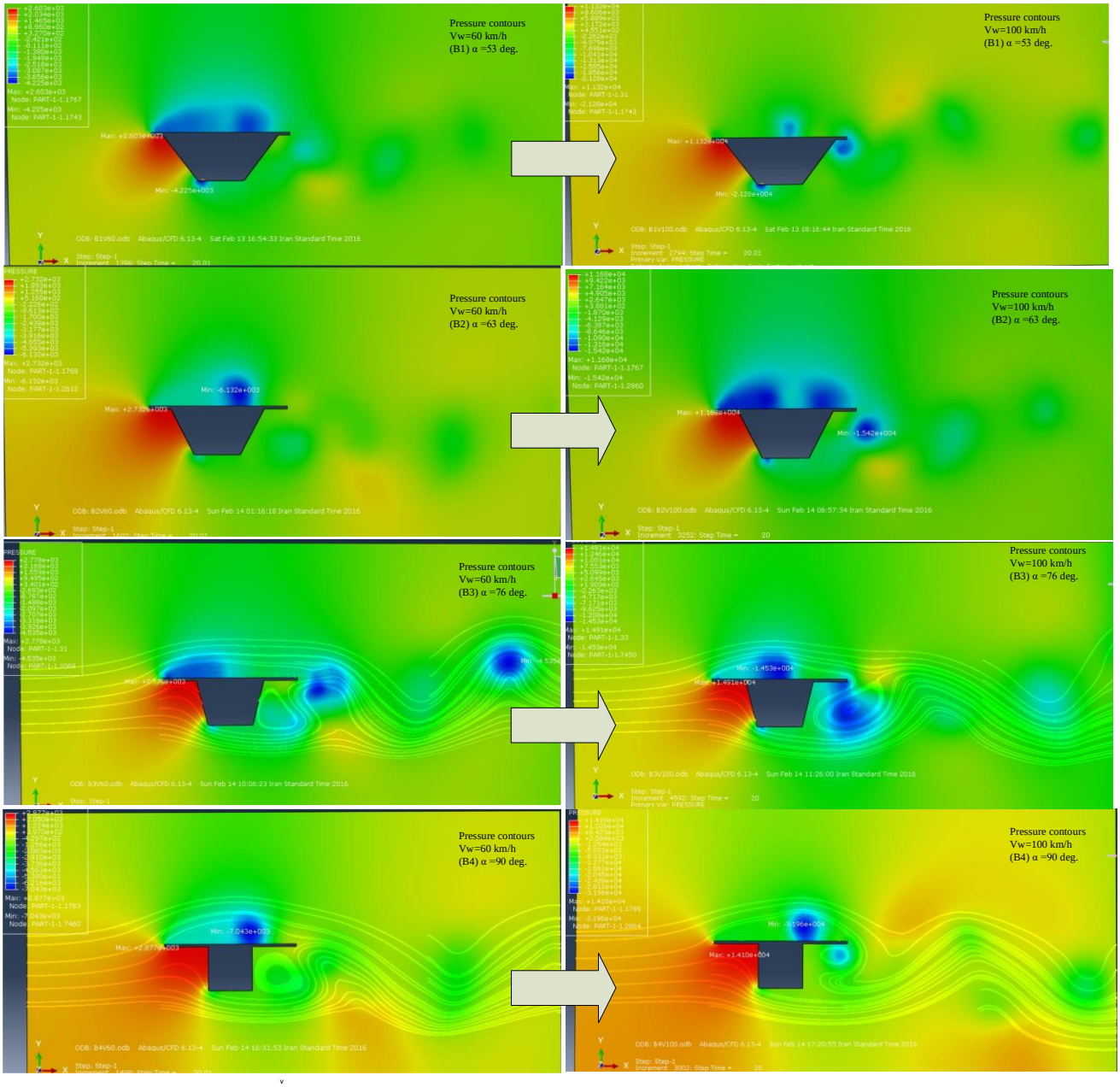

Fig. 15. Distribution of pressure and flow lines around box decks with different web angles under the influence of increasing wind speed

6.5 Variation of Flow velocity and Pressure contours around the box girder with (a) cells linked by top flanges and (b) cells linked both by top and bottom flanges

Both models of continuous cell box beam (with cells linked both by the top and bottom flanges) and double cells box beam (with cells linked by top flanges) are made and put them subjected to flutter condition at a wind speed of 100 km/h (See Fig. 16). The vortex shedding path at the back of the wind in both sections is similar. Fig. 17 shows how the pressure is distributed around the deck cross-section. According to pressure countors, there is no appreciable force in the gap area between the cells. In general, the pressure distribution is similar for both sections. The single cell box or a pair of cells will not have much effect on the turbulence of the flow around the wall of the deck. The goal in deck section designing is to establish a more uniform flow around the section as much as possible. In general, fixed vortex currents can be used to push the laminar flows and wind energy dissipation to get the optimal section. In this case, maybe the fixed vortex shedding formed between the two modules plays a positive role in dissipating incoming wind energy.

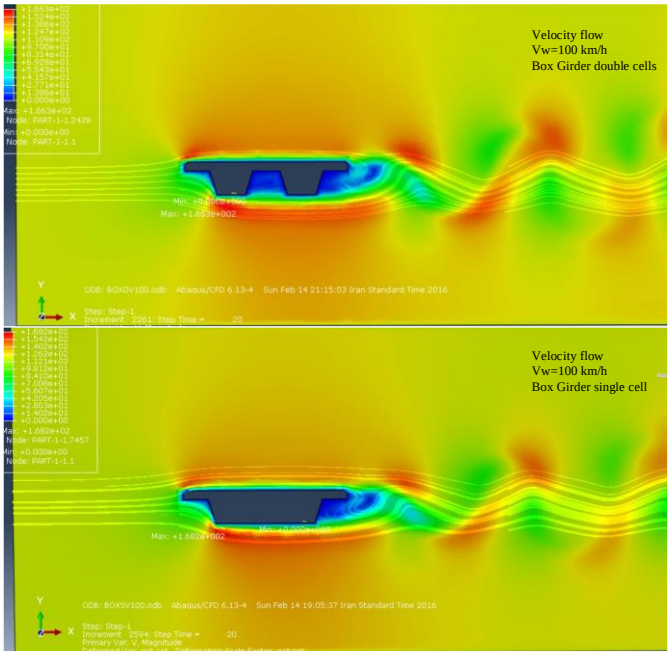

Fig. 16. The velocity of the flow around the box girder with (a) cells linked by top flanges and (b) cells linked both by top and bottom flanges

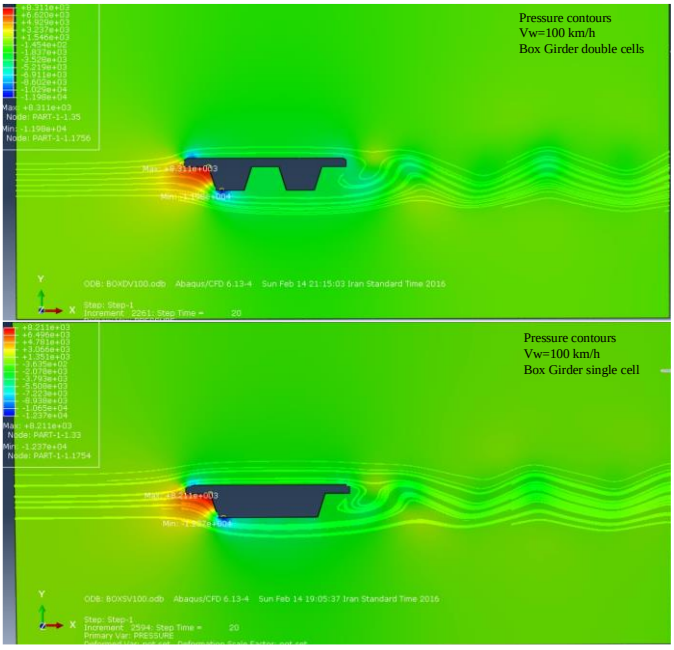

Fig. 17. The pressure countor of the flow around the box girder with (a) cells linked by top flanges and (b) cells linked both by top and bottom flanges

6.6 Comparison of velocity vector around the bridge decks with different cross sections

Bridges with flat trapezoidal decks have a higher critical flutter wind velocity compared to closed box section decks. Due to aerodynamic characteristics of sharp-edged trapezoidal decks, wind flows cross around the deck uniformly. The absence of turbulence and all kinds of vortex shedding causes fewer flactuations and impact loads to the deck. In brief, the flat shape of the deck improves the dynamic balance of the bridge. But in the case of box decks, turbulent flows due to the cross-sectional shape leads to the formation of vortex shedding at the leeward side of the deck section which imposed additional dynamic forces on the deck and even leads to resonance conditions.

It has been observed that the high ratio of the width of the section to its height has a positive role in the wind flow passing above and below the section. In trapezoidal deck sections with a higher ratio of width to height, wind flow crosses the contact surface of the deck without creating severe vortices, which in turn will cause fewer vibrations. The vortex road formed in the leeward side of box sections indicates the need for further investigations and tests in using single-cell box sections for long-span bridges, particularly those prone to strong winds.

Fig. 18 shows the velocity vectors inside the flow domain. It is found that the wind flows cross above and below the flat deck uniformly and the separation of the wind flow is not observed at the point of contact with the wall and leeward side. However, the separation of the wind flow from the upper surface of the deck is clearly seen in single-cell box sections. The most critical condition is related to the single-cell box section with vertical webs. Vortex shedding on the deck cause vibrations and in turn dynamic forces at the entrance sector of the deck. The wind flow separation of single-cell box decks is seen clearly when wind flow cross-section.

Using Equation (1) and the values provided for air at 30°C (Table 1), the Reynolds number values for the proposed sections can be calculated. This value of Reynolds number is obtained for trapezoidal flat deck section, box sections with one double cell, and box sections with single-cell, 5’250’490, 6’058’256 and 14’135’932 respectively. As can be seen, Reynolds’ values are relatively large, increasing by about 14 million, leading to severe vortex shedding leeward the sections. The calculation of turbulent wind flows for large-size and sections with real dimension gives the large Reynolds numbers. On the other hand, it is known that the flow patterns and the consequent pressure and wind forces change with Reynolds numbers. This also makes it difficult to use wind tunnel results directly on real structures. Qualitative treatments of wind flow over a deck section depends largely on the Reynolds number; similar wind flow patterns often appear when the shape and Reynolds number is matched. Other factors such as surface roughness have a serious effect as well. CFD-Simulation methods also have some deficiencies for large Reynolds numbers and require additional measures for use in practical work.

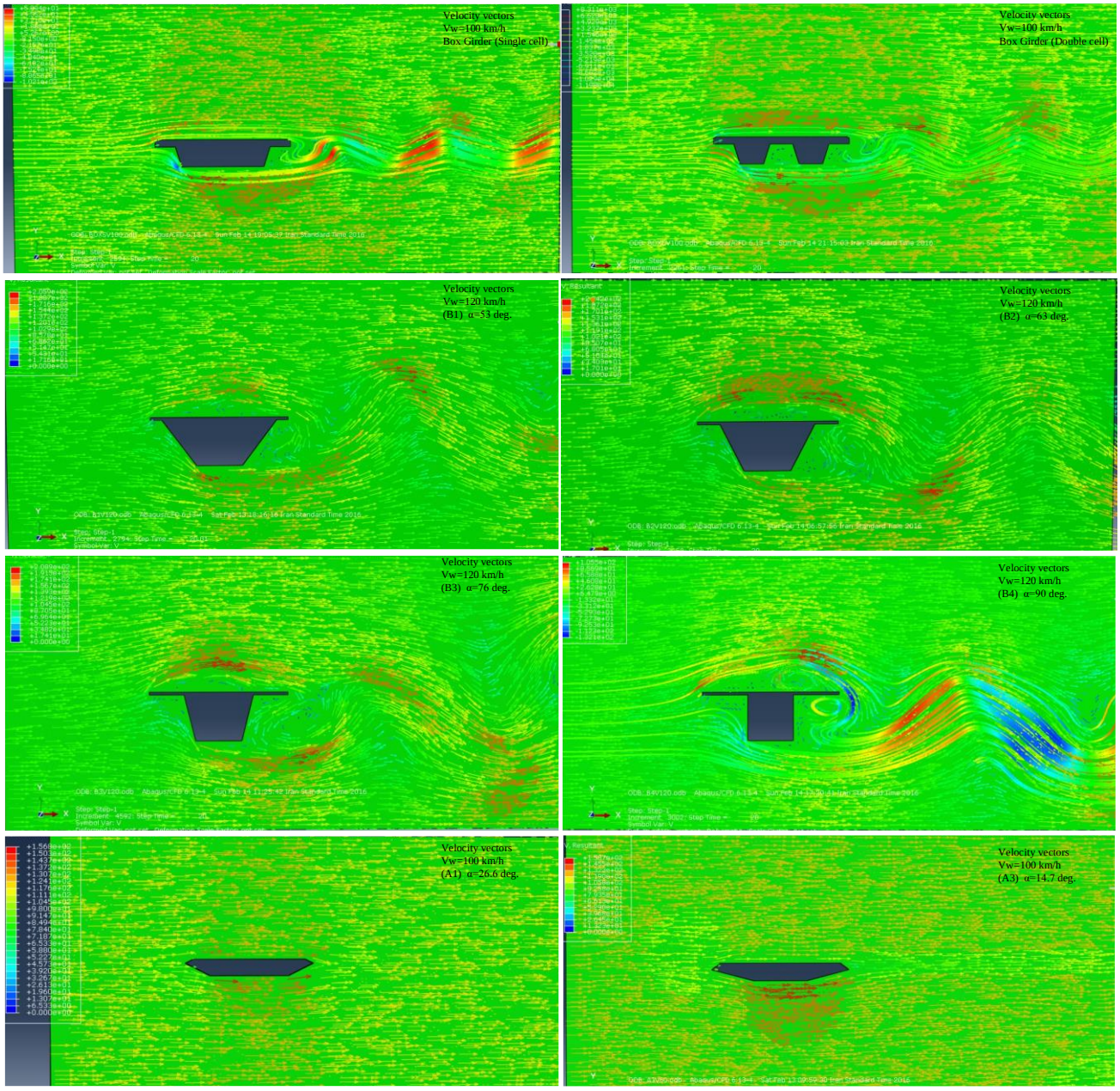

Fig. 18. Flow velocity vector in the perimeter of bridge decks with different cross section

7. Conclusions

A brief overview of laboratory experiments and modeling of bridge deck air flutter is discussed. The geometry of the deck cross-section and their aerodynamic behavior are considered in the present study. The main focus is the geometric parameters of the sections were considered as a design variable and previously tested in wind tunnels. An attempt has been made to compare and validate the results of the dynamic analysis of the current study with identical laboratory results.

- The phenomena of wind flow, turbulence, vortex shedding, and aerodynamic instability of the wind in flutter are introduced. Then, the assumptions used in fluid dynamics analysis, including deck design variables, wind flutter domain, boundary conditions, and meshing, are described and interpreted. The steps of performing dynamic analysis and the parameters and material properties introduced to ABAQUS platform V6.14 [24] are presented and the results of the analyzes are compared and interpreted. Based on the results obtained from several bridge deck models under wind flutter conditions and fluid dynamic analyzes, the following results can be mentioned.
- Due to the relatively long length of the deck, wind currents are expected to stick to the deck surface. Then the eddy boundary layers are reattached to the end of the deck. The sharp edges facing the bridge deck, vortices are expected to form periodically behind the deck, which is called (vortex road). To obtain all these phenomena, a fine-grained mesh is needed.

- Long-span Bridges with flat trapezoidal decks have a higher critical flutter wind speed than closed box decks, owing to the wind flows smoothly pass through the top and bottom of the deck. In the case of box decks, turbulent currents due to the section shape causes the occurrence of vortex shedding behind the section (See Fig. 17). In other words, the flat trapezoidal shape of the deck improves the dynamic instability of the bridge.
- The shape of the bridge deck is very important for dynamic responses. The aerodynamic behavior of trapezoidal flat sections under the influence of wind forces is better than box sections. That's why, the majority of long-length modern suspension bridge decks were constructed using a variety of trapezoidal flat sections (or sections with sharp edges), when compared to box sections. The results show the high sensitivity of the aerodynamic behavior of the bridges to changes in the geometry of the end edges of the decks.
- Calculating turbulent flows for large and real size sections yields large numbers. The flow patterns and the consequent pressure/wind forces that change with Reynolds numbers reduces the reliability of direct use of wind tunnel results. Dynamic flow calculations for large Reynolds numbers show that as Reynolds values increase, the vortex shedding behind the cross-section becomes more severe.
- In the study of the aerodynamic effect of the geometric shape of the bridge deck, the angle of the web plate of a box girder relative to the vertical line, which is one of the important characteristics of box decks is examined. The results showed that the pressures applying to rotate the cross-section acts counter-clockwise direction, increase with rising angle, and the most critical state is related to the vertical upright position (Fig. 13). The pressure on the box girder web in the vertical position is about 25% higher than the case where the web position is at an angle of 53 degrees to the bottom flange.
- By increasing the width-to-height ratio of trapezoidal flat sections, the uniform flow conduction is improved and less vortex shedding is seen. By reducing shocks and oscillating movements on the bridge deck, fewer dynamic forces are applied to the surface of the bridge deck (Fig. 12).
- The lower angle (approximately 15 degrees between the bottom flange plate and the side web panel is the optimal value for the side edge of flat trapezoidal cross-section, has a positive effect on the uniform passage of airflow around the deck, and the lack of vortex shedding around the cross-section reduces the oscillating vibrations and in turn decrease the applied forces and probability of resonance condition. (Fig. 9).
- In the investigation of the effect of increasing flutter velocity on box sections with different web angles, it is observed that with increasing the speed of the flutter, the pressure on the wall facing the wind is about 4.5 times, so that this increase is more critical in the vertical upright webs up to 5 times.
- An increase in suction pressure in the opposite direction of the wind is also seen, and the torsional moments rotate the section counterclockwise. The pressure distribution around the decks showed that the existing pressure creates lifting forces at the loaded edge of the deck. Negative pressures cause the vortex shedding on the right of the deck and act against the edge pressure towards the wind. The distributed negative pressure field affects the bridge deck almost uniformly. The pressure field increases due to the counterclockwise rotation. Considering these works, it can be seen as a result of moving to the right of the vortices on the deck. When they are scattered from the deck surface when an increase in the positive moment is observed.

References

[1] Eurocode 1, 1991-1-4, Actions on Structures - Part 1-4: General actions – Wind actions, 2004.

[2] H. Lee and J. Moon, "Static wind load evaluation under steady-state wind flow for 2-edge sloped box girder by using wind tunnel test", Hindawi, Advances in Civil Engineering, https://doi.org/10.1155/2019/9397527, 9397527, pp.12, 2019.

[3] X. Ying, F. Xu, M. Zhang, Zh. Zhang, "Numerical explorations of the limit cycle flutter characteristics of a bridge deck", Journal of Wind Engineering and Industrial Aerodynamics, http://dx.doi.org/10.1016/j.jweia.2017.06.020, Vol.169, pp.30–38, 2017.

[4] H. Tang, K.M. Shum, Y. Li, "Investigation of flutter performance of a twin-box bridge girder at large angles of attack", Journal of Wind Engineering & Industrial Aerodynamics, https://doi.org/10.1016/j.jweia.2019.01.010, Vol.186, pp. 192–203, 2019.

[5] M. C Montoya, S. Hernandez, F. Nieto, A. Kareem, "Aero-structural design of bridges focusing on the buffeting response: Formulation, parametric studies and deck shape tailoring", Journal of Wind Engineering and Industrial Aerodynamics, https://doi.org/10.1016/j.jweia.2020.104243, Vo. 204, 104243, 2020.

[6] I. Kusano, J. B. Jakobsen and J. T. Snæbjörnsson, "CFD simulations of a suspension bridge deck for different deck shapes with railings and vortex mitigating devices", IOP Conf. Series: Materials Science and Engineering, doi:10.1088/1757-899X/700/1/012003, 700, 012003, 2019.

[7] Sh. Liu, C. S. Cai and Y. Han, "Time-domain simulations of turbulence effects on the aerodynamic flutter of longspan bridges", Advances in Bridge Engineering, https://doi.org/10.1186/s43251-020-00007-6, Vol.1(7), 2020.

[8] Y. Yang, R. Zhou, Y. Ge, Y. Du and L. Zhang, "Sensitivity analysis of geometrical parameters on the aerodynamic performance of closed-box girder bridges", Sensors, doi:10.3390/s18072053, Vol.18, 2053, 2018.

[9] S. O. Hansen and T. Thorbek Lars, Analysis of Critical Flutter Wind Velocities During Construction, 1996.

[10] S. O. Hansen and T. Thorbek Lars, Buffeting Response of the Great Belt Suspension Bridge During Construction, 1997.

[11] S. O. Hansen and T. Thorbek Lars, Aerodynamic Derivatives for The Completed Great Belt Bridge Aerodynamic Derivatives Recieved from Lars Thorbek In an Excel Spreadsheet. The data is based on wind tunnel tests carried out in 1996, 2008.

[12] J. B. Frandsen, "Numerical bridge deck studies using finite elements. Part I: flutter, Journal of Fluids and Structures", https://doi.org/10.1016/j.jfluidstructs.2003.12.005, Vol.19, No. 2, pp. 171-191. 2004.

[13] A. M. Awruch and A. L. Braun, "Numerical simulation of the wind action on a long-span bridge deck", Journal of the Brazilian Society of Mechanical Sciences and Engineering, https://doi.org/10.1590/S1678-58782003000400007, pp. 1678-5878, 2003.

[14] A. Cigada, G. Diana, E. Zappa, "On the response of a bridge deck to turbulent wind: a new approach", Journal of Wind Engineering and Industrial Aerodynamics, https://doi.org/10.1016/S0167-6105(02)00230-1, Vol. 90, pp. 1173–1182, 2002.

[15] A. Larsen and A. Wall, "Shaping of bridge box girders to avoid vortex shedding response", Journal of Wind Engineering and Industrial Aerodynamics, https://doi.org/10.1016/j.jweia.2012.04.018, Vol. 104–106, pp. 159–165, 2012.

[16] A. Larsen, G. L. Larose, "Dynamic wind effects on suspension and cable-stayed bridges", Journal of Sound and Vibration, https://doi.org/10.1016/j.jsv.2014.06.009, Vol. 334, pp.2–28, 2015.

[17] C. Anina, H. Rüdiger, B. Stanko, "Numerical simulations and experimental validations of force coefficients and flutter derivatives of a bridge deck", Journal of Wind Engineering and Industrial Aerodynamics, https://doi.org/10.1016/j.jweia.2015.04.017, Vol. 144, pp. 172–182, 2015.

[18] Y. Han, C. S. Cai, J. Zhang, S. Chen, Xu. He, "Effects of aerodynamic parameters on the dynamic responses of road vehicles and bridges under cross winds", Journal of Wind Engineering and Industrial Aerodynamics, https://doi.org/10.1016/j.jweia.2014.08.013, Vol.134, pp.78–95, 2014.

[19] S. Pindado, J. Meseguer, S. Franchini, "Short note: The influence of the section shape of box-girder decks on the steady aerodynamic yawing moment of double cantilever bridges under construction", Journal of Wind Engineering and Industrial Aerodynamics, doi:10.1016/j.jweia.2005.05.005, Vol. 93, pp. 547–555, 2005.

[20] G. L. Larose, H. Tanaka, N.J. Gimsing and C. Dyrbye, "Direct measurements of buffeting wind forces on bridge decks", Journal of Wind Engineering and Industrial Aerodynamics, https://doi.org/10.1016/S0167-6105(98)00073-7, Vol. 74-76, pp.809-818, 1998.

[21] G. Morgenthal and F.A. McRobie, "A comparative study of numerical methods for fluid-structure interaction analysis in long-span bridge design", Wind and Structures an International Journal. DOI: 10.12989/was.2002.5.2_3_4.101, 2000.

[22] G. Morgenthal, Fluid-Structure interaction in Bluff-Body aerodynamics and long-span bridge design: phenomena and methods, University of Cambridge, Department of Engineering. Technical Report No. CUED/D-STRUCT/TR.187, 2001.

[23] S. O. Hansen and O. C. Dyrbye, Wind Loads on Structures, 0 471 95651 1, 1997.

[24] S. Michael, ABAQUS/Standard User's Manual, Version 6.14. Providence, RI, Dassault Systèmes Simulia Corp, 2014.

Improvement of Cluster Head Selection in LEACH for Reducing Energy Consumption in Wireless Sensor Networks

Ali Qasim Alrubaye*, Indrit Myderrizi**

*Institute of Graduate Studies, Electrical and Electronics Engineering Program, Istanbul Gelisim University, Istanbul, Türkiye.
**Department of Avionics, Faculty of Applied Sciences, Istanbul Gelisim University, Istanbul, Türkiye.
(alialmezel87@gmail.com, imyderrizi@gelisim.edu.tr)

‡Ali Qasim Alrubaye, Indrit Myderrizi, Tel: +90 212 422 70 00,
alialmezel87@gmail.com

Received: 27.03.2022 Accepted: 21.10.2022

Abstract- Sensor nodes (motes) are randomly dispersed in wireless sensor network (WSN) domains. Motes in WSNs coordinate for producing information of high quality and each scattered mote routes that information back to fixed or mobile base stations (BSs). One of the problems with sensor nodes is battery constraints that limit network lifetime, meaning mots contain limited power depending on size, battery life, and memory. Aggregation-based routing algorithm, low energy adaptive clustering hierarchy (LEACH), is envisaged as a highly adequate solution to reduce power consumption. The main objective of this work is to optimize the LEACH protocol primarily in terms of power consumption. There are two reasons to explore hierarchical routing. First, sensor networks have high density and there is a large amount of redundancy in communication. The second is to increase the scalability of the sensor network by considering the security aspects of the communication. In many studies using the LEACH algorithm, the performance analysis of WSNs with the MATLAB simulator has revealed some flaws that need to be eliminated in the algorithm. The proposed research uses the improved IV-LEACH protocol to ensure an even distribution of selected cluster heads of motes over the network to increase the efficiency of the LEACH protocol. Using MATLAB, average life, energy consumption, and efficiency are analyzed to determine mots suitability for use in WSNs. The IV-LEACH protocol outperforms the LEACH protocol, improving energy consumption, lifetime and throughput in a simulated network of 150 nodes.
Keywords: WSN; LEACH protocol; average lifetime; energy consumption.

1. Introduction

With technological advances, sensors are in high demand for monitoring and surveillance applications. Small, autonomous and inexpensive sensors can be used to monitor various parameters such as chemical structure, velocity, voltage and temperature. Most of these sensors wirelessly send the measured parameters to a base station (BS), i.e. a sink. Receivers and transmitters feed the sensors and enable wireless communication. These autonomous sensors are distributed in an area and communicate with each other to form a WSN. WSNs are typically used to monitor applications in areas where replacing or accessing sensor nodes is not possible or practicable from an economic point of view (for example, in high voltage substations) [1-2].

To ensure the continuity of these applications, short-lived sensors need to be operated for longer periods of time. Transmissions from sensor nodes in WSNs consume a significant amount of energy, which is considered one of the primary reasons for the premature failure of nodes. Therefore, network lifetime and energy consumption stand out as major concerns in WSNs. As WSNs grow in popularity in networking fields, researchers use a broad range of energy effective approaches to decrease the energy consumption of nodes and extend the network lifetime [3]. Despite their positive aspects, WSNs have some limitations. To overcome these formidable problems, multiple algorithms have emerged over time to increase network lifetime. These algorithms configure routes with minimal delay for sensor broadcast and communication, reduce power cost, and provide adequate, error-free data transmission. Among them, the Low Energy

Adaptive Clustering Hierarchy (LEACH) algorithm is consistently popular. LEACH is a cluster-based routing protocol that performs well and is an adaptive algorithm [4-9].

A modified LEACH algorithm is presented in [10], which calculates the optimal cluster head (CH) proportion in the selection of CH nodes, considering the residuary energy and current location problem, and uses the Stable Election Protocol (SEP) algorithm to compute the divergent CH selection probability for ahead and standard nodes. The enhanced energy efficient LEACH (EEE-LEACH) algorithm proposed in [11] decreases energy consumption in the WSN by utilizing multiple-input multiple-output (MIMO) method and selects the shortest route for data transmission in channel undergoing fading. The research in [12] first analyzes the basic operations related to LEACH and performs optimization using a Genetic Algorithm (GA) to make longer the life span of the network. A LEACH-based clustering algorithm, which minimizes the energy consumption from sensors pending data transmission, is presented in [13]. The LEACH protocol has been customized to extend the lifetime of the WSN. In [14], the high packet loss of LEACH routing is solved through network optimization by adding a Delay Tolerant Network (DTN) structure that allows transmission in exceptional conditions such as a crowded WSN. In the optimization algorithm based on the LEACH algorithm presented in [15], the energy efficiency of the BS is increased to share the energy consumption with the network, resulting in approximately twice the network's lifetime in contrast to the classic LEACH algorithm. A new CH selection mechanism is developed in [16] to increase energy performance of the Two-Level Hierarchy for the Low Energy Adaptive Clustering Hierarchy (TL-LEACH). Extended TL-LEACH outperforms in terms of energy consumption, node's service life, and communication latency is significantly reduced. In [17], a Residual Energy-Aware Clustering Transformation (REACT) protocol is proposed for LEACH, which improves its achievement by providing a clustering technique. A modified end-to-end reliable LEACH (ME-LEACH) algorithm is presented in [18] to boost the lifetime of a WSN by altering the data communication from a CH to the BS. Another proposed modified version of LEACH, which uses an intermediary CH to transmit data in [19], aims to extend network lifetime and forward a greater amount of data compared to the classic protocol.

The issue of energy consumption is very important in WSNs, so it is vital to decrease energy consumption and increase network lifetime. As mentioned above, LEACH is one of the major accepted routing protocols, as it is characterized by saving energy, resulting in increased network lifetime by random selection of the CH. However, this protocol has some limitations; the CH excludes the residual node energy in the selection process, resulting in the node's death. Also, the distance between the BS and the nodes is excluded when choosing CH. The power consumption process of the CH distant from the BS is higher than the nodes' power consumption near to the BS. These limitations need to be evaluated when designing the WSN protocol. The main factor to consider is the amount of energy consumed by the sensor and how reducing the energy consumed increases the network lifetime.

In this article, an optimized LEACH-based protocol has been developed. It takes advantage of the energy features of protocols such as TL-LEACH, E-LEACH and PEGASIS to increase the efficiency of the LEACH protocol by establishing the even distribution of the selected CHs in WSN. Using MATLAB®, the performance of the proposed protocol has been validated compared to several LEACH-based protocols. The LEACH algorithm is a cluster-based protocol of routing, so it performs well and is adaptable.

2. Theoretical Background

2.1 Protocols Used in WSN

The most important purpose of routing a WSN is to provide highly efficient, continuous networks. Flat direction, hierarchical direction, and positional (location-based) direction are three possible classifications for the protocol based on the shape of the network [20-22]. The protocols used in WSNs are shown in Fig. 1.

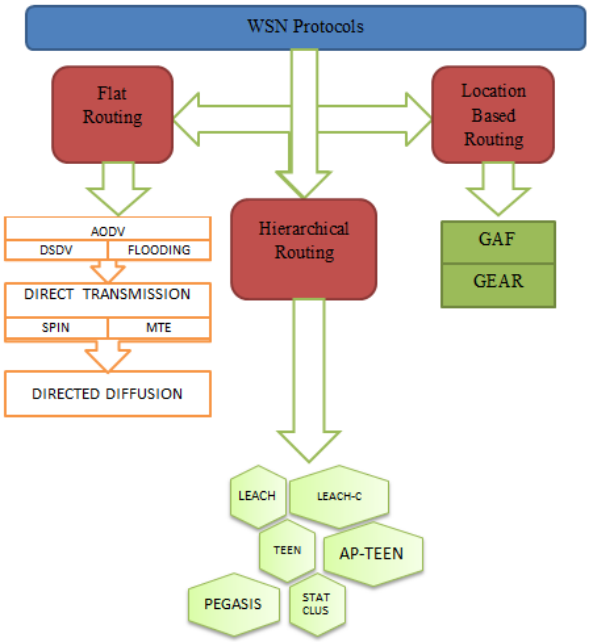

Figure 1: WSN protocols

Flat Routing Protocol: The flat routing protocol can be defined as a multi-hop protocol in which each node has a fixed functional role, all nodes participate in the operation to complete the sensing process, and each node cannot be

identified individually as a result of many nodes. Flat routing consists of several protocols as: Ad-hoc On-demand Distance Vector (AODV), Flooding, Minimum Transmission Energy (MTE), Sensor Protocol for Information via Negotiation (SPIN), Destination Sequenced Distance Vector (DSDV), Direct Transmission and Directed Diffusion (DD).

Hierarchical Routing Protocol: Hierarchical algorithms divide nodes into subregions called clusters. One CH is selected from each cluster to allow communication between clusters. CHs are then responsible for the management and transmission of data aggregated inside of the area they supervise. Hierarchical or cluster-based routing generally comprises of two layers of routing: one layer is related to CH selection and the other is related to routing [23]. Hierarchical routing consists of several protocols as: LEACH, LEACH-Centralised (C), Threshold-sensitive Energy Efficient sensor Network (TEEN), Adaptive TEEN (APTEEN), and Power Efficient GAthering in Sensor Information Systems (PEGASIS).

Location-Based Routing Protocol: Location-based algorithms use a node's location information to find and transmit data to a destination in a specific network area [23]. Network nodes do not require complex calculations to find the next hop in this protocol; direction decision is based on location information. This protocol consists of a set of facts of network nodes. First, the nodes must be identified by a Global Positioning System (GPS) device. Second, each of the nodes must know the location of adjacent nodes. Third, the source node must be aware of the destination node's location [24]. Location-based routing consists of several protocols, such as Geographic Adaptive Fidelity (GAF) and Geographical and Energy-Aware Routing (GEAR).

2.2 LEACH Protocol

This protocol is a self-organizing, adaptive clustering protocol that uses randomization to uniformly allocate the energy load between the sensors in the network. Nodes here arrange themselves into local clusters with one node performing as the local BS or CH. To prevent premature death of selected CHs LEACH involves random rotation of the high-energy CH location to rotate between diverse sensors i.e. precautions are taken to avoid draining the battery of a single sensor [4]. When CH is selected, it sends a message to other nodes to join that cluster. However, sensor nodes other than CH select their CH based on the minimum transmit energy required for communication. After a cluster is created, the CH determines the communication schedule for its nodes [25]. The topology of the LEACH clustering structure is illustrated in Fig. 2.

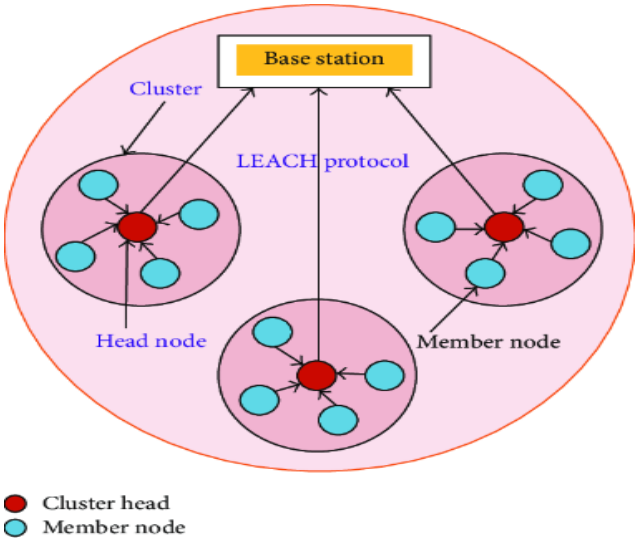

Figure 2: LEACH clustering structure [25].

LEACH Algorithm: The LEACH process is separated into rounds. Every round starts with the set-up phase where the clusters are arranged. Following this is the steady-state phase where data is transmitted to the BS. To reduce the overhead, the steady-state phase is longer compared to the set-up phase [4]. The main steps involved in the operation of LEACH are listed below.

I. Set-up Phase

At this phase, the nodes are dynamically divided out into various clusters and per cluster, a CH is randomly selected from among the cluster nodes. During the time that clusters are created, a random number in the range of 0 to 1 is chosen and compared with the threshold *T(n)*. If the selected value is smaller than *T(n)*, the node is made as a CH for the present round; else, the node remains a member node [26]. The threshold *T(n)* is calculated using the following equation:

$$T(n) = \begin{cases} \frac{p}{1-p\times(r \bmod \frac{1}{p})} & if\ n \in G \\ 0 & otherwise \end{cases} \quad (1)$$

where *p* is the percentage of the CHs amid all the nodes, *r* is the number of the round, and *G* is the collections of the nodes that have not been CHs in the course of the last *1/p* rounds [4].

After some nodes are identified as CH, the entire network is announced by sending control message packets. These messages are received by all network nodes and then stored in their memory. These nodes then determine whichever cluster to participate based on the strength of the received signal. The strength of the signal indicates the distance between nodes and CHs. Nodes will be closest to one of the clusters. This process helps reduce energy consumption. After the cluster to join is determined, standard nodes (not CHs) send a control packet to the CHs, informing them that they have joined certain clusters [25].

After formation of the clusters, all CHs decide on the communication timeline for their cluster. CH and other members utilise Time Division Multiple Access (TDMA) for communication within the cluster. The CH shares out the data transmission time slot when each cluster member can transmit data to its CH. TDMA time schedule assists nodes reduce the number of unneeded communications [27].

II. Steady-State Phase

In the steady-state phase where the data transmission occurs, every sensor node accumulates data from the environment and transmits it to its own CH. Each sensor node acts in accordance with the timeline for communication. CHs acquire data from cluster members and conduct data fusion. Data fusion process brings down large amounts of data and shrinks data packets, which assists CHs utilize far less energy to send data to the BS. Sending data packets from CHs to the BS constitutes the final stage for the steady-state phase [27].

Later, the network goes back to the cluster creation procedure, which involves new set-up and steady-state phases. The periodic process keeps going on until the entire network dies [27]. The description of the two phases above explains how individual clusters communicate between nodes in the respective cluster. But radio, by its very nature, is a broadcast medium. Therefore, transmission in one cluster has an effect on (and therefore disrupts) communication in the neighboring cluster. To lower such interference, each cluster transmits utilizing different CDMA codes [4]. The first-order radio model, consisting of both transmitter and receiver electronics, and a transmitter amplifier presented in [4], [27-30], provides a simple low-energy radio model in terms of energy requirements suitable for a complete analysis of radio signals to be filtered from neighboring clusters. Fig. 3 shows the flowchart of LEACH.

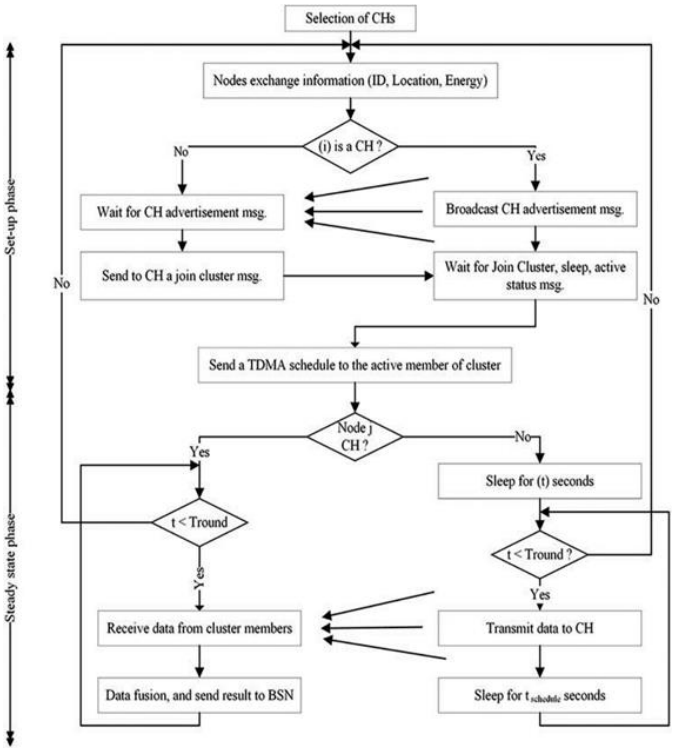

Figure 3: Flowchart of LEACH algorithm [31]

3. Overview of the Proposed IV-LEACH Protocol

At the core of the proposed IV-LEACH protocol, besides the original protocol of LEACH, there are advantages provided by TL-LEACH and E-LEACH protocols for energy consumption, and there is also the PEGASIS protocol used for equal distribution of energy in the WSN [32]. The flow diagram of the IV-LEACH protocol is displayed in Fig. 4. The most substantial features of the protocols incorporated in the IV-LEACH are described in the sections below.

3.1 TL-LEACH Protocol

Different from the LEACH, where CHs send data directly to the BS in a single hop, the TL-LEACH protocol introduced in [33] works in a two-level hierarchy [5]. TL-LEACH applies arbitrary rotation of local cluster BSs (primary CHs and secondary CHs) [33], that is, it uses one of the CHs located between CH and BS as a relay terminal. The bi-level nature of TL-LEACH decreases the number of nodes allocated for data transfer to BS and then efficaciously lowers the overall energy consumption [7], [9]. TL-LEACH utilizes two methods to attain energy and delay efficiency: random, adaptive, self-configuring cluster formation and localized control for data transmissions [22].

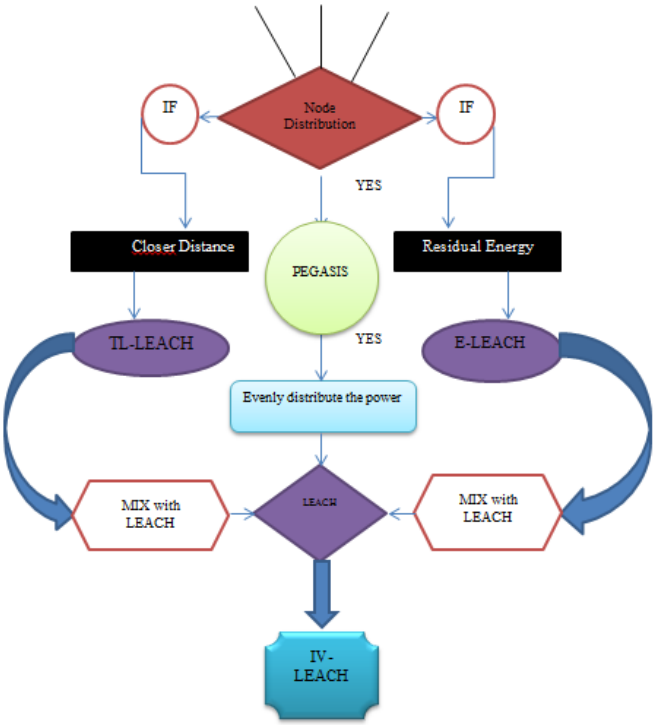

Figure 4: Flowchart of the proposed IV-LEACH protocol

3.2 E-LEACH Protocol

Enhanced-LEACH (E-LEACH) upgrades the CH selection process by making the residual energy of the node the primary metric in determining whether the node is a CH in the next round [9]. In the E-LEACH protocol, initially all nodes have the same energy and the same probability of being the CH, i.e. in the first round, each node has a chance to be the CH, indicating that the selection is random like in the LEACH protocol [5]. After the first round, the remaining energy of each node is determined and considered in the selection of CH. Communication between CHs and BS requires more energy than communication between CHs and cluster members. E-LEACH selects nodes with large residual energy at the root node as CH [7]. LEACH-E extends the service life of the network by balancing the energy load between all nodes in the network [5].

3.3 PEGASIS Protocol

PEGASIS is an improved near-optimal chain-based protocol over LEACH. In PEGASIS, every node communicates solely with its nearby neighbor and transmits to the BS in turn, hence decreasing the amount of energy consumed per round [34]. The chain is created using the greedy method and the leader of chain is responsible of transmitting the data to BS, where every network node changes its task as the leader permitting a better even distribution of energy load among WSN nodes and thus the energy consumption for each round is balanced [35]. In PEGASIS, the sensor nodes are randomly located, and each of them is capable of data sensing, wireless communication, data fusion and positioning. The energy load is evenly shared out between the sensor nodes in the WSN [22].

control. It also shows the definition of the server name, server port, and key assigned to the server.

3.4 IV-LEACH Protocol

The IV-LEACH protocol uses distributed clustering method unlike LEACH. The entire sensor area is divided into sub-regions that are similar to each other. Cluster head selection from each sub-region is provided by the threshold method as selected in the LEACH protocol. Every regular node in this network can be shut down until the allotted time of transmission, minimizing the energy consumption in the nodes [32].

The inclusion of the E-LEACH protocol is to improve the CHs selection procedure. After the first round, the main measure in deciding which nodes can be CHs is the residuary energy of each of the nodes. Like the LEACH, the E-LEACH algorithm is divided into rounds. In round 1, each of the nodes has the same probability of turning into CH. This is an indication that CH is chosen at random. In subsequent rounds, since the residuary energy of each of the nodes differs after the first round of communication, it is used in the selection of the CHs. Nodes higher in energy become CHs.

In IV-LEACH, to further increase energy efficiency, one of the CHs located between the cluster and the BS is used as a relay point, as in the TL-LEACH, instead of transferring data straight-forward to the BS.

Like the LEACH, IV-LEACH has 2 phases: set-up and steady-state phases. The protection mechanism detailed in [27] has also been added to the IV-LEACH protocol to lower the number of re-clustering operations required.

Once cluster heads are selected, a WSN uses the CSMA MAC protocol to announce its state. The remaining nodes make CH decisions in the current round relying on the strength of the received signal of the advertisement message. A TDMA schedule is applied to all cluster group members to send a message to the CH. Then CH sends the data to BS. When a CH is selected for a particular area, the steady-state phase begins. A flowchart of this distributed clustering algorithm is shown in Fig. 5 [36].

As soon as the clusters are formed and the TDMA time schedule is determined, the transmission of data begins and the steady-state phase is initiated. Assuming that the nodes always contain all the data, the nodes communicate during the transmission times allocated to the CH. Such a type of transmission utilizes minimum energy (the level is selected according to the received strength of the CH advertisement

message). Then the radios of the nodes are closed until the allocated transmission time. The IV-LEACH protocol ensures a homogeneous distribution of selected CHs throughout the network.

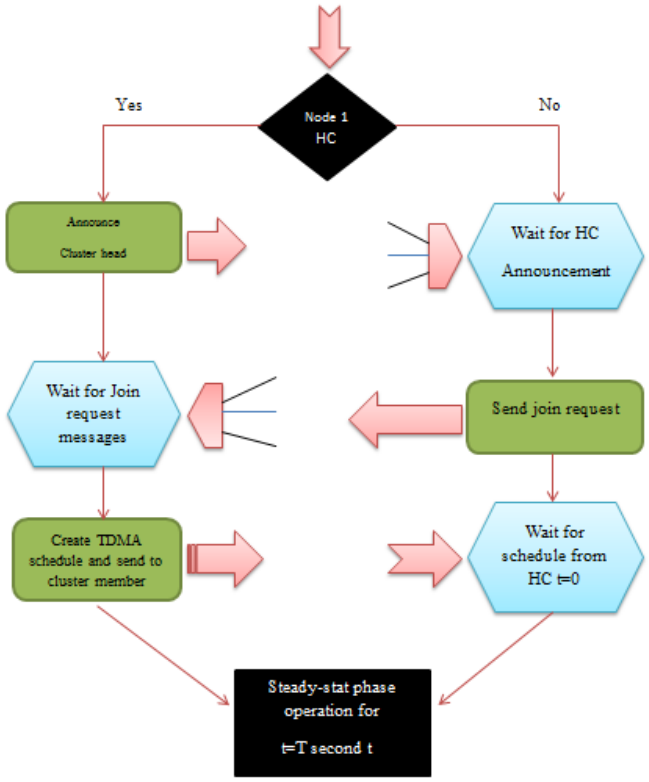

Figure 5: Cluster formation algorithm flowchart for IV-LEACH [36]

4. Protocol Performance Simulation and Analysis

The efficiency of the IV-LEACH protocol is validated by using MATLAB simulation tool and evaluation is peformed based on the period of network stability, i.e. network throughput, network lifetime and energy dissipation. Parameters used in simulations are categorized in Table 1. The nodes of the WSN are simulated to be randomly distributed over an area of 900×900 m^2 with the BS located at the central point (450, 450), as is shown in Fig. 6.

Table 1. Simulation parameters

Parameter	Value
Sensing area (W×L)	900 × 900 m^2
Number of nodes (N)	150
Initial energy of nodes (E_0)	0.5 J
Desired percentage of cluster heads	0.1 J
Position of BS	X = 450, Y = 450
Packet size for CH per round	6400 bits
Max number of simulated rounds	500
The energy of free space model amplifier	0.34 nJ
Energy for transmitting and receiving one bit	50 nJ
Amount of energy that is spent by the amplifier for transmitting bits	100 pJ
Energy of data aggregation	5 nJ

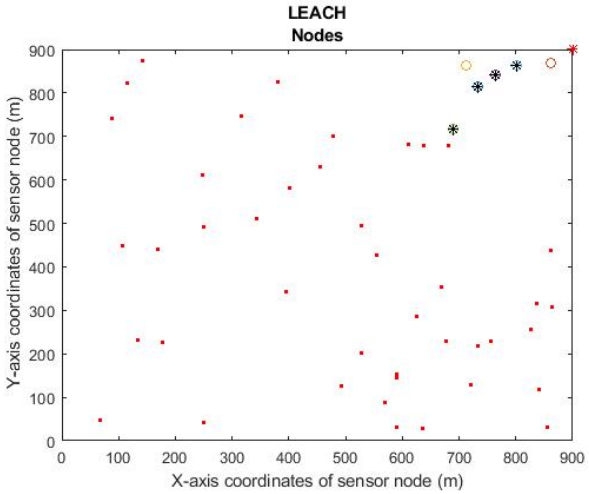

Figure 6: Location of nodes in WSN

4.1 Performance Analysis of IV-LEACH over LEACH

Lifetime of the Network: Network's lifetime represents the interval of time from the start of communication to the sensor node's death. Following 460 rounds of the IV-LEACH protocol and 300 rounds of the LEACH protocol, 10 live nodes remained. This is demonstrated in Fig. 7.

Total Energy Dissipation: The performance of WSN is greatly improved with IV-LEACH protocol over traditional LEACH protocol. As shown in Fig. 8, the average residual energy was 300 J after 250 rounds were completed in the conventional protocol, while it was 300 J over 480 rounds for the IV-LEACH protocol.

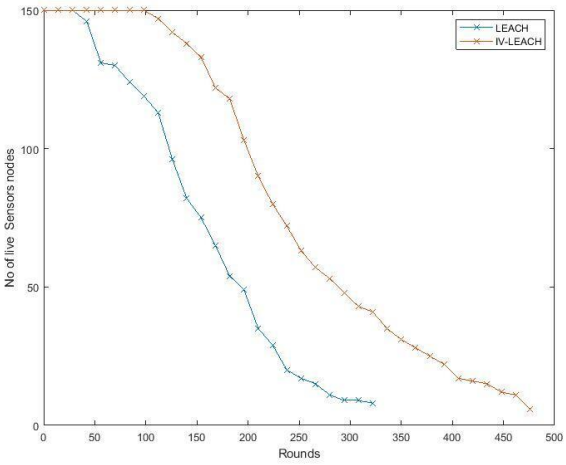

Figure 7: Lifetime of the sensor nodes

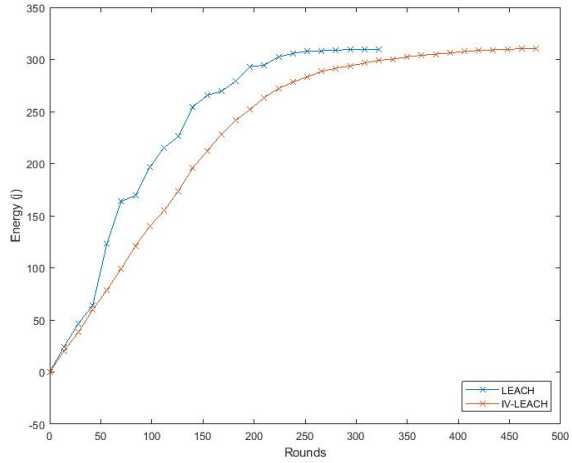

Figure 8: Total energy dissipation

Throughput of the Network: The IV-LEACH protocol outperforms the original LEACH protocol regarding the throughput of the network i.e. the number of the received data packets, as shown in Fig. 9. In the LEACH protocol, the number of packets was 7.5×10^5 per 300 rounds. But in the IV-LEACH protocol, the number of packets was 11×10^5 in 300 rounds.

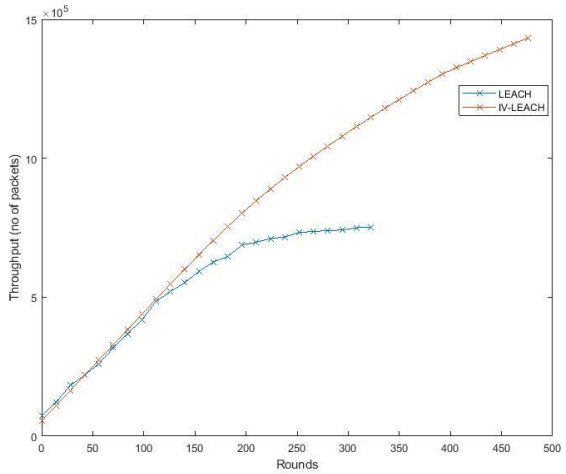

Figure 9: Throughput of the network

4.2 Comparison of Network Stability Period

The stability period of the network is represented by the first dead node (FDN), i.e. the moment when the death of the 1st sensor node occurs relative to the time after the start of the rounds. The simulation results show that the IV-LEACH protocol has higher stability compared to the E-LEACH, TL-LEACH and LEACH protocols. As shown in Fig. 10, after several simulation runs, FDN for LEACH, E-LEACH and TL-LEACH protocols occurs in five seconds, six seconds, and seven seconds, respectively. FDN for the IV-LEACH protocol takes place in eight seconds.

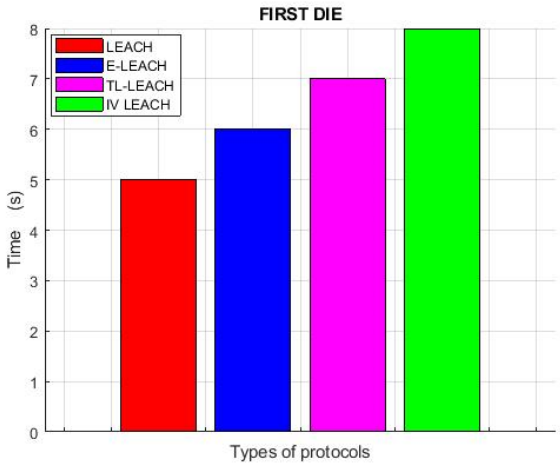

Figure 10: FDN lifetime of different LEACH protocols

Similarly, the last dead node (LDN) is also used for network stability. As shown in Fig. 11, LDN for the LEACH protocol occurs in 150 seconds. For the E-LEACH and TL-LEACH protocols, LDN occurs in 225 and 325 seconds, respectively. In the IV-LEACH protocol, LDN occurs in 450 seconds.

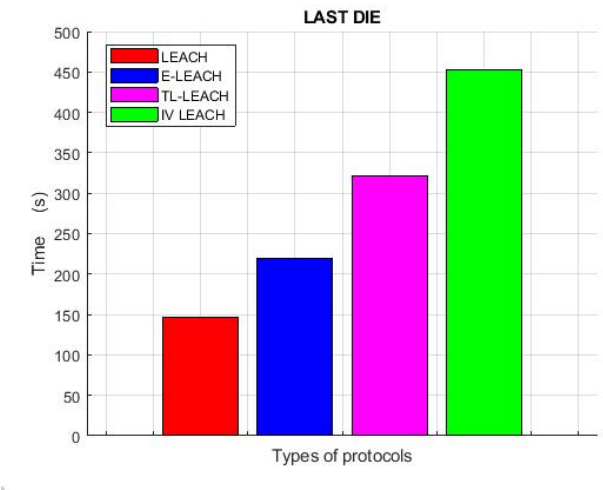

Figure 11: LDN lifetime of different LEACH protocols

5. Conclusion

Energy saving is an important issue in WSNs. In order to enhance energy efficiency and extend the service life of sensor nodes, multiple energy-aware cluster-based techniques are developed. CH selection is an essential step in cluster formation that affects network lifetime and throughput. The IV-LEACH protocol presented in this paper provides the advantageous features of E-LEACH, TL-LEACH and PEGASIS protocols as well as the selection of cluster heads evenly distributed throughout the network. The IV-LEACH routing protocol has been optimized to extend the lifetime of the sensor nodes, taking into account their residuary energy and their distance from the BS. This protocol makes it possible to extend the lifetime of the WSN. Network stability cycle is still considered short for many applications requiring reliable network feedback. IV-LEACH has been modified to enhance the stability of the network by increasing the FDN and LDN times. The simulation results obtained indicate that the IV-LEACH protocol can come through the restrictions of the LEACH protocol in terms of energy consumption, throughput and network lifetime.

References

[1] I. F. Akyildiz, et al. 'Wireless sensor networks: a survey', Computer Networks, 38 (2002), pp. 393-422.

[2] D. Jin, and S. Lin (Eds.), 'Advances in Computer Science and Information Engineering', Springer, (2012).

[3] M. Mishra, et al. 'Network Lifetime Improvement through Energy-Efficient Hybrid Routing Protocol for IoT Applications' Sensors, 21 (2021), pp. 1-26.

[4] W. R. Heinzelman, et al. 'Energy-Efficient Communication Protocol for Wireless Microsensor Networks', Proceedings of the 33rd Annual Hawaii International Conference on System Sciences, January 7-8, Maui, HI, USA (2000), pp. 1-10.

[5] H. Dhawan, and S. Waraich. 'A Comparative Study on LEACH Routing Protocol and its Variants in Wireless Sensor Networks: A Survey', International Journal of Computer Applications, 95(8) (2014), pp. 21-27.

[6] R. M. Dilip Charaan, and R. Ramash, 'Correlative Analysis On Enhanced Descendants Of LEACH Protocol For Wireless Sensor Networks', Journal of Theoretical and Applied Information Technology, 68(2) (2014), pp. 427-442.

[7] A. Kaur, and A. Grover, 'LEACH and Extended LEACH Protocols in Wireless Sensor Network-A Survey', International Journal of Computer Applications, 116(10) (2015), pp. 1-5.

[8] J. Huo, et al. 'Design and Improvement of Routing Protocol for Field Observation Instrument Networking Based on LEACH Protocol', Hindawi Journal of Electrical and Computer Engineering, (2020), pp. 1-19.

[9] D. Prabha, and V. K. Arora, 'A Survey on LEACH and its Descendant Protocols in Wireless Sensor Network', Proceedings of the International Conference on Communication, Computing & Systems, August 8-9, Punjab, India (2014), pp. 162-167.

[10] T. Yang, et al. 'Wireless Routing Clustering Protocol Based on Improved LEACH Algorithm', Proceedings of the IEEE International Conference on RFID Technology & Application (RFID-TA), September 26-28, Macau, Macao (2018), pp. 1-6.

[11] A. Bharti, et al. 'Enhanced energy efficient LEACH (EEE-LEACH) algorithm using MIMO for wireless sensor network', Proceedings of the IEEE International Conference on Computational Intelligence and Computing Research (ICCIC), December 10-12, Madurai, India (2015), pp. 1-4.

[12] R. Sujee, and K. E. Kannammal, 'Energy efficient adaptive clustering protocol based on genetic algorithm and genetic algorithm inter cluster communication for wireless sensor networks', Proceedings of the International Conference on Computer Communication and Informatics (ICCCI), January 5-7, Coimbatore, India (2017), pp. 1-6.

[13] R. Regmi, et al. 'Modified LEACH algorithm for wireless sensor networks in agricultural field', Proceedings of the IEEE International Conference on Power, Control, Signals and Instrumentation Engineering (ICPCSI), September 21-22, Chennai, India (2017). pp. 3100-3104.

[14] M. A. Rahmadhani, et al. 'Energy Consumption and Packet Loss Analysis of LEACH Routing Protocol on WSN Over DTN', Proceedings of the 4th International Conference on Wireless and Telematics (ICWT), July 12-13, Bali, Indonesis (2013), pp. 1-5.

[15] Y. Chen, et al. 'LEACH Algorithm Based on Energy Consumption Equilibrium', Proceedings of the International Conference on Intelligent Transportation, Big Data & Smart City (ICITBS), January 25-26, Xiamen, China (2018), pp. 677-680.

[16] K. Manzoor, et al. 'Enhanced TL-LEACH routing protocol for large-scale WSN applications', Proceedings of the Cybersecurity and Cyberforensics Conference (CCC), May 8-9, Melbourne, Australia (2019), pp. 35-39.

[17] P. Ullas, and K. S. Shivaprakasha, 'Residual Energy-Aware Clustering Transformation for LEACH Protocol', Journal of Telecommunications and Information Technology, 2, (2021), pp. 31-37.

[18] M. Abdurohman, et al. 'A Modified E-LEACH Routing Protocol for Improving the Lifetime of a Wireless Sensor Network', Journal of Information Processing Systems, 16(4) (2020), pp. 845-858.

[19] H. Ouldzira, et al. 'MG-leach: an enhanced leach protocol for wireless sensor network', International Journal of Electrical and Computer Engineering (IJECE), 9(4) (2019), pp. 3139-3145.

[20] J. N. Al-Karaki, and A. E. Kamal, 'Routing techniques in wireless sensor networks: a survey', IEEE Wireless Communications, 11(6) (2004), pp. 6-28.

[21] A. Rady, et al. 'Comprehensive survey of routing protocols for Mobile Wireless Sensor Networks', International Journal of Communication Systems, 34(15) (2021), pp. 1-30.

[22] X. Liu, 'A Survey on Clustering Routing Protocols in Wireless Sensor Networks', Sensors, 12(8) (2012), pp. 11113-11153.

[23] J. N. Anisi, et al. 'An Overview of Data Routing Approaches for Wireless Sensor Networks', Sensors, 12(8) (2012), pp. 3964-3996.

[24] M. Ilyas, and I. Mahgoub (Eds.), 'Handbook of Sensor Networks: Compact Wireless and Wired Sensing Systems', CRC Press, (2005).

[25] S. Ananda Kumar, et al. 'A Modified LEACH Protocol for Increasing Lifetime of the Wireless Sensor Network', Cybernetics and Information Technologies, 16(3) (2016), pp. 154-164.

[26] R. K. Kodali, et al. 'Energy Efficient m− level LEACH protocol', International Conference on Advances in Computing, Communications and Informatics (ICACCI), August 10-13, Kochi, India (2015), pp. 973-979.

[27] X. Qu, 'Energy efficient wireless sensor network with modified LEACH algorithm', Master Thesis, Blekinge Institute of Technology, (2012).

[28] H. K. Sarma, et al. 'Energy efficient communication protocol for wireless sensor networks with mobile node', International Conference on Recent Advances and Innovations in Engineering (ICRAIE), May 9-11, Jaipur, India (2014), pp. 1-6.

[29] P. Sivakumar, and M. Radhika, 'Performance Analysis of LEACH-GA over LEACH and LEACH-C in WSN', Procedia Computer Science, 125 (2018), pp. 248-256.

[30] C. Lin, and F. Jiang, 'Research of Multidimensional Optimization of LEACH Protocol Based on Reducing Network Energy Consumption', Journal of Electrical and Computer Engineering, (2021), pp. 1-9.

[31] H. Faris, et al. 'Optimization of Head Cluster Selection in WSN by Human-Based Optimization Techniques', Computers, Materials & Continua, 72(3) (2022), pp. 5643-5661.

[32] A. Q. Mohammed, 'Improvement of cluster head selection in LEACH protocol to reducing energy consumption in wireless sensor networks', Master Thesis, Istanbul Gelisim University, (2021).

[33] V. Loscri, et al. 'A Two-Levels Hierarchy for Low-Energy Adaptive Clustering Hierarchy (TL-LEACH)', IEEE Conference on Vehicular Technology (VTC), September 28-28, Dallas, TX, USA (2005), pp. 1809-1813.

[34] S. Lindsey, and C.S. Raghavendra, 'Pegasis: Power efficient gathering in sensor information systems', IEEE Aerospace Conference Proceedings, March 9-16, Big Sky, MT, USA (2002), pp. 1125–1130.

[35] A. M. Khedr, et al. 'Successors of PEGASIS protocol: A comprehensive survey', Computer Science Review, 39 (2021), pp. 1-24.

[36] W. R. Heinzelman, et al. 'An Application-Specific Protocol Architecture for Wireless Micro-Sensor Networks', IEEE Transactions on Wireless Communications, 1(4) (2002), pp. 660-670.

INTERNATIONAL JOURNAL OF ENGINEERING TECHNOLOGIES-IJET

Guide for Authors

The **International Journal of Engineering Technologies (IJET)** seeks to promote and disseminate knowledge of the various topics of engineering technologies. The journal aims to present to the international community important results of work in the fields of engineering such as imagining, researching, planning, creating, testing, improving, implementing, using and asking. The journal also aims to help researchers, scientists, manufacturers, institutions, world agencies, societies, etc. to keep up with new developments in theory and applications and to provide alternative engineering solutions to current.

The *International Journal of Engineering Technologies* is a quarterly published journal and operates an online submission and peer review system allowing authors to submit articles online and track their progress via its web interface. The journal aims for a publication speed of **60 days** from submission until final publication.

The coverage of IJET includes the following engineering areas, but not limited to:

All filed of engineering such as;

Chemical engineering

- Biomolecular engineering
- Materials engineering
- Molecular engineering
- Process engineering

Civil engineering

- Environmental engineering
- Geotechnical engineering
- Structural engineering
- Transport engineering
- Water resources engineering

Electrical engineering

- Computer engineering
- Electronic engineering
- Optical engineering
- Power engineering

Mechanical engineering

- Acoustical engineering
- Manufacturing engineering
- Thermal engineering
- Vehicle engineering

Systems (interdisciplinary) engineering

- Aerospace engineering
- Agricultural engineering
- Applied engineering
- Biological engineering
- Building services engineering
- Energy engineering
- Railway engineering
- Industrial engineering
- Mechatronics
- Military engineering
- Nano engineering
- Nuclear engineering
- Petroleum engineering

Types of Articles submitted should be original research papers, not previously published, in one of the following categories,

- Applicational and design studies.
- Technology development,

– Comparative case studies.

– Reviews of special topics.

– Reviews of work in progress and facilities development.

– Survey articles.

– Guest editorials for special issues.

Ethic Responsibilities

The publication of an article in peer-reviewed *"International Journal of Engineering Technologies"* is an essential building block in the development of a coherent and respected network of knowledge. It is a direct reflection of the quality of the work. Peer-reviewed articles support and embody the scientific method. It is therefore important to agree upon standards of expected ethical behavior for all parties involved in the act of publishing: the author, the journal editor, the peer reviewer, the publisher and the society of society-owned or sponsored journals.

All authors are requested to disclose any actual or potential conflict of interest including any financial, personal or other relationships with other people or organizations within three years of beginning the submitted work that could inappropriately influence, or be perceived to influence, their work.

Submission of an article implies that the work described has not been published previously that it is not under consideration for publication elsewhere. The submission should be approved by all authors and tacitly or explicitly by the responsible authorities where the work was carried out, and that, if accepted, it will not be published elsewhere in the same form, in English or in any other language, including electronically without the written consent of the copyright-holder.

Upon acceptance of an article, authors will be asked to complete a "Copyright Form". Acceptance of the agreement will ensure the widest possible dissemination of information. An e-mail will be sent to the corresponding author confirming receipt of the manuscript together with a "Copyright Form" form or a link to the online version of this agreement.

Author Rights

As a journal author, you retain rights for a large number of author uses, including use by your employing institute or company. These rights are retained and permitted without the need to obtain specific permission from *IJET.* These include:

- The right to make copies (print or electronic) of the journal article for your own personal use, including for your own classroom teaching use;
- The right to make copies and distribute copies (including via e-mail) of the journal article to research colleagues, for personal use by such colleagues for scholarly purposes;
- The right to post a pre-print version of the journal article on internet web sites including electronic pre-print servers, and to retain indefinitely such version on such servers or sites for scholarly purposes
- the right to post a revised personal version of the text of the final journal article on your personal or institutional web site or server for scholarly purposes
- The right to use the journal article or any part thereof in a printed compilation of your works, such as collected writings or lecture notes.

Article Style

Authors must strictly follow the guide for authors, or their articles may be rejected without review. Editors reserve the right to adjust the style to certain standards of uniformity. Follow Title, Authors, Affiliations, Abstract, Keywords, Introduction, Materials and Methods, Theory/Calculation, Conclusions, Acknowledgements, References order when typing articles. The corresponding author should be identified with an asterisk and footnote. Collate

acknowledgements in a separate section at the end of the article and do not include them on the title page, as a footnote to the title or otherwise.

Abstract and Keywords:

Enter an abstract of up to 250 words for all articles. This is a concise summary of the whole paper, not just the conclusions, and is understandable without reference to the rest of the paper. It should contain no citation to other published work. Include up to six keywords that describe your paper for indexing purposes.

Abbreviations and Acronyms:

Define abbreviations and acronyms the first time they are used in the text, even if they have been defined in the abstract. Abbreviations such as IEEE, SI, MKS, CGS, sc, dc, and rms do not have to be defined. Do not use abbreviations in the title unless they are unavoidable.

Text Layout for Peer Review:

Use single column layout, double spacing and wide (3 cm) margins on white paper at the peer review stage. Ensure that each new paragraph is clearly indicated. Present tables and figure legends in the text where they are related and cited. Number all pages consecutively; use 12 pt font size and standard fonts; Times New Roman, Helvetica, or Courier is preferred.

Research Papers should not exceed 12 printed pages in two-column publishing format, including figures and tables.

Technical Notes and *Letters* should not exceed 2,000 words.

Reviews should not exceed 20 printed pages in two-column publishing format, including figures and tables.

Equations:

Number equations consecutively with equation numbers in parentheses flush with the right margin, as in (1). To make equations more compact, you may use the solidus (/), the exp function, or appropriate exponents. Italicize Roman symbols for quantities and variables, but not Greek symbols. Use an dash (–) rather than a hyphen for a minus sign. Use parentheses to avoid ambiguities in denominators. Punctuate equations with commas or periods when they are part of a sentence, as in

$$C = a + b \qquad (1)$$

Symbols in your equation should be defined before the equation appears or immediately following. Use “Eq. (1)” or “equation (1),” while citing.

Figures and Tables:

All illustrations must be supplied at the correct resolution:

* Black and white and colour photos - 300 dpi

* Graphs, drawings, etc - 800 dpi preferred; 600 dpi minimum

* Combinations of photos and drawings (black and white and color) - 500 dpi

In addition to using figures in the text, upload each figure as a separate file in either .tiff or .eps format during submission, with the figure number.

Table captions should be written in the same format as figure captions; for example, “Table 1. Appearance styles.”. Tables should be referenced in the text unabbreviated as “Table 1.”

References:

Please ensure that every reference cited in the text is also present in the reference list (and viceversa). Any references cited in the abstract must be given in full. Unpublished results and personal communications are not recommended in the reference list, but may be mentioned in the text. Citation of a reference as “in press” implies that the item has been accepted for publication. Number citations consecutively in square brackets [1]. Punctuation follows the bracket [2]. Refer simply to the reference number, as in [3]. Use “Ref. [3]” or Reference [3]” at the beginning of a sentence: “Reference [3] was …”. Give all authors’ names; use “et al.” if there are six authors or more. For papers published in translated journals, first give the English citation, then the original foreign-language citation.

Books

[1] J. Clerk Maxwell*, A Treatise on Electricity and Magnetism,* 3rd ed., vol. 2. Oxford:Clarendon Press, 1892, pp.68-73.

Journals

[2] Y. Yorozu, M. Hirano, K. Oka, and Y. Tagawa, “Electron spectroscopy studies on magneto-optical media and plastic substrate interface”, *IEEE Transl. J. Magn. Japan*, vol. 2, pp. 740-741, August 1987.

Conferences

[3] Çolak I., Kabalci E., Bayindir R., and Sagiroglu S, “The design and analysis of a 5-level cascaded voltage source inverter with low THD”, *2nd PowerEng Conference*, Lisbon, pp. 575-580, 18-20 March 2009.

Reports

[4] IEEE Standard 519-1992, Recommended practices and requirements for harmonic control in electrical power systems, *The Institute of Electrical and Electronics Engineers*, 1993.

Text Layout for Accepted Papers:

A4 page margins should be margins: top = 24 mm, bottom = 24 mm, side = 15 mm. Main text should be given in two column. The column width is 87mm (3.425 in). The space between the two columns is 6 mm (0.236 in). Paragraph indentation is 3.5 mm (0.137 in). Follow the type sizes specified in Table. Position figures and tables at the tops and bottoms of columns. Avoid placing them in the middle of columns. Large figures and tables may span across both columns. Figure captions should be centred below the figures; table captions should be centred above. Avoid placing figures and tables before their first mention in the text. Use the abbreviation “Fig. 1,” even at the beginning of a sentence.

Type size (pts.)	Appearance		
	Regular	**Bold**	*Italic*
10	Authors' affiliations, Section titles, references, tables, table names, first letters in table captions,figure captions, footnotes, text subscripts, and superscripts	**Abstract**	
12	Main text, equations, Authors' names, [a]		*Subheading (1.1.)*
24	Paper title		

Submission checklist:

It is hoped that this list will be useful during the final checking of an article prior to sending it to the journal's Editor for review. Please consult this Guide for Authors for further details of any item. Ensure that the following items are present:

- ❖ One Author designated as corresponding Author:

• E-mail address

• Full postal address

• Telephone and fax numbers

- ❖ All necessary files have been uploaded

• Keywords: a minimum of 4

• All figure captions (supplied in a separate document)

• All tables (including title, description, footnotes, supplied in a separate document)

- ❖ Further considerations

• Manuscript has been "spellchecked" and "grammar-checked"

• References are in the correct format for this journal

• All references mentioned in the Reference list are cited in the text, and vice versa

• Permission has been obtained for use of copyrighted material from other sources (including the Web)

• Color figures are clearly marked as being intended for color reproduction on the Web (free of charge) and in print or to be reproduced in color on the Web (free of charge) and in black-and-white in print.

Article Template Containing Author Guidelines for Peer-Review

First Author*, Second Author**‡, Third Author***

*Department of First Author, Faculty of First Author, Affiliation of First Author, Postal address

**Department of Second Author, Faculty of First Author, Affiliation of First Author, Postal address

***Department of Third Author, Faculty of First Author, Affiliation of First Author, Postal address

(First Author Mail Address, Second Author Mail Address, Third Author Mail Address)

‡ Corresponding Author; Second Author, Postal address, Tel: +90 312 123 4567, Fax: +90 312 123 4567,corresponding@affl.edu

Received: xx.xx.xxxx Accepted:xx.xx.xxxx

Abstract- Enter an abstract of up to 250 words for all articles. This is a concise summary of the whole paper, not just the conclusions, and is understandable without reference to the rest of the paper. It should contain no citation to other published work. Include up to six keywords that describe your paper for indexing purposes. Define abbreviations and acronyms the first time they are used in the text, even if they have been defined in the abstract. Abbreviations such as IEEE, SI, MKS, CGS, sc, dc, and rms do not have to be defined. Do not use abbreviations in the title unless they are unavoidable.

Keywords- Keyword1; keyword2; keyword3; keyword4; keyword5.

2. Introduction

Authors should any word processing software that is capable to make corrections on misspelled words and grammar structure according to American or Native English. Authors may get help by from word

processor by making appeared the paragraph marks and other hidden formatting symbols. This sample article is prepared to assist authors preparing their articles to IJET.

Indent level of paragraphs should be 0.63 cm (0.24 in) in the text of article. Use single column layout, double-spacing and wide (3 cm) margins on white paper at the peer review stage. Ensure that each new paragraph is clearly indicated. Present tables and figure legends in the text where they are related and cited. Number all pages consecutively; use 12 pt font size and standard fonts; Times New Roman, Helvetica, or Courier is preferred. Indicate references by number(s) in square brackets in line with the text. The actual authors can be referred to, but the reference number(s) must always be given. Example: "..... as demonstrated [3, 6]. Barnaby and Jones [8] obtained a different result ...."

IJET accepts submissions in three styles that are defined as Research Papers, Technical Notes and Letter, and Review paper. The requirements of paper are as listed below:

- Research Papers should not exceed 12 printed pages in two-column publishing format, including figures and tables.
- Technical Notes and Letters should not exceed 2,000 words.
- Reviews should not exceed 20 printed pages in two-column publishing format, including figures and tables.

Authors are requested write equations using either any mathematical equation object inserted to word processor or using independent equation software. Symbols in your equation should be defined before the equation appears or immediately following. Use “Eq. (1)” or “equation (1),” while citing. Number equations consecutively with equation numbers in parentheses flush with the right margin, as in Eq. (1). To make equations more compact, you may use the solidus (/), the exp function, or appropriate exponents. Italicize Roman symbols for quantities and variables, but not Greek symbols. Use an dash (–) rather than a hyphen for a minus sign. Use parentheses to avoid ambiguities in denominators. Punctuate equations with commas or periods when they are part of a sentence, as in

$$C = a + b \tag{1}$$

Section titles should be written in bold style while sub section titles are italic.

3. Figures and Tables

3.1. Figure Properties

All illustrations must be supplied at the correct resolution:

- Black and white and colour photos - 300 dpi
- Graphs, drawings, etc - 800 dpi preferred; 600 dpi minimum
- Combinations of photos and drawings (black and white and colour) - 500 dpi

In addition to using figures in the text, Authors are requested to upload each figure as a separate file in either .tiff or .eps format during submission, with the figure number as Fig.1., Fig.2a and so on. Figures are cited as “Fig.1” in sentences or as “Figure 1” at the beginning of sentence and paragraphs. Explanations related to figures should be given before figure. Figures and tables should be located at the top or bottom side of paper as done in accepted article format.

Figure 1. Engineering technologies.

Table captions should be written in the same format as figure captions; for example, “Table 1. Appearance styles.”. Tables should be referenced in the text unabbreviated as “Table 1.”

Table 1. Appearance properties of accepted manuscripts

Type size (pts.)	Appearance		
	Regular	**Bold**	*Italic*
10	Authors’ affiliations, Abstract, keywords, references, tables, table names, figure captions, footnotes, text subscripts, and superscripts	**Abstract**	
12	Main text, equations, Authors’ names, Section titles		*Subheading (1.1.)*
24	Paper title		

4. Submission Process

The *International Journal of Engineering Technologies* operates an online submission and peer review system that allows authors to submit articles online and track their progress via a web interface. Articles that are prepared referring to this template should be controlled according to submission checklist given in “Guide f Authors”. Editor handles submitted articles to IJET primarily in order to control in terms of compatibility to aims and scope of Journal.

Articles passed this control are checked for grammatical and template structures. If article passes this control too, then reviewers are assigned to article and Editor gives a reference number to paper. Authors registered to online submission system can track all these phases.

Editor also informs authors about processes of submitted article by e-mail. Each author may also apply to Editor via online submission system to review papers related to their study areas. Peer review is a critical element of publication, and one of the major cornerstones of the scientific process. Peer Review serves two key functions:

- Acts as a filter: Ensures research is properly verified before being published
- Improves the quality of the research

5. Conclusion

The conclusion section should emphasize the main contribution of the article to literature. Authors may also explain why the work is important, what are the novelties or possible applications and extensions. Do not replicate the abstract or sentences given in main text as the conclusion.

Acknowledgements

Authors may acknowledge to any person, institution or department that supported to any part of study.

References

[1] J. Clerk Maxwell, *A Treatise on Electricity and Magnetism*, 3rd ed., vol. 2. Oxford:Clarendon Press, 1892, pp.68-73. (Book)

[2] H. Poor, *An Introduction to Signal Detection and Estimation*, New York: Springer-Verlag, 1985, ch. 4. (Book Chapter)

[3] Y. Yorozu, M. Hirano, K. Oka, and Y. Tagawa, "Electron spectroscopy studies on magneto-optical media and plastic substrate interface", *IEEE Transl. J. Magn. Japan*, vol. 2, pp. 740-741, August 1987. (Article)

[4] E. Kabalcı, E. Irmak, I. Çolak, "Design of an AC-DC-AC converter for wind turbines", *International Journal of Energy Research*, Wiley Interscience, DOI: 10.1002/er.1770, Vol. 36, No. 2, pp. 169-175. (Article)

[5] I. Çolak, E. Kabalci, R. Bayindir R., and S. Sagiroglu, "The design and analysis of a 5-level cascaded voltage source inverter with low THD", *2nd PowerEng Conference*, Lisbon, pp. 575-580, 18-20 March 2009. (Conference Paper)

[6] IEEE Standard 519-1992, Recommended practices and requirements for harmonic control in electrical power systems, *The Institute of Electrical and Electronics Engineers*, 1993. (Standards and Reports)

Article Template Containing Author Guidelines for Accepted Papers

First Author*, Second Author**‡, Third Author***

*Department of First Author, Faculty of First Author, Affiliation of First Author, Postal address

**Department of Second Author, Faculty of First Author, Affiliation of First Author, Postal address

***Department of Third Author, Faculty of First Author, Affiliation of First Author, Postal address

(First Author Mail Address, Second Author Mail Address, Third Author Mail Address)

‡ Corresponding Author; Second Author, Postal address, Tel: +90 312 123 4567,

Fax: +90 312 123 4567,corresponding@affl.edu

Received: xx.xx.xxxx Accepted:xx.xx.xxxx

Abstract- Enter an abstract of up to 250 words for all articles. This is a concise summary of the whole paper, not just the conclusions, and is understandable without reference to the rest of the paper. It should contain no citation to other published work. Include up to six keywords that describe your paper for indexing purposes. Define abbreviations and acronyms the first time they are used in the text, even if they have been defined in the abstract. Abbreviations such as IEEE, SI, MKS, CGS, sc, dc, and rms do not have to be defined. Do not use abbreviations in the title unless they are unavoidable.

Keywords Keyword1, keyword2, keyword3, keyword4, keyword5.

1. Introduction

Authors should any word processing software that is capable to make corrections on misspelled words and grammar structure according to American or Native English. Authors may get help by from word processor by making appeared the paragraph marks and other hidden formatting symbols. This sample article is prepared to assist authors preparing their articles to IJET.

Indent level of paragraphs should be 0.63 cm (0.24 in) in the text of article. Use single column layout, double-spacing and wide (3 cm) margins on white paper at the peer review stage. Ensure that each new paragraph is clearly indicated. Present tables and figure legends in the text where they are related and cited. Number all pages consecutively; use 12 pt font size and standard fonts; Times New Roman, Helvetica, or Courier is preferred. Indicate references by number(s) in square brackets in line with the text. The actual authors can be referred to, but the reference number(s) must always be given. Example: "..... as demonstrated [3,6]. Barnaby and Jones [8] obtained a different result ...."

IJET accepts submissions in three styles that are defined as Research Papers, Technical Notes and Letter, and Review paper. The requirements of paper are as listed below:

- Research Papers should not exceed 12 printed pages in two-column publishing format, including figures and tables.
- Technical Notes and Letters should not exceed 2,000 words.
- Reviews should not exceed 20 printed pages in two-column publishing format, including figures and tables.

Authors are requested write equations using either any mathematical equation object inserted to word processor or using independent equation software. Symbols in your equation should be defined before the equation appears or immediately following. Use “Eq. (1)” or “equation (1),” while citing. Number equations consecutively with equation numbers in parentheses flush with the right margin, as in Eq. (1). To make equations more compact, you may use the solidus (/), the exp function, or appropriate exponents. Italicize Roman symbols for quantities and variables, but not Greek symbols. Use an dash (-) rather than a hyphen for a

minus sign. Use parentheses to avoid ambiguities in denominators. Punctuate equations with commas or periods when they are part of a sentence, as in

$$C = a + b \quad (1)$$

Section titles should be written in bold style while sub section titles are italic.

6. Figures and Tables

6.1. Figure Properties

All illustrations must be supplied at the correct resolution:

- Black and white and colour photos - 300 dpi
- Graphs, drawings, etc - 800 dpi preferred; 600 dpi minimum
- Combinations of photos and drawings (black and white and colour) - 500 dpi

In addition to using figures in the text, Authors are requested to upload each figure as a separate file in either .tiff or .eps format during submission, with the figure number as Fig.1., Fig.2a and so on. Figures are cited as "Fig.1" in sentences or as "Figure 1" at the beginning of sentence and paragraphs. Explanations related to figures should be given before figure.

Fig. 1. Engineering technologies.

Figures and tables should be located at the top or bottom side of paper as done in accepted article format. Table captions should be written in the same format as figure captions; for example, "Table 1. Appearance styles.". Tables should be referenced in the text unabbreviated as "Table 1."

Table 1. Appearance properties of accepted manuscripts

Type size (pts.)	Appearance		
	Regular	**Bold**	*Italic*
10	Main text, section titles, authors' affiliations, abstract, keywords, references, tables, table names, figure captions, equations, footnotes, text subscripts, and superscripts	**Abstract-**	*Subheading (1.1.)*
12	Authors' names,		
24	Paper title		

6.2. Text Layout for Accepted Papers

A4 page margins should be margins: top = 24 mm, bottom = 24 mm, side = 15 mm. The column width is 87mm (3.425 in). The space between the two columns is 6 mm (0.236 in). Paragraph indentation is 3.5 mm (0.137 in). Follow the type sizes specified in Table. Position figures and tables at the tops and bottoms of columns. Avoid placing them in the middle of columns. Large figures and tables may span across both columns. Figure captions should be centred below the figures; table captions should be centred above. Avoid placing figures and tables before their first mention in the text. Use the abbreviation "Fig. 1," even at the beginning of a sentence.

7. Submission Process

The International Journal of Engineering Technologies operates an online submission and peer review system that allows authors to submit articles online and track their progress via a web interface. Articles that are prepared referring to this template should be controlled according to submission checklist given in "Guide f Authors". Editor handles submitted articles to IJET primarily in order to control in terms of compatibility to aims and scope of Journal. Articles passed this control are checked for grammatical and template structures. If article passes this control too, then reviewers are assigned to article and Editor gives a reference number to paper. Authors registered to online submission system can track all these phases. Editor also informs authors about processes of submitted article by e-mail. Each author may also apply to Editor via online

submission system to review papers related to their study areas. Peer review is a critical element of publication, and one of the major cornerstones of the scientific process. Peer Review serves two key functions:

- Acts as a filter: Ensures research is properly verified before being published
- Improves the quality of the research

8. Conclusion

The conclusion section should emphasize the main contribution of the article to literature. Authors may also explain why the work is important, what are the novelties or possible applications and extensions. Do not replicate the abstract or sentences given in main text as the conclusion.

Acknowledgements

Authors may acknowledge to any person, institution or department that supported to any part of study.

References

[7] J. Clerk Maxwell, A Treatise on Electricity and Magnetism, 3rd ed., vol. 2. Oxford:Clarendon Press, 1892, pp.68-73. (Book)

[8] H. Poor, An Introduction to Signal Detection and Estimation, New York: Springer-Verlag, 1985, ch. 4. (Book Chapter)

[9] Y. Yorozu, M. Hirano, K. Oka, and Y. Tagawa, "Electron spectroscopy studies on magneto-optical media and plastic substrate interface", IEEE Transl. J. Magn. Japan, vol. 2, pp. 740-741, August 1987. (Article)

[10] E. Kabalcı, E. Irmak, I. Çolak, "Design of an AC-DC-AC converter for wind turbines", International Journal of Energy Research, Wiley Interscience, DOI: 10.1002/er.1770, Vol. 36, No. 2, pp. 169-175. (Article)

[11] I. Çolak, E. Kabalci, R. Bayindir R., and S. Sagiroglu, "The design and analysis of a 5-level cascaded voltage source inverter with low THD", 2nd PowerEng Conference, Lisbon, pp. 575-580, 18-20 March 2009. (Conference Paper)

[12] IEEE Standard 519-1992, Recommended practices and requirements for harmonic control in electrical power systems, The Institute of Electrical and Electronics Engineers, 1993. (Standards and Reports)

INTERNATIONAL JOURNAL OF ENGINEERING TECHNOLOGIES (IJET)
COPYRIGHT AND CONSENT FORM

This form is used for article accepted to be published by the IJET. Please read the form carefully and keep a copy for your files.

TITLE OF ARTICLE (hereinafter, "The Article"):

……..…….....……

……..…….....……

……...……...……

LIST OF AUTHORS:

……..……...…..……

……..…….....……

……...……...……

CORRESPONDING AUTHOR'S ("The Author") NAME, ADDRESS, INSTITUTE AND EMAIL:

……...……

……..…….....……

……...……...……..…

COPYRIGHT TRANSFER

The undersigned hereby transfers the copyright of the submitted article to International Journal of Engineering Technologies (the "IJET"). The Author declares that the contribution and work is original, and he/she is authorized by all authors and/or grant-funding agency to sign the copyright form. Author hereby assigns all including but not limited to the rights to publish, distribute, reprints, translates, electronic and published derivates in various arrangements or any other versions in full or abridged forms to IJET. IJET holds the copyright of Article in its own name.

Author(s) retain all rights to use author copy in his/her educational activities, own websites, institutional and/or funder's web sites by providing full citation to final version published in IJET. The full citation is provided including Authors list, title of the article, volume and issue number, and page number or using a link to the article in IJET web site. Author(s) have the right to transmit, print and share the first submitted copies with colleagues. Author(s) can use the final published article for his/her own professional positions, career or qualifications by citing to the IJET publication.

Once the copyright form is signed, any changes about the author names or order of the authors listed above are not accepted by IJET.

Authorized/Corresponding Author **Date/ Signature**